

Genome-wide determination of on-target and off-target characteristics for RNA-guided DNA Methylation by dCas9 methyltransferases

--Manuscript Draft--

Manuscript Number:	GIGA-D-17-00040R3	
Full Title:	Genome-wide determination of on-target and off-target characteristics for RNA-guided DNA Methylation by dCas9 methyltransferases	
Article Type:	Research	
Funding Information:	Teknologi og Produktion, Det Frie Forskningsråd (DFF-1337-00128)	Prof. Yonglun Luo
	Teknologi og Produktion, Det Frie Forskningsråd (DFF-1335-00763A)	Prof. Yonglun Luo
	Innovation Fund Denmark (BrainStem)	Prof. Yonglun Luo
	Lundbeckfonden (R173-2014-1105)	Prof. Yonglun Luo
	Lundbeckfonden (R151-2013-14439)	Prof. Lars Bolund
	Lundbeckfonden (R219-2016-1375)	Dr. Lin Lin
	Toyota Foundation (JP)	Prof. Anders Lade Nielsen
	Lundbeckfonden	Prof. Anders Lade Nielsen
Abstract:	<p>Background Fusion of DNA methyltransferase domains to the nuclease-deficient clustered regularly interspaced short palindromic repeat (CRISPR) associated protein 9 (dCas9) has been used for epigenome editing, but the specificities of these dCas9 methyltransferases have not been fully investigated.</p> <p>Findings We generated CRISPR-guided DNA methyltransferases by fusing the catalytic domain of DNMT3A or DNMT3B to the C terminus of the dCas9 protein from <i>S. pyogenes</i> and validated its on-target and global off-target characteristics. Using targeted quantitative bisulfite pyrosequencing, we prove that dCas9-BFP-DNMT3A and dCas9-BFP-DNMT3B can efficiently methylate the CpG dinucleotides flanking its target sites at different genomic loci (uPA and TGFBR3) in human embryonic kidney cells (HEK293T). Furthermore, we conducted whole genome bisulfite sequencing (WGBS) to address the specificity of our dCas9 methyltransferases. WGBS revealed that although dCas9-BFP-DNMT3A and dCas9-BFP-DNMT3B did not cause global methylation changes, a substantial number (over 1000) of off-target differentially methylated regions (DMRs) were identified. The off-target DMRs, which were hypermethylated in cells expressing dCas9 methyltransferase and gRNAs, were predominantly found in promoter regions, 5' untranslated regions, CpG islands, and DNase I hypersensitivity sites, whereas, unexpected hypomethylated off-target DMRs were significantly enriched in repeated sequences. Through chromatin immunoprecipitation with massive parallel DNA sequencing analysis, we further revealed that these off-target DMRs were weakly correlated with dCas9 off-target binding sites. Using qPCR, RNA sequencing and fluorescence reporter cells, we also found that dCas9-BFP-DNMT3A and dCas9-BFP-DNMT3B can mediate transient inhibition of gene expression, which might be caused by dCas9-mediated de novo DNA methylation as well as interference with transcription.</p> <p>Conclusion Our results prove that dCas9 methyltransferases cause efficient RNA-guided methylation of specific endogenous CpGs. However, there is significant off-target methylation indicating that further improvements of the specificity of CRISPR-dCas9 based DNA methylation modifiers are required.</p>	

Corresponding Author:	Yonglun Luo Aarhus Universitet Health Aarhus, DENMARK
Corresponding Author Secondary Information:	
Corresponding Author's Institution:	Aarhus Universitet Health
Corresponding Author's Secondary Institution:	
First Author:	Lin Lin
First Author Secondary Information:	
Order of Authors:	Lin Lin
	Yong Liu
	Fengping Xu
	Jingrong Huang
	Tina Fuglsang Daugaard
	Trine Skov Petersen
	Bettina Hansen
	Lingfei ye
	Qing Zhou
	Fang Fang
	Ling Yang
	Shengting Li
	Lasse Fløe
	Kristopher Torp Jensen
	Ellen Shrock
	Fang Chen
	Huanming Yang
	Jian Wang
	Xin Liu
	Xun Xu
	Lars Bolund
	Anders Lade Nielsen
	Yonglun Luo
Order of Authors Secondary Information:	
Response to Reviewers:	Dear Editor and Reviewers, Thanks again for the constructive comments and the approval of our study. We have now include a paragraph in the discussion section describing the difference in off-target effects between Cas9 and dCas9 methyltransferases and effector proteins. Kr Alun
Additional Information:	
Question	Response

<p>Are you submitting this manuscript to a special series or article collection?</p>	<p>No</p>
<p>Experimental design and statistics</p> <p>Full details of the experimental design and statistical methods used should be given in the Methods section, as detailed in our Minimum Standards Reporting Checklist. Information essential to interpreting the data presented should be made available in the figure legends.</p> <p>Have you included all the information requested in your manuscript?</p>	<p>Yes</p>
<p>Resources</p> <p>A description of all resources used, including antibodies, cell lines, animals and software tools, with enough information to allow them to be uniquely identified, should be included in the Methods section. Authors are strongly encouraged to cite Research Resource Identifiers (RRIDs) for antibodies, model organisms and tools, where possible.</p> <p>Have you included the information requested as detailed in our Minimum Standards Reporting Checklist?</p>	<p>Yes</p>
<p>Availability of data and materials</p> <p>All datasets and code on which the conclusions of the paper rely must be either included in your submission or deposited in publicly available repositories (where available and ethically appropriate), referencing such data using a unique identifier in the references and in the “Availability of Data and Materials” section of your manuscript.</p> <p>Have you have met the above requirement as detailed in our Minimum Standards Reporting Checklist?</p>	<p>Yes</p>

1
2
3
4 **1 Genome-wide determination of on-target and off-target characteristics for RNA-guided**
5 **2 DNA Methylation by dCas9 methyltransferases**
6
7
8
9

10 4 Lin Lin ^{1,7,§}, Yong Liu ^{1,§}, Fengping Xu ^{2,3,4,§}, Jinrong Huang ^{2,3,4,§}, Tina Fuglsang Daugaard ¹,
11 5 Trine Skov Petersen ¹, Bettina Hansen ¹, Lingfei Ye ², Qing Zhou ^{2,3}, Fang Fang ^{2,3}, Ling Yang ²,
12 6 ³, Shengting Li ^{1,2}, Lasse Fløe ¹, Kristopher Torp Jensen ¹, Ellen Shrock ⁶, Fang Chen ^{2,3,4},
13 7 Huanming Yang ^{2,4,5}, Jian Wang ^{2,4}, Xin Liu ^{2,3}, Xun Xu ^{2,3,*}, Lars Bolund ^{1,2,3,7,9}, Anders Lade
14 8 Nielsen ¹, Yonglun Luo ^{1,2,3,7,8,9*}
15
16
17
18

19 10 Initials for authors:

20 11 L.L., Y.Liu., F.X., J.H., T.F.D., T.S.P., B.H., L.Y., Q.Z., F.F., L.Y., S.L., L.F., K.T.J., E.S., F.C.,
21 12 H.Y., J.W., X.L., X.X., L.B., A.L.N., Y.L.
22
23

24 14 Affiliations for authors:

- 25 15 1. Department of Biomedicine, Aarhus University, Aarhus, Denmark
26 16 2. BGI-Shenzhen, Shenzhen 518083, China
27 17 3. China National GeneBank-Shenzhen, BGI-Research, Shenzhen 518083, China
28 18 4. Department of Biology, University of Copenhagen, Copenhagen, Denmark
29 19 5. James D. Watson Institute of Genome Sciences, Hangzhou 310058, China
30 20 6. Department of Genetics, Harvard Medical School, Boston, MA, USA.
31 21 7. Danish Regenerative Engineering Alliance for Medicine (DREAM), Department of Biomedicine,
32 22 Aarhus University, Aarhus, Denmark
33 23 8. BrainStem - Stem Cell Center of Excellence in Neurology, Copenhagen, Denmark
34 24 9. BGI-Qingdao, 2877 Tuanjie Road, Sino-German Ecopark, Qingdao, 266000, China

35 25 §. These authors contributed equally to the study

36 26 *. All correspondence should be addressed to Xun Xu (XUXUN@GENOMICS.CN) and Yonglun
37 27 Luo (ALUN@BIOMED.AU.DK)
38
39

40 28
41 29 **Emails:**

42 30 Lin Lin: lin.lin@biomed.au.dk

43 31 Yong Liu: liyongbox@gmail.com

44 32 Jinrong Huang: huangjinrong@genomics.cn

45 33 Fengping Xu: xufengping@genomics.cn

46 34 Tina Fuglsang Daugaard: tfm@biomed.au.dk

47 35 Trine Skov Petersen: trinesp@biomed.au.dk

48 36 Bettina Hansen: bhansen@biomed.au.dk

49 37 Lingfei Ye: yelingfei@genomics.cn
50
51
52
53
54
55
56
57
58
59
60
61
62
63
64
65

1
2
3
4 38 Qing Zhou: zhouqing1@genomics.cn
5
6 39 Fang Fang: fangfang@genomics.org.cn
7
8 40 Ling Yang: yangling2@genomics.cn
9
10 41 Shengting Li: lishengting@gmail.com
11
12 42 Lasse Fløe: lassefloe@gmail.com
13
14 43 Kristopher Torp Jensen: kristopher.torp@gmail.com
15
16 44 Ellen Shrock: ellen_shrock@g.harvard.edu
17
18 45 Fang Chen: fangchen@genomics.cn
19
20 46 Huanming Yang: yanghm@genomics.cn
21
22 47 Jian Wang: wangjian@genomics.cn
23
24 48 Xin Liu: [<liuxin@genomics.cn>](mailto:liuxin@genomics.cn)
25
26 49 Xun Xu: xuxun@genomics.cn
27
28 50 Lars Bolund: bolund@biomed.au.dk
29
30 51 Anders Lade Nielsen: aln@biomed.au.dk
31
32 52 Yonglun Luo: alun@biomed.au.dk
33
34 53
35
36
37
38
39
40
41
42
43
44
45
46
47
48
49
50
51
52
53
54
55
56
57
58
59
60
61
62
63
64
65

1
2
3
4
5
6
7
8
9
10
11
12
13
14
15
16
17
18
19
20
21
22
23
24
25
26
27
28
29
30
31
32
33
34
35
36
37
38
39
40
41
42
43
44
45
46
47
48
49
50
51
52
53
54
55
56
57
58
59
60
61
62
63
64
65

55 **1. Abstract**

56 **Background**

57 Fusion of DNA methyltransferase domains to the nuclease-deficient clustered regularly
58 interspaced short palindromic repeat (CRISPR) associated protein 9 (dCas9) has been used for
59 epigenome editing, but the specificities of these dCas9 methyltransferases have not been fully
60 investigated.

61

62 **Findings**

63 We generated CRISPR-guided DNA methyltransferases by fusing the catalytic domain of
64 DNMT3A or DNMT3B to the C terminus of the dCas9 protein from *S. pyogenes* and validated its
65 on-target and global off-target characteristics. Using targeted quantitative bisulfite
66 pyrosequencing, we prove that dCas9-BFP-DNMT3A and dCas9-BFP-DNMT3B can efficiently
67 methylate the CpG dinucleotides flanking its target sites at different genomic loci (*uPA* and
68 *TGFBR3*) in human embryonic kidney cells (HEK293T). Furthermore, we conducted whole
69 genome bisulfite sequencing (WGBS) to address the specificity of our dCas9 methyltransferases.
70 WGBS revealed that although dCas9-BFP-DNMT3A and dCas9-BFP-DNMT3B did not cause
71 global methylation changes, a substantial number (over 1000) of off-target differentially
72 methylated regions (DMRs) were identified. The off-target DMRs, which were hypermethylated in
73 cells expressing dCas9 methyltransferase and gRNAs, were predominantly found in promoter
74 regions, 5' untranslated regions, CpG islands, and DNase I hypersensitivity sites, whereas,
75 unexpected hypomethylated off-target DMRs were significantly enriched in repeated sequences.
76 Through chromatin immunoprecipitation with massive parallel DNA sequencing analysis, we
77 further revealed that these off-target DMRs were weakly correlated with dCas9 off-target binding
78 sites. Using qPCR, RNA sequencing and fluorescence reporter cells, we also found that dCas9-
79 BFP-DNMT3A and dCas9-BFP-DNMT3B can mediate transient inhibition of gene expression,
80 which might be caused by dCas9-mediated *de novo* DNA methylation as well as interference with
81 transcription.

82

83 **Conclusion**

84 Our results prove that dCas9 methyltransferases cause efficient RNA-guided methylation of
85 specific endogenous CpGs. However, there is significant off-target methylation indicating that
86 further improvements of the specificity of CRISPR-dCas9 based DNA methylation modifiers are
87 required.

88

89 **Key words**

90 DNA methylation – CRISPR – Cas9 – DNMT3A – DNMT3B – dCas9 – specificity – off-targets –
91 epigenome editing

1
2
3
4
5
6
7
8
9
10
11
12
13
14
15
16
17
18
19
20
21
22
23
24
25
26
27
28
29
30
31
32
33
34
35
36
37
38
39
40
41
42
43
44
45
46
47
48
49
50
51
52
53
54
55
56
57
58
59
60
61
62
63
64
65

92 **2. Background**

93 Owing to its simplicity, efficiency and potential for multiplicity, the type II Clustered Regularly
94 Interspaced Short Palindromic Repeats (CRISPR) and CRISPR-associated protein 9 (Cas9) with
95 engineered variants have been widely used for genome and epigenome editing in many species
96 [1-5]. The Cas9 protein is guided to a specific genomic locus containing a protospacer adjacent
97 motif (PAM) by a small single guide RNA (gRNA), which contains a conserved scaffold sequence
98 and a programmable guide sequence (typically 20 nt) for base pairing with the taret [1]. By
99 introducing double mutations (D10A and H840A) in the *S.pyogenes* Cas9 protein (dCas9) to
100 inactivate its catalytic activity and fusing functional effectors to the C terminus of the dCas9, the
101 applications of CRISPR/Cas9 are expanded to regulation of gene expression (CRISPRa and
102 CRISPRi) [6-8], targeted DNA purification [9], visualization of specific gene regions [10], and
103 acetylation or methylation of chromatin components [11, 12].

104
105 Genome-wide studies have revealed fundamental functional roles of DNA methylation as well as
106 associations between aberrant DNA methylation and human diseases including cancer [13, 14].
107 Methylation of cytosine residues (5mC) in the mammalian genome mainly occurs at CpG
108 dinucleotides. In promoter regions CpG methylation normally associated with repression of gene
109 expression. Currently, insights into DNA methylation-associated biological processes are largely
110 based on correlative data. Methods have been developed to methylate desired gene loci
111 selectively by fusing programmable DNA binding proteins (zinc finger proteins (ZFs) or
112 transcription-activator-like effectors (TALEs)) to DNA methyltransferases ³⁻⁹. However, the
113 laborious generation of ZFs- and TALEs hampers their broader applications. Engineered dCas9
114 has been harnessed for targeted DNA methylation by fusing dCas9 to the catalytic domain of
115 mammalian DNA methyltransferases, thus providing an alternative tool for more easily
116 programmable DNA methylation [15, 16].

117
118 Currently, genome-wide characterization of the specificity of dCas9-based epigenetic modifiers is
119 lacking. To gain more insights into the efficiency and specificity of targeted DNA methylation by
120 CRISPR gRNA-guided dCas9 methyltransferases, we used quantitative bisulfite pyrosequencing,
121 whole genome bisulfite sequencing, and ChIP-seq to investigate the characteristics of dCas9
122 methyltransferase-mediated DNA methylation in human cells.

123
124

1
2
3
4
5
6
7
8
9
10
11
12
13
14
15
16
17
18
19
20
21
22
23
24
25
26
27
28
29
30
31
32
33
34
35
36
37
38
39
40
41
42
43
44
45
46
47
48
49
50
51
52
53
54
55
56
57
58
59
60
61
62
63
64
65

125 **3. Methods**

126 **3.1 Cell Culture**

127 Human embryonic kidney HEK293T cells (ATCC) were cultured in Dulbecco's modified Eagle's
128 medium (DMEM, Life Technologies), 10% fetal bovine serum (Sigma), 1% penicillin-streptomycin
129 (Sigma), 1X GlutaMAX (Life Technologies) at 37 °C, 5% CO₂.

130

131 **3.2 dCas9 methyltransferases plasmids**

132 The dCas9 coding sequence was derived from pHR-SFFV-dCas9-BFP-KRAB (Addgene ID
133 46911) (a gift from Stanley Qi & Jonathan Weissman). The catalytic domains of DNMT1,
134 DNMT3A and DNMT3B were PCR-amplified from pcDNA3/Myc-DNMT1 (Addgene ID 36939),
135 pcDNA3/Myc-DNMT3A (Addgene ID 35521) and pcDNA3/Myc-DNMT3B1 (Addgene ID 35522) (a
136 gift from Arthur Riggs), respectively. The DNMT3A (E752A) and DNMT3B (E697A) catalytically
137 inactivating mutations were introduced by site-directed mutagenesis. All plasmids described in
138 this study have been validated by Sanger sequencing and will be publically available through
139 Addgene (https://www.addgene.org/Yonglun_Luo/) (**Supplementary Table S1**).

140

141 **3.3 CRISPR gRNA design**

142 Based on the observation that dCas9 methyltransferases could efficiently methylate the CpGs
143 flanking the target sites, a web-based gRNA designing tool (dCas9 methyltransferases **gRNA**
144 **finder**, <http://luolab.au.dk/views/gRNA.cgi>) was developed to facilitate dCas9
145 methyltransferase-based gRNA design. All updates regarding the dCas9 methyltransferase
146 protocol are available on the website (<http://luolab.au.dk/>). All gRNA sequences are listed in
147 **Supplementary Table S1**.

148

149 **3.4 Transfection and enrichment transfected cells**

150 Unless stated elsewhere, cells were transfected with gRNAs (total 500 ng) and a dCas9
151 methyltransferase expression vector (500 ng) in six-well plates using X-tremeGENE 9 DNA
152 transfection reagent (Roche). For single gRNA or pUC19 control transfections, the amount of
153 plasmid added was equivalent to the total amount of plasmid added for multiple gRNA
154 transfections. For BFP-based enrichment, cells were harvested 48 hours after transfection, and
155 dCas9 methyltransferase-expressing cells were sorted by FACS. Briefly, transfected cells were
156 harvested by trypsinization, washed twice with 2% FBS-PBS, and re-suspended in 500 µL 2%
157 FBS-PBS. Cells were stained with Propidium Iodide (PI) before sorting. PI negative and BFP
158 positive or negative cells were sorted with a 4 Laser BD FACS Aria III instrument. All transfections
159 were performed in at least two independent experiments.

160

161 **3.5 Quantitative PCR (qPCR)**

1
2
3
4
5
6
7
8
9
10
11
12
13
14
15
16
17
18
19
20
21
22
23
24
25
26
27
28
29
30
31
32
33
34
35
36
37
38
39
40
41
42
43
44
45
46
47
48
49
50
51
52
53
54
55
56
57
58
59
60
61
62
63
64
65

162 Total RNA was extracted from cells with the RNeasy Plus Mini Kit (Qiagen, 74136) according to
163 the manufacturer's instructions and quantified using a Nanodrop 1000 Spectrophotometer. The
164 first strand cDNA was synthesized from 100-500 ng total RNA with the iScript cDNA synthesis kit
165 (Bio-Rad, 170-8891) following the manufacturer's instructions. qPCR was performed in triplicate
166 for each sample, using the Light Cycler 480 SYBR Green I Master mix (Roche Life Science,
167 04887352001) and a Light Cycler 480 qPCR machine. Each qPCR reaction contained 1 μ L cDNA
168 template (5 times diluted), 7.5 μ L qPCR Master mix (2X), and 5 pmol of each qPCR primer in a
169 total volume of 15 μ L. The following qPCR program was used for *uPA*, *TGFBR3* and *GAPDH*: 1
170 cycle at 95 °C for 5 min; 45 cycles at 95 °C for 10s, 57 °C for 10s, and 72 °C for 10s during which
171 the fluorescence signal was measured. The final product was subjected to melting curve analysis.
172 Primers for qPCR are listed in **Supplementary Table S1**. Relative gene expression was
173 calculated using the $2^{-\Delta\Delta CT}$ method by first normalizing to the internal control *GAPDH* (ΔCT) and
174 then calibrating to the transfection control pUC19 ($\Delta\Delta CT$) [17].
175

176 **3.6 DNA methylation analysis by bisulfite pyrosequencing with PyroMark Q24**

177 Genomic DNA was extracted using the DNeasy Blood & Tissue Kit (Qiagen, 69506) according to
178 the manufacturer's instructions. A total of 200 ng of genomic DNA was bisulfite treated using the
179 EpiTect Bisulfite Kit (Qiagen, 59104) according to the manufacturer's instructions. This converts
180 unmethylated cytosines to uracils. The bisulfite converted DNA was eluted with 20 μ L elution
181 buffer provided by the kit. Bisulfite PCR reactions for all genes described in this study were
182 performed in a 25 μ L volume containing 0.15 μ L Hotstar Taq polymerase (5U/ μ L) (New England
183 Biolabs, M0495L), 2.5 μ L 10xStandard buffer, 0.5 μ L of 10 mM dNTPs, 1.0 μ L of each primer (10
184 μ M) and 1.5 μ L bisulfite converted genomic DNA. PCR was performed under the following
185 conditions: 95 °C for 5 min followed by 45 cycles of 94 °C for 30 sec, 58 °C for 1 min, and 72 °C
186 for 45 sec, and, finally, by 72 °C for 7 min. 4 μ L PCR product was checked by gel electrophoresis.
187 Pyrosequencing was performed with the PyroMark Q24 Advanced Reagents (Qiagen, 970922)
188 using 20 μ L PCR product from the bisulfite treated DNA and 20 μ L sequencing primer (0.375 μ M)
189 according to the PyroMark Q24 CpG protocol. The general degree of cytosine methylation was
190 determined by pyrosequencing of the bisulfite converted genomic DNA, using the PyroMark Q24
191 Advanced system (Qiagen).

192
193 **3.7 DNA methylation analysis by bisulfite Sanger sequencing**

194 Bisulfite converted DNA was used as template for PCR amplifications with the BS specific PCR
195 primers listed in **Supplementary Table S1**, using the DreamTaq DNA Polymerase (Life
196 Technologies, EP0701). PCR products were gel purified, sub-cloned in a TA-cloning vector (Life
197 Technologies, 450030) and transformed into chemically competent *E.coli* cells. Cell clones were

1
2
3
4
5
6
7
8
9
10
11
12
13
14
15
16
17
18
19
20
21
22
23
24
25
26
27
28
29
30
31
32
33
34
35
36
37
38
39
40
41
42
43
44
45
46
47
48
49
50
51
52
53
54
55
56
57
58
59
60
61
62
63
64
65

198 manually picked, sub-cultured in 250 ul LB medium overnight, lysed, subjected to Sanger
199 sequencing and analyzed by BISMA [18].

200

201 **3.8 Fluorescence reporter cell assay**

202 Five stable fluorescence reporter cell clones were established by randomly inserting various
203 copies of the CMV promoter-driven mCherry expression cassette into HEK293T (pLV-mCherry
204 was a gift from Pantelis Tsoulfas, Addgene ID 36084). Cells were transfected separately with
205 each dCas9 methyltransferase expression vector (50 ng) and gRNAs (total 50 ng) in 24-well
206 plates. One-third of the transfected cells were seeded to a new plate every 2-3 days and the
207 remainder used for flow cytometry analysis. Median mCherry intensity was measured with the BD
208 LSRFortessa™ cell analyzer (FACS CORE facility, Aarhus University). Identical instrument
209 settings and control beads were applied during the time course experiment to ensure valid
210 comparison across different time points. 20,000 events were recorded for each sample. Flow
211 cytometry data were analyzed using the Flowjo software.

212

213 **3.9 Immunostaining**

214 48 hours after transfection, cells were fixed with freshly-made 4% PFA for 15 min at room
215 temperature, followed by three washes with DPBS. Cells were permeabilized in 0.3% Triton X-
216 100 DPBS for 10 min and blocked in 5% goat serum-DPBS for 30 min. Cells were incubated with
217 a primary rabbit anti-HA-tag antibody (C29F4, Cell Signaling 3724, 1:1000) overnight, followed by
218 secondary antibody staining with Alexa Fluor 555 donkey anti-rabbit IgG (A-31572, Life
219 technologies) at room temperature for 2 hours. Images were obtained with a confocal microscope
220 (LSM710, Carl Zeiss).

221

222 **3.10 Southern blot analysis**

223 Genomic DNA (15 µg) was digested with *EcoRI* restriction enzyme overnight and then analyzed
224 by gel electrophoresis with vacuum blotting. Primers for generating the mCherry probe are listed
225 in **Supplementary Table S1**. Probe labelling was performed using the Prime-It II Random Primer
226 Labeling Kit according to the manufacturer's instructions. Pre-hybridization and hybridization
227 steps were carried out at 42 °C. Excess probe was washed from the membrane with SSC buffer,
228 and the hybridization pattern was visualized on X-ray film by autoradiography.

229

230 **3.11 RNA sequencing**

231 Integrity and quantity of extracted RNA was evaluated with an Agilent 2100 Bioanalyzer
232 according to the manufacturer's instructions. After DNase I treatment, mRNA was isolated with
233 Oligo (dT) magnetic beads. Fragmentation buffer was added to generate short fragments of
234 mRNA. cDNA was synthesized using the mRNA fragments as templates, resolved with EB buffer

1
2
3
4
5
6
7
8
9
10
11
12
13
14
15
16
17
18
19
20
21
22
23
24
25
26
27
28
29
30
31
32
33
34
35
36
37
38
39
40
41
42
43
44
45
46
47
48
49
50
51
52
53
54
55
56
57
58
59
60
61
62
63
64
65

235 for end repair and ligated with adaptors. After size selection and purification by agarose gel
236 electrophoresis, cDNA with sizes of approximately 240 bp were used for PCR amplification (12
237 cycles) and library construction. Libraries were sequenced on an Ion Proton platform (>30 million
238 reads per sample). Sequencing reads that contained low quality, adaptor, and/or short (< 30nt)
239 read sequences were filtered out before mapping. tmap was used to align the clean reads to the
240 hg19 UCSC RefSeq (RNA sequences, GRCh37). No more than 3 mismatches were allowed in
241 the alignment. Gene expression levels were calculated by transforming uniquely mapped
242 transcript reads to TPM (transcript per million) [19]. Differentially expressed genes were defined
243 as genes with a Benjamini-Hochberg-adjusted P value (FDR) ≤ 0.001 and fold change ≥ 2
244 compared to pUC19 control.

245
246 **3.12 ChIP-seq**

247 HEK293T cells were transfected with dCas9 methyltransferase and five *uPA* gRNAs (triplicates).
248 48 hours after transfection, transfected cells were subjected to ChIP with a commercially
249 available kit CHIP-IT Express Enzymatic (53009-AF, ActivMotif, distributed by Nordic Biolabs) and
250 an anti-HA tag antibody (C29F4, Cell Signaling) according to the manufacturer's instructions.
251 Next generation sequencing libraries were prepared for Chip and input samples. SE50
252 sequencing was performed on Illumina HiSeq2500. Clean reads were mapped to human genome
253 hg19 using SOAP2 with the parameter "-p 4 -v 2 -s 35". Unique mapping reads was sampled
254 randomly and equally (62723057 reads). Peaks were called using MACS with P value $1e-3$
255 compared to the input samples. Common peaks found in the triplicates were selected.
256 Furthermore, ChIP peaks loated in repeat sequences and rDNA were removed. Sequence motifs
257 enriched within 70 bp of peak summits were identified using MEME-ChIP.

258
259 **3.13 WGBS library preparation and sequencing**

260 Genomic DNA was fragmented by sonication to a mean size of 250bp using a Bioruptor
261 (Diagenode, Belgium), followed by the blunt-ending, dA addition to 3'-end, and adaptor ligation
262 using the TruSeq Sample Preparation kit (Illumina Inc.) according to the manufacturer's
263 instructions. Then, bisulfite conversion was conducted with the EZ DNA Methylation-Gold kit
264 (ZYMO). The fragments with different insert size were excised from the same lane of a 2% TAE
265 agarose gel. Products were purified by using QIAquick Gel Extraction kit (Qiagen) and amplified
266 by 18 PCR cycles. The library quality was monitored using the Agilent 2100 BioAnalyzer (Agilent)
267 and the concentration of the library was determined by quantitative PCR. Finally, the WGBS
268 libraries were paired-end sequenced on Illumina HiSeq X Ten.
269 After filtering out adaptor and low-quality reads, a total of 953.7Gb 150bp paired-end clean data
270 was generated. An average of 106Gb clean data was obtained for each sample. Clean reads
271 were aligned to the human reference genome (hg19) by BSMAP(v2.74) with the parameter "-u -v

1
2
3
4
5
6
7
8
9
10
11
12
13
14
15
16
17
18
19
20
21
22
23
24
25
26
27
28
29
30
31
32
33
34
35
36
37
38
39
40
41
42
43
44
45
46
47
48
49
50
51
52
53
54
55
56
57
58
59
60
61
62
63
64
65

272 5 -z 33 -p 6 -n 0 -w 20 -s 16 -r 0 -f 10 -L 140" [20]. Only the CpG sites with read depths ≥ 4 were
273 taken into consideration for DNA methylation level calculation. The 48502 bp lambda DNA
274 genome was used as an extra reference for calculating the bisulphite conversion rate. Nearly
275 complete ($>99\%$) bisulfite conversion was documented in all libraries. For repeat WGBS
276 experiment, HEK293T cells were transfected with pUC19 as controls or transfected with dCas9-
277 BFP-DNMT3A and uPA gRNAs. Transfections were conducted in triplicates. Genomic DNA were
278 purified from all cells 48 hours after transfection without BFP-based FACS enrichment of
279 transfected cells. WGBS library construction and sequencing were conducted as above but
280 sequenced with less depth, of 10-15X coverage.

281
282 **3.14 Identification of differentially methylated regions (DMRs) and attempts to exclude**
283 **stochastic DMRs unrelated to the dCas9 methyltransferase treatment**

284 The bioconductor package DSS was used to identify DMRs with the parameter " $\delta \geq 0.1$,
285 $pvalue \leq 0.01$, CpG sites ≥ 3 , DMR length ≥ 10 bp, smoothing window 100 bp". Since
286 expressing high amount of dCas9-BFP-DNMT3A and either uPA or TGFBR3 gRNAs caused the
287 highest *de novo* on-target methylation, we reasoned that the authentic off-target DMRs should be
288 detected in these two comparisons. We first compared group 1 (dCas9-BFP-DNMT3A (500 ng) +
289 uPA gRNAs (500 ng)) or group 3 (dCas9-BFP-DNMT3A (500 ng) + TGFBR3 gRNAs (500 ng)) to
290 group 9 (pUC19 control).

291
292 Based on the observation of (1) dose- and gRNA-dependent *de novo* methylation of *uPA*,
293 *TGFBR3* and *GAPDH* by dCas9 methyltransferases and (2) dCas9-BFP-DNMT3A being more
294 efficient than dCas9-BFP-DNMT3B, we reasoned that the authentic DMRs caused by dCas9
295 methyltransferases and uPA gRNAs should have a methylation pattern as described below:

296
297 **Hypermethylated DMRs by dCas9 methyltransferases and uPA gRNAs should meet:**

- 298 % mCpG:
299 **(1) group 9** (pUC19) \leq **group 5** (dCas9-DNMT-3A only (500 ng)) \leq **group 7** (dCas9-DNMT-3A
300 (50 ng) + uPA gRNAs (50 ng)) \leq **group 1** (dCas9-DNMT-3A (500 ng) + uPA gRNAs (500 ng)).
301 **(2) group 2** (dCas9-DNMT-3B (500 ng) + uPA gRNAs (500 ng)) \leq **group 1** (dCas9-DNMT-3A
302 (500 ng) + uPA gRNAs (500 ng))
303 **(3) group 6** (dCas9-DNMT-3B (500 ng)) \leq **group 2** (dCas9-DNMT-3B (500 ng) + uPA gRNAs
304 (500 ng))

305
306 **Hypomethylated DMRs by dCas9 methyltransferases and uPA gRNAs should meet:**

307 % mCpG:

1
2
3
4
5
6
7
8
9
10
11
12
13
14
15
16
17
18
19
20
21
22
23
24
25
26
27
28
29
30
31
32
33
34
35
36
37
38
39
40
41
42
43
44
45
46
47
48
49
50
51
52
53
54
55
56
57
58
59
60
61
62
63
64
65

308 **(1) group 9** (pUC19) >= **group 5** (dCas9-DNMT-3A only (500 ng)) >= **group 7** (dCas9-DNMT-3A
309 (50 ng) + uPA gRNAs (50 ng)) >= **group 1** (dCas9-DNMT-3A (500 ng) + uPA gRNAs (500 ng)).
310 **(2) group 2** (dCas9-DNMT-3B (500 ng) + uPA gRNAs (500 ng)) >= **group 1** (dCas9-DNMT-3A
311 (500 ng) + uPA gRNAs (500 ng))
312 **(3) group 6** (dCas9-DNMT-3B (500 ng)) >= **group 2** (dCas9-DNMT-3B (500 ng) + uPA gRNAs
313 (500 ng))

314
315 Similarly, the authentic DMRs caused by dCas9 methyltransferases and *TGFBR3* gRNAs should
316 have a methylation pattern as described below:

317
318 **Hypermethylated DMRs by dCas9 methyltransferases and TGFBR3 gRNAs should meet:**

319 % mCpG:

320 **(1) group 9** (pUC19) =< **group 5** (dCas9-DNMT-3A only (500 ng)) =< **group 8** (dCas9-DNMT-3A
321 (50 ng) + TGFBR3 gRNAs (50 ng)) =< **group 3** (dCas9-DNMT-3A (500 ng) + TGFBR3 gRNAs
322 (500 ng)).

323 **(2) group 4** (dCas9-DNMT-3B (500 ng) + TGFBR3 gRNAs (500 ng)) =< **group 3** (dCas9-DNMT-
324 3A (500 ng) + TGFBR3 gRNAs (500 ng))

325 **(3) group 6** (dCas9-DNMT-3B (500 ng)) =< **group 4** (dCas9-DNMT-3B (500 ng) + TGFBR3
326 gRNAs (500 ng))

327
328 **Hypomethylated DMRs by dCas9 methyltransferases and TGFBR3 gRNAs should meet:**

329 % mCpG:

330 **(1) group 9** (pUC19) >= **group 5** (dCas9-DNMT-3A only (500 ng)) >= **group 8** (dCas9-DNMT-3A
331 (50 ng) + TGFBR3 gRNAs (50 ng)) >= **group 3** (dCas9-DNMT-3A (500 ng) + TGFBR3 gRNAs
332 (500 ng)).

333 **(2) group 4** (dCas9-DNMT-3B (500 ng) + TGFBR3 gRNAs (500 ng)) >= **group 3** (dCas9-DNMT-
334 3A (500 ng) + TGFBR3 gRNAs (500 ng))

335 **(3) group 6** (dCas9-DNMT-3B (500 ng)) >= **group 4** (dCas9-DNMT-3B (500 ng) + TGFBR3
336 gRNAs (500 ng))

337
338 We applied this methylation level-based filtering criteria to further remove potential stochastic
339 DMRs. The remaining DMRs were subjected to all analyses as described in this study.

340
341 **3.15 Analysis of 5nt-SEED-NGG motif density**

342 The 5nt-SEED-NGG density was calculated by counting the frequency of the sequence
343 containing the 5 nt SEED sequences preceding a NGG site on either DNA strand. The PAM
344 density was calculated by counting the frequency of PAM sites (NGG) on either DNA strand. The

1
2
3
4
5
6
7
8
9
10
11
12
13
14
15
16
17
18
19
20
21
22
23
24
25
26
27
28
29
30
31
32
33
34
35
36
37
38
39
40
41
42
43
44
45
46
47
48
49
50
51
52
53
54
55
56
57
58
59
60
61
62
63
64
65

345 median density with standard deviation is shown in the plots. Fisher’s exact test was conducted to
346 compare densities between different sequence datasets.

347

348 **3.16 Statistics**

349 All values in this study were presented as mean ± standard deviation. The one-way Analysis of
350 Variance (ANOVA) with Bonferroni multiple testing, linear regression, Wilcoxon matched-pairs
351 signed-rank test, Fisher’s exact test and Benjamini-Hochberg–adjusted P value were used for
352 statistical analysis. A p-value < 0.05 was considered statistically significant.

353

354

1
2
3
4
5
6
7
8
9
10
11
12
13
14
15
16
17
18
19
20
21
22
23
24
25
26
27
28
29
30
31
32
33
34
35
36
37
38
39
40
41
42
43
44
45
46
47
48
49
50
51
52
53
54
55
56
57
58
59
60
61
62
63
64
65

355 4 Results

356 4.1 On-target DNA methylation by dCas9 methyltransferases: dCas9-BFP-DNMT3A and 357 dCas9-BFP-DNMT3B

358 In mammalian cells, DNA methylation is established by *de novo* DNA methyltransferases
359 (DNMT3A and DNMT3B), and maintained upon replication by DNMT1 [21]. Using a similar
360 approach as Vojta *et al.* and McDonald *et al.* [15, 16]., we fused DNMT1 catalytic domain,
361 DNMT3A catalytic domain, DNMT3B catalytic domain or EGFP to the C-terminal end of dCas9
362 with a blue fluorescent protein (BFP) and a triple tandem repeated flexible linker (3XG4S, Gly-
363 Gly-Gly-Gly-Ser) (**Fig. 1a and Supplementary Fig. S1a**). Enrichment of cells expressing the
364 fusion dCas9 methyltransferases were validated by BFP-based Fluorescence Activated Cell
365 Sorting (FACS) (**Supplementary Fig. S1b**) and immunofluorescence staining using anti-HA tag
366 antibody (**Supplementary Fig. S1c**).

367
368 To validate that dCas9 methyltransferases can methylate endogenous CpGs, the dCas9
369 methyltransferases were first targeted by five gRNAs (*uPA* gRNA T1 to T5, **Fig. 1b**) to the *uPA*
370 promoter, which contains a dense CpG island that is hypomethylated in human cancer cells [22].
371 HEK293T cells were transfected with *uPA* gRNAs and individual dCas9 fusion expression
372 vectors. Following BFP-based FACS enrichment of transfected cells, the percentage of
373 methylated CpGs (mCpGs) at individual CpG sites in the *uPA* promoter (*uPA*-MR1 and *uPA*-MR2
374 genomic regions) was quantified by bisulfite pyrosequencing (**Fig. 1c**). Compared to the pUC19
375 control, cells expressing *uPA* gRNAs and dCas9-BFP-DNMT3A or dCas9-BFP-DNMT3B, but not
376 dCas9-BFP-DNMT1 or dCas9-BFP-EGFP, had significantly higher mCpG levels (*P* value < 0.01,
377 ANOVA test). This is consistent with previous reports showing that the C-terminal catalytic
378 domains of DNMT3A and DNMT3B, but not DNMT1, are active [23, 24]. The CpGs most
379 efficiently *de novo* methylated were located 10-50 bp upstream and downstream of the gRNA
380 target sites. CpGs located in the gRNA binding sites were not methylated by the dCas9
381 methyltransferases, most likely because CRISPR/dCas9 binding blocks the interaction of the
382 methyltransferase domain with the CpGs (**Fig. 1c**). *De novo* methylation by dCas9-BFP-DNMT3A
383 and gRNAs was further validated by bisulfite Sanger sequencing (**Supplementary Fig. S1d**).

384
385 To investigate dCas9 methyltransferase-mediated methylation of another genomic locus, we
386 generated three gRNAs targeting the transforming growth factor beta receptor 3 (*TGFBR3*)
387 promoter. Similar *de novo* methylation effects were observed for dCas9-BFP-DNMT3A or dCas9-
388 BFP-DNMT3B with *TGFBR3* gRNAs (**Fig. 1d-g; Supplementary Fig. S2**). Our results collectively
389 reveal that fusion of dCas9 to the catalytic domain of DNMT3A/3B can mediate targeted *de novo*
390 DNA methylation.

391

1
2
3
4
5
6
7
8
9
10
11
12
13
14
15
16
17
18
19
20
21
22
23
24
25
26
27
28
29
30
31
32
33
34
35
36
37
38
39
40
41
42
43
44
45
46
47
48
49
50
51
52
53
54
55
56
57
58
59
60
61
62
63
64
65

392 4.2 Off-target methylation by dCas9 methyltransferases

393 Since high frequency off-target mutagenesis has been observed in previous applications of
394 CRISPR-Cas9 [25], we investigated the specificity of dCas9 methyltransferases. For this purpose,
395 we repeated the experiment with two additional controls: (1) cells expressing dCas9-BFP-
396 DNMT3A or dCas9-BFP-DNMT3B only; (2) cells expressing dCas9-BFP-DNMT3A or dCas9-
397 BFP-DNMT3B and three scrambled gRNAs (gRNAs targeting the CMV promoter). We found that
398 expression of dCas9 methyltransferases and scrambled gRNAs could cause some unspecific *de*
399 *novo* methylation of the *uPA* promoter, but at much lower levels compared to that obtained for
400 *uPA* gRNAs (**Supplementary Fig. S3**). A slightly increased *uPA* promoter methylation, although
401 not significant, was also observed in cells expressing dCas9 methyltransferase only
402 (**Supplementary Fig. S3**).

403
404 To further assess the off-target methylation, we investigated three genomic regions with various
405 sequence similarities to the *uPA* gRNA target sites: *SH2D3C* (3 mismatches, **Supplementary**
406 **Fig. S4a**), *FAM221A* (3 mismatches, **Supplementary Fig. S4b**), and *GAPDH* promoter (9
407 mismatches, **Fig. 2a**). We did not observe significant changes in CpG methylation at *SH2D3C*
408 and *FAM221A* genomic sites. Surprisingly, several CpG sites in the *GAPDH* promoter were
409 significantly methylated in cells expressing dCas9-BFP-DNMT3A and *uPA*, *TGFBR3*, or
410 scrambled (CMV) gRNAs (**Fig. 2b-c**). The same was observed, but to a lesser extent, in cells
411 expressing dCas9-BFP-DNMT3B (**Fig. 2d-e**). This effect was less prominent in cells expressing
412 dCas9 methyltransferase only, indicating that unspecific methylation of the *GAPDH* promoter is
413 RNA-guided. Our results collectively reveal the existence of site dependent off-target methylation
414 by dCas9 methyltransferases.

415 416 4.3 Effects of DNMT3A/3B catalytic activity and dCas9 methyltransferase expression level 417 on on-target and off-target DNA methylation

418 *De novo* methylation by dCas9 methyltransferases could be mediated either by the catalytic
419 activity of DNMT3A and DNMT3B, or by the recruitment of additional DNA methylation enzymes
420 to the binding sites facilitated by protein interactions. To elucidate the mechanism of on-target
421 and off-target DNA methylation, we introduced the E752A and E697A catalytically inactivating
422 mutations [26] in the DNMT3A and DNMT3B catalytic domains, respectively. To investigate the
423 effect of dCas9 methyltransferase expression levels on on-target and off-target DNA methylation,
424 cells were sorted into four populations based on BFP signal intensity, a marker of dCas9
425 methyltransferase expression level: 1. very low: +; 2. low: ++; 3. medium: +++; and 4. high: ++++
426 (**Fig. 3a**). Bisulfite pyrosequencing analysis of the *uPA* (**Fig. 3b**) and *TGFBR3* (**Fig. 3c**,
427 **Supplementary Fig. S5**) promoters revealed that only dCas9 methyltransferases but not dCas9
428 methyltransferase catalytic mutants cause dose-dependent *de novo* methylation, suggesting that

1
2
3
4 429 *de novo* on-target methylation by dCas9 methyltransferases is mediated by the catalytic activity of
5 430 DNMT3A and DNMT3B.

6
7 431

8 432 We next investigated the effect of dCas9 methyltransferase expression level on off-target
9 433 methylation by analyzing the *GAPDH* promoter methylation in the FACS-sorted cells with different
10 434 BFP signal intensity (+, ++, +++, and ++++). Consistent with previous results, co-expression of
11 435 dCas9-BFP-DNMT3A or dCas9-BFP-DNMT3B (**Fig. 4a, b**) with either *uPA* or *TGFBR3* gRNAs
12 436 significantly increased *de novo* methylation of *GAPDH* promoter CpGs compared to cells
13 437 expressing dCas9 methyltransferase without gRNAs or pUC19. Furthermore, titrating dCas9
14 438 methyltransferase expression levels decreased unspecific methylation of the *GAPDH* promoter
15 439 (**Fig. 4a, b**). Similarly, methyltransferase catalytic mutants do not cause *de novo* methylation of
16 440 *GAPDH*. Since *de novo* methylation of gRNA-targeted genes was also decreased by dCas9
17 441 methyltransferase titration (**Fig. 3**), our results collectively suggest that altering dCas9
18 442 methyltransferase expression levels cannot efficiently reduce unspecific methylation relative to
19 443 targeted methylation.

20
21 444

22 445 To investigate global methylation levels, repetitive *LINE1* elements were investigated as they
23 446 represent a surrogate marker for global DNA methylation [27]. We measured the *LINE1* 5'UTR
24 447 methylation by bisulfite pyrosequencing which revealed that expression of dCas9-BFP-DNMT3A
25 448 and *uPA* gRNAs did not result in significant *LINE1* methylation changes (**Fig. 4c**).

26
27 449

28 450 **4.4 Genome-wide bisulfite sequencing revealed off-target methylation by dCas9** 29 451 **methyltransferases**

30 452 Prompted by the unspecific methylation of *GAPDH* promoter by dCas9 methyltransferases, we
31 453 investigated the genome-wide off-target methylation characteristics by CRISPR dCas9
32 454 methyltransferases using whole-genome bisulfite sequencing (WGBS). WGBS were conducted in
33 455 HEK293T cells transfected with (i) pUC19 (control), (ii) dCas9-BFP-DNMT3A or dCas9-BFP-
34 456 DNMT3B alone, and (iii) dCas9-BFP-DNMT3A or dCas9-BFP-DNMT3B with either *uPA* or
35 457 *TGFBR3* gRNAs with two difference doses (50 ng or 500 ng) (**Supplementary Fig. S6a**). Using
36 458 the Illumina HiSeq X platform, we generated over 100 giga bases (Gb) of clean data for each
37 459 sample (more than 30X coverage with a 99.5% bisulfite conversion rate). This allowed us to
38 460 analyze the methylation pattern at single-base pair resolution. Since mainly CpG dinucleotides
39 461 are subject to methylation in HEK293T cells (**Supplementary Fig. S6b**), all following analyses
40 462 are based on CpG methylation in the entire genome (approximately 40,000,000 CpG sites). We
41 463 firstly examined *uPA*, *TGFBR3* and *GAPDH* promoter methylation as revealed by WGBS in all
42 464 nine groups. WGBS confirmed that the *uPA* and *TGFBR3* gRNAs could target dCas9-BFP-
43 465 DNMT3A or dCas9-BFP-DNMT3B to the *uPA* and *TGFBR3* loci and methylate CpGs flanking the

1
2
3
4 466 gRNA binding sites in a dose- and gRNA-dependent manner (**Fig. 5**). Furthermore, our WGBS
5 467 data revealed that some dCas9 methyltransferase-mediated *de novo* methylation of *uPA*,
6 468 *TGFBR3* and *GAPDH* (*off-target*) promoters occurred in a broad region surrounding the gRNA
7
8 469 binding site.
9

10 470
11 471 Next, we analyzed the global DNA methylation profile. Consistent with the *LINE1* assay (**Fig. 3c**),
12 472 expression of dCas9 methyltransferase alone or together with gRNAs was not associated with
13 473 global methylation changes (**Supplementary Fig. S6c, d**). Since we have only one replicate per
14 474 group and stochastic methylations frequently occur in cancer cells during cultivation [28], we
15 475 analyzed the data with DSS-single (a method developed by Wu et al. for detecting differentially
16 476 methylated regions (DMRs) from WGBS data without replicates [29]) to identify differentially
17 477 methylated regions (DMRs) caused by dCas9 methyltransferase and gRNAs. Firstly, we
18 478 compared cells transfected with dCas9 methyltransferases with or without gRNAs to control cells
19 479 (transfected with pUC19 control plasmid). Over 10,000 hyper or hypo DMRs were identified by
20 480 DSS-single (**Supplementary Fig. S7**). Secondly, based on the observation that: **(1)** there is
21 481 dose- and gRNA-dependency of *uPA*, *TGFBR3* and *GAPDH* methylation by dCas9
22 482 methyltransferase and **(2)** dCas9-BFP-DNMT3A is more efficient than dCas9-BFP-DNMT3B, we
23 483 applied a stringent filtering step to remove potentially stochastic DMRs. Following this filtering, we
24 484 identified over 1000 DMRs resulting from dCas9 methyltransferase together with either *uPA*
25 485 gRNAs (hypermethylated DMRs (hyper-DMRs) = 3671; hypomethylated DMRs (hypo-DMRs) =
26 486 1807) or *TGFBR3* gRNAs (hyper-DMRs = 2267; hypo-DMRs = 1662) (**Supplementary Table S2-**
27 487 **S5**). These DMRs were on average 63-81 bp and contained an average of 5-9 CpGs
28 488 (**Supplementary Fig. S8**). The average methylation levels of these hyper/hypo-DMRs differ
29 489 significantly between pUC19 control cells, cells expressing dCas9 methyltransferase only, cells
30 490 expressing low amounts of dCas9 methyltransferase and gRNAs, and cells expressing high
31 491 amounts of dCas9 methyltransferase and gRNAs (**Fig. 6a, Supplementary Fig. S9a**). Only a
32 492 very small portion of the DMRs (hyper-DMRs = 192; hypo-DMRs = 81) were commonly found
33 493 among DMRs caused by dCas9 methyltransferase and *uPA* compared to *TGFBR3* gRNAs (**Fig.**
34 494 **6b**), suggesting that the majority of the off-target DMRs are RNA-guided. Taken together, our
35 495 WGBS result revealed that expression of dCas9 methyltransferases together with gRNAs can
36 496 cause substantial off-target methylation.
37
38
39
40
41
42
43
44
45
46
47
48
49
50

51 497 52 498 **4.5 Characteristics of dCas9 methyltransferase off-targets**

53 499 To better describe the characteristics of dCas9 methyltransferase off-targets, we stratified hyper-
54 500 and hypo-DMRs according to their localization in particular types of genomic regions, including
55 501 promoters, coding sequences (CDS), introns, 5' untranslated regions (5-UTR), 3-UTR, CpG
56 502 islands (CGI), CGI shores, Alu sequences, LINE1 (L1) sequences, and LINE2 (L2) sequences.
57
58
59
60
61
62
63
64
65

1
2
3
4
5
6
7
8
9
10
11
12
13
14
15
16
17
18
19
20
21
22
23
24
25
26
27
28
29
30
31
32
33
34
35
36
37
38
39
40
41
42
43
44
45
46
47
48
49
50
51
52
53
54
55
56
57
58
59
60
61
62
63
64
65

503 Our results showed that hyper-DMRs were predominantly enriched in promoters, 5-UTR and CGI,
504 whereas hypo-DMRs were enriched in repeated sequences Alu and LINE1 (**Fig. 6c-d,**
505 **Supplementary Fig. S9b-c**). Consistent with this finding, a metaplot of average methylation
506 levels for all genes before the DSS-single call also showed that transcription start site flanking
507 regions (overlapping with promoters and 5'UTR) were hypermethylated in cells expressing dCas9
508 methyltransferase and gRNAs (**Supplementary Fig. 10**).

509
510 Since dCas9 preferentially binds open chromatin regions [30], we further analyzed DNase I
511 hypersensitivity regions based on ENCODE data from HEK293T cells (GEO#: GSM1008573) and
512 quantified the average methylation level in DNase I hypersensitivity sites (DHS) (as an indication
513 of sites with an open chromatin state). The DHS flanking regions (1 kb upstream and
514 downstream) were used as a control. Compared to cells transfected with pUC19, cells expressing
515 dCas9 methyltransferase and gRNAs had significantly higher methylation levels in the DHS sites
516 (P value < 0.05; Wilcoxon matched-pairs signed-rank test) (**Fig. 6e, Supplementary Fig. 9d**).
517 Furthermore, only hyper-DMRs but not hypo-DMRs were significantly enriched in DHS (P value <
518 $1e-300$, Fisher's exact test, **Fig. 6f-g** and **Supplementary Fig. 9e-f**), which collectively suggests
519 that open chromatin regions are prone to unspecific methylation by dCas9 methyltransferase and
520 gRNAs.

521
522 Previous studies have discovered that complementary base pairing between gRNA guide
523 sequences and the PAM-proximal 5nt region (5ntSEED-PAM) is crucial for off-target binding [30,
524 31]. We also assessed the density of individual gRNA 5ntSEED-PAM sequence (5'-**NNNNN**NGG-
525 3') in the hyper- and hypo-DMRs. For each DMR, we included the 100-bp flanking sequences
526 when calculating the presence of 5ntSEED-PAM sequence density. This is based on the previous
527 observation that dCas9 methyltransferases methylate CpGs flanking the gRNA binding site. We
528 consistently observed significant enrichment of 5ntSEED-PAM sequences for all gRNAs in the
529 hyper-DMRs but not hypo-DMRs (**Fig. 6h, Supplementary Fig. 9g**). Taken together, this shows
530 that, if guided by gRNAs, dCas9 methyltransferases can cause substantial off-target methylation
531 of genomic regions with open chromatin accessibility i.e. promoters and 5'UTR, as well as CpG
532 islands. Our finding between the off-target methylation and the chromatin accessibility is also
533 consistent with our recent discovery that CRISPR/Cas9 cleaves more efficiently in euchromatin
534 than heterochromatin regions [32].

535
536 **4.6 dCas9 methyltransferase-mediated hypermethylated DMRs are weakly correlated with**
537 **off-target binding**

538 To further investigate the association between dCas9 methyltransferase off-target methylation
539 and dCas9 off-target DNA binding, we studied off-target binding sites in HEK293T cells

1
2
3
4
5
6
7
8
9
10
11
12
13
14
15
16
17
18
19
20
21
22
23
24
25
26
27
28
29
30
31
32
33
34
35
36
37
38
39
40
41
42
43
44
45
46
47
48
49
50
51
52
53
54
55
56
57
58
59
60
61
62
63
64
65

540 expressing dCas9 methyltransferase and *uPA* gRNAs using ChIP-seq. Using pair-wise
541 comparison as previous approach for dCas9 [31], 805 enriched peaks (P value < 0.001,
542 **Supplementary Table S6**) were identified. These ChIP peaks were scattered throughout the
543 genome and significantly enriched in DHS genomic regions (**Fig. 7a, b**). Using MEME motif
544 scanning of ChIP peaks [33], we identified the most significant motif GGGAGAGGGAGNGG (P =
545 1.0e-593). This motif is identical to the 11-bp seed sequences of *uPA* gRNA T2
546 (GAGCCGGGCGGGAGAGGGAG(GGG)) and the PAM (NGG) site (**Fig. 7c**), suggesting that T2
547 is dominant compared to other *uPA* gRNAs in mediating off-target binding. Analysis of 5ntSEED-
548 PAM sequence density further confirmed that *uPA* T2 binding sites were over-represented in the
549 ChIP peaks (**Fig. 7d**). A previous study has shown that the choice of gRNAs has a great effect on
550 dCas9 off-target binding [31]. The *uPA* gRNA T2 is highly G-rich or AG-rich in the seed region.
551 This can potentially be the cause of most of the off-target activities. This could be the explanation
552 of why we have found 40 times more off-target binding sites compared to the study by Liu et al.
553 [34].

554
555 We next analyzed the correlation between the ChIP peaks and the *uPA* DMRs (including the
556 flanking 100 bp of each DMR). There is a significantly increased overlap between ChIP peaks
557 and *uPA* hyper-DMRs (p = 0.006, Fisher's exact test) but not *uPA* hypo-DMRs (p = 1, Fisher's
558 exact test) (**Fig. 7e**). However, the percentage of *uPA* hyper-DMRs overlaps with ChIP peaks is
559 still very low (11 out of 3671 hyper DMRs, 0.3%). Since the average methylation level of all ChIP
560 peak regions exceeds 60% (**Supplementary Fig. 11**), and this may partially explain why there is
561 a low correlation between ChIP peaks and DMRs given potential functional difficulty in further
562 increasing the methylation level. Furthermore, ChIP-seq only identified sites to which the dCas9
563 methyltransferase binds strongly.

564 565 **4.7 Effects of dCas9 methyltransferases on gene expression**

566 Methylation of promoter DNA can be correlated with inhibition of gene transcription. To determine
567 whether the dCas9 methyltransferase-mediated *uPA* and *TGFBR3* promoter methylation could
568 inhibit gene expression, we measured *uPA* and *TGFBR3* mRNA levels by quantitative PCR
569 (qPCR) in HEK293T cells. Compared to the pUC19 transfection control, both *uPA* and *TGFBR3*
570 expression was significantly decreased in cells expressing dCas9-BFP-DNMT3A or dCas9-BFP-
571 DNMT3B and either *uPA* or *TGFBR3* gRNAs (**Fig. 8a**). However, the reduced *uPA* and *TGFBR3*
572 expression does not appear to be only associated with the *de novo* DNA methylation by dCas9
573 methyltransferases (**Fig. 8a**), as inactivating dCas9 methyltransferase mutants dCas9-BFP-
574 DNMT3A(E752A) and dCas9-BFP-DNMT3B(E697A) also cause similar degrees of expression
575 inhibition despite their lack of *de novo* DNA methylation activity.

576

1
2
3
4
5
6
7
8
9
10
11
12
13
14
15
16
17
18
19
20
21
22
23
24
25
26
27
28
29
30
31
32
33
34
35
36
37
38
39
40
41
42
43
44
45
46
47
48
49
50
51
52
53
54
55
56
57
58
59
60
61
62
63
64
65

577 To investigate whether the inhibition of gene expression is specific to the gRNA targeted genes,
578 we conducted RNA sequencing in HEK293T cells expressing dCas9 methyltransferase and *uPA*
579 gRNAs. A large number (> 1000) of differentially expressed genes (DEG) significantly (FDR *P*
580 value < 0.001, fold change > 2) were found in cells expressing *uPA* gRNAs and either dCas9-
581 BFP-DNMT3A or dCas9-BFP-DNMT3B (**Fig. 8b-c**). However, similar effects on the global
582 transcription profile were observed in cells expressing *uPA* gRNAs with dCas9-BFP-DNMT1 or
583 with dCas9-BFP-EGFP lacking *de novo* DNA methylation activity (**Fig. 8d-e**). We cross-compared
584 DEGs among the four groups and 342 (18-32%) genes were commonly identified (**Fig. 8f**). For
585 DEGs found in cells expressing dCas9-BFP-DNMT3A and *uPA* gRNAs, we also performed
586 integrative analyses of the expression change, promoter methylation, and promoter binding
587 intensity (**Fig. 8g**). Very weak but significant correlation was identified for a few clusters of DEGs.
588 Taken together, these results suggest that the non-specific alteration of transcription is not merely
589 caused by promoter methylation or binding of dCas9 methyltransferase. Since *uPA* is an
590 important factor in regulating cell proliferation and inhibition of cell growth was found in cells
591 expressing dCas9 methyltransferases and *uPA* gRNAs (**Supplementary Fig. S12**), the large
592 number of differentially expressed genes might be a result of altered cellular functions. Taken
593 together, our results clearly indicate that inhibition of *uPA* and *TGFBR3* expression by dCas9
594 methyltransferase and corresponding gRNAs is not merely due to *de novo* DNA methylation of
595 their promoters.

596
597 To investigate whether longer term inhibition of gene expression can be facilitated by dCas9
598 methyltransferases, five HEK293T fluorescent reporter cell clones carrying different copies of a
599 CMV-mCherry expression cassette (**Supplementary Fig. 13a, b**) were generated. We quantified
600 mCherry level by FACS for two weeks after transfection. We observed that the number of dCas9
601 methyltransferase-expressing cells peaked on day 2 and decreased gradually (**Supplementary**
602 **Fig. 13c**). Maximal inhibition of mCherry levels were observed on day 5 after transfection
603 (**Supplementary Fig. 13d-h**). Compared to other dCas9 fusion proteins, the dCas-BFP-DNMT3A
604 fusion resulted in the highest and longest inhibition of mCherry expression in the reporter cells
605 (four out of five clones) (**Supplementary Fig. 13d-h**). The transient and prolonged inhibition
606 efficacy varied among the five cell clones. For example, clone 2, which has the lowest copy
607 number of transgene, showed the highest transient and longest inhibition by dCas-BFP-DNMT3A
608 (**Supplementary Fig. 13e**). However, expression of mCherry was, in all clones, not significantly
609 different from the pUC19 control after two weeks, suggesting that inhibition of gene expression by
610 dCas9 methyltransferases is not stably maintained.

611
612 **Discussion**

1
2
3
4
5
6
7
8
9
10
11
12
13
14
15
16
17
18
19
20
21
22
23
24
25
26
27
28
29
30
31
32
33
34
35
36
37
38
39
40
41
42
43
44
45
46
47
48
49
50
51
52
53
54
55
56
57
58
59
60
61
62
63
64
65

613 Since dCas9 methyltransferases are targeted to a specific genomic locus simply by a small
614 gRNA, this system is more convenient than ZF- or TALE-based methyltransferases [26, 35, 36].
615 Recently, Vojta *et al.* and McDonald *et al.* reported that directly fusing DNMT3A to dCas9 could
616 be used to induce DNA methylation at specific loci in HEK293T cells [15, 16]. Consistent with
617 that, we show that dCas9-BFP-DNMT3A can methylate CpGs flanking the gRNA binding sites in
618 genomic loci, further proving the general applicability of dCas9 methyltransferases for targeted
619 DNA methylation in mammalian cells. In addition, our study shows for the first time that the fusion
620 of dCas9 to DNMT3B is also capable of inducing specific DNA methylation, although the
621 efficiency is lower than that of DNMT3A. Additionally, Peter *et al.* showed that the dCas9-
622 DNMT3A-DNMT3L fusion can further improve *de novo* methylation efficiency compared to
623 dCas9-DNMT3A [37]. Together with the reported systems, the dCas9 methyltransferases system
624 reported in this study further broadens the availability and applicability of CRISPR-based
625 reprogramming of DNA methylation. Based on the observation that dCas9 methyltransferases
626 can efficiently methylate the flanking CpG sites from the gRNA binding site, we have developed
627 an open-source web-based gRNA designing tool for dCas9 methyltransferase gRNAs
628 (<http://luolab.au.dk/views/gRNA.cgi>).

629
630 On the basis of extensive gene-specific bisulfite pyrosequencing and whole-genome bisulfite
631 sequencing (WGBS), we identified novel off-target methylation characteristics that appear to be
632 predominantly enriched in promoter, 5'UTR, CGI, and open chromatin regions. Since most of
633 these genomic regions are hypomethylated in HEK293T cells, it was expected that the off-target
634 DMRs were enriched in such regions. In other genomic regions, which already have a high level
635 of methylation, a further methylation by dCas9 methyltransferase is not achievable. We
636 discovered that open chromatin regions are highly prone to off-target methylation by dCas9-
637 methyltransferase. Since the *GAPDH* promoter is located a DHS region, this explains why this
638 region is subjected to highly off-target methylation. To further confirm our finding, we repeat the
639 WGBS experiment in triplicates (**Supplementary Fig. 14**). Our result confirmed that the hyper-
640 methylated DMRs identified in previous WGBS experiment (**Fig. 6a**) are significantly increased in
641 cells overexpressing dCas9-BFP-DNMT3A and *uPA* in the repeated experiments
642 (**Supplementary Fig. 14a**). Consistently, DHS regions were significantly methylated in cells
643 expressing dCas9-BFP-DNMT3A and *uPA* (**Supplementary Fig. 14b**).

644
645 Our study also revealed the gRNA-dependency of off-target methylation. This is consistent with
646 the observations of McDonald *et al.* and Vojta *et al.* [15, 16]. Additionally, we have discovered
647 that even in the absence of gRNAs, expression of the dCas9-BFP-DNMT3A or dCas9-BFP-
648 DNMT3B alone can cause some unspecific DNA methylation. This gRNA-independent off-target
649 methylation effect is even more pronounced when too many dCas9 methyltransferases, or the

1
2
3
4
5
6
7
8
9
10
11
12
13
14
15
16
17
18
19
20
21
22
23
24
25
26
27
28
29
30
31
32
33
34
35
36
37
38
39
40
41
42
43
44
45
46
47
48
49
50
51
52
53
54
55
56
57
58
59
60
61
62
63
64
65

650 DNMT3A catalytic domain, enter the nucleus. For example, increasing dCas9 methyltransferase
651 expression level, fusing the catalytic domain of DNMT3A or DNMT3B directly to Cas9 without the
652 BFP linker, or overexpressing the DNMT3A catalytic domain will cause increased gRNA-
653 independent off-target methylation (see extended data and description in **Supplementary File 1**).

654
655 In this study, we found that expressing dCas9 methyltransferases and gRNAs could also cause
656 significant demethylation of genomic regions enriched in repeated sequences. Repeated
657 sequences, which make up more than half of the human genome, are generally highly
658 methylated, and their dynamics, to some extent, are associated with normal development and
659 tumorigenesis. A previous study of methylation in repeated sequences has shown that, with
660 increasing age from adulthood, there is a global decrease in DNA methylation in repeated
661 sequences and intergenic genome sequences [38]. We also observed that expression of dCas9
662 methyltransferase alone or together with gRNA can inhibit HEK293T cell growth (**Supplementary**
663 **Fig. 12**). The hypo-methylated DMRs could potentially be the result of inhibited cell proliferation by
664 dCas9 methyltransferase and gRNAs. This should be investigated in future studies.

665
666 Improvement of dCas9 methyltransferase specificity, to minimize the gRNA-dependent and
667 gRNA-independent off-target activity, is crucial for future applications of the technology.
668 McDonald, et al., has observed significant reduction in off-target methylation using DOX inducible
669 dCas9-DNMT3A. Consistent with these findings, we found that reducing the dCas9
670 methyltransferase and gRNA expression levels, as well as lowering the dCas9 methyltransferase
671 nuclear entry efficiency (**Supplementary File 1**), can reduce off-target methylation. However, this
672 approach also reduced on-target methylation levels accordingly. Thus, this may not represent a
673 plausible way of increasing the specificity of the system. New approaches should be developed to
674 reduce off-target methylation while maintaining sufficient on-target methylation efficiencies. The
675 results presented in this study highlight the importance of inclusion of extensive controls in
676 subsequent experiments, such as catalytically inactive dCas9 methyltransferase mutants,
677 scrambled gRNAs, and gRNA free settings. This is necessary for reliable interpretations of
678 correlations between specific DNA methylation events by dCas9 methyltransferase, gene
679 expression regulation and phenotypic effects.

680
681 **Off-target effect is one of the major concerns in CRISPR/Cas9 based DNA manipulation**
682 **technologies and applications. Unlike the original CRISPR/Cas9 technology, of which the**
683 **endonuclease activity of Cas9 depends heavily on the base-pairing between the guide sequences**
684 **and the target site (proto-spacer), the dead Cas9 (dCas9) derived CRISPR technologies and**
685 **applications are more depending on the physical interaction between dCas9/gRNA complex and**
686 **the DNA loci, and more tolerance to mismatches. The dCas9 in such CRISPR-derived systems is**

1
2
3
4
5
6
7
8
9
10
11
12
13
14
15
16
17
18
19
20
21
22
23
24
25
26
27
28
29
30
31
32
33
34
35
36
37
38
39
40
41
42
43
44
45
46
47
48
49
50
51
52
53
54
55
56
57
58
59
60
61
62
63
64
65

687 acting as a cargo protein bringing whatever proteins/domains to a specific genomic locus guided
688 by the small gRNA. As already demonstrated in Figure 2 and Supplementary Figure 4 of this
689 study and several previous investigations by ChIP-seq [39-41], the criteria of defining off-target
690 sites (simply based on mismatches) from wild type Cas9 is not suitable for the dCas9-derived
691 effector proteins, such as the dCas9 methyltransferases. Although our study only evaluated the
692 dCas9 methyltransferases, we speculate that this off-target effects are most likely to be the same
693 for other kind of dCas9 based effectors.

694
695 In this study, we also observed that dCas9 methyltransferases can efficiently inhibit expression of
696 genes in human cells. However, the transient inhibition of gene expression could be resulted from
697 both promoter methylation and blockage of transcription by dCas9 methyltransferases. A previous
698 study reported that targeted DNA methylation by a zinc finger-based methyltransferase is not
699 stably maintained [42]. Our time-course experiments to study the inhibition of gene expression is
700 gradually decreased during *in vitro* expansion of the transfected cells. This could be the result of
701 removal of the *de novo* established epigenetic marks, dilution of the dCas9 methyltransferase
702 expression plasmids, and/or negative selection of the cells expressing dCas9 methyltransferases.
703 We also realize that DNA methylation and gene expression analyses were conducted in cells
704 transiently transfected with dCas9 methyltransferase expression plasmids, which might lead to
705 severe overexpression of the dCas9 methyltransferases. Thus, future studies could benefit from
706 being conducted in cells stably or conditionally expressing low copy numbers of dCas9
707 methyltransferase to minimize off-target methylation. Taken together, our study is the first to
708 reveal novel characteristics of the on-target and off-target DNA methylation by dCas9
709 methyltransferases on a genome-wide scale with single-base resolution and highlights the need
710 for development of CRISPR DNA methylation editing systems with higher specificity.

711
712 **Conclusions**

713 The dCas9 methyltransferases presented here, and other dCas9 fusion protein systems
714 described previously [11, 12, 15, 16], provide useful tools for targeted epigenome editing.
715 Continued improvement of the specificities of these systems and combining tools to enable
716 simultaneous modification of multiple histones and DNA loci will enable more precise and stable
717 regulation of gene structure and function. Such CRISPR gRNA-guided programmable epigenetic
718 modification tools will hopefully have broad research applications to delineate the association
719 between specific epigenetic changes, gene-expression regulation, and phenotypes.

720
721 **Availability of supporting data**

722 RNA sequencing, WGBS, and ChIP-seq data are available from the publicly available repository
723 (GEO).

1
2
3
4
5
6
7
8
9
10
11
12
13
14
15
16
17
18
19
20
21
22
23
24
25
26
27
28
29
30
31
32
33
34
35
36
37
38
39
40
41
42
43
44
45
46
47
48
49
50
51
52
53
54
55
56
57
58
59
60
61
62
63
64
65

724 RNA-seq: GSE74935
725 WGBS: GSE92310, GSE92311
726 ChIP-seq: GSE92261
727

728 **Declarations**

729 **Competing Interests Statement**

730 The authors declare no competing financial interests.

731

732 **Author contributions**

733 L.L., L.B. and Y.L., conceived the idea.

734 H.Y., J.W., L.B., X.L. X.X., A.L.N., and Y.L. planned and oversaw the study

735 L.L., Y.Liu., F.X., J.H., T.F.D., T.S.P., B.H., L.Y., Q.Z., F.F., L.Y., S.L., K.T.J. L.F., E.S., and Y.L.
736 performed experiments and analyzed the data.

737 L.L., J.H., and Y.L. prepared the figures.

738 L.L. and Y.L. drafted the manuscript and all authors revised the manuscript.

739

740 **Acknowledgements**

741 This work was partially supported by grants from Danish Research Council for Independent
742 Research DFF-1337-00128 (Y.L.), the Sapere Aude Young Research Talent Prize DFF-1335-
743 00763A (Y.L.), the Innovation Fund Denmark (BrainStem, Y.L.) and the Lundbeck Foundation:
744 R173-2014-1105 (Y.L.); R151-2013-14439 (L.B.); R219-2016-1375 (L.L.) A.L.N. was supported
745 by the Toyota-Foundation and the Lundbeck Foundation. FACS was performed with help from
746 Charlotte Christie Petersen and Anni Skovbo at the FACS Core Facility, Aarhus University,
747 Denmark.

748

749 **Abbreviations**

750 CRISPR: Clustered Regularly Interspaced Short Palindromic Repeats

751 Cas9: CRISPR-associated protein 9

752 dCas9: Nuclease deficient Cas9 or dead Cas9

753 FACS: Fluorescence-activated cell sorting

754 WGBS: whole-genome bisulfite sequencing

755 CGI: CpG island

756 UTR: Untranslated region

757 DHS: DNase I hypersensitivity sites

758 PAM: Protospacer adjacent motif

759 gRNA: guide RNA

760 ZF: zinc finger protein

1
2
3
4
5
6
7
8
9
10
11
12
13
14
15
16
17
18
19
20
21
22
23
24
25
26
27
28
29
30
31
32
33
34
35
36
37
38
39
40
41
42
43
44
45
46
47
48
49
50
51
52
53
54
55
56
57
58
59
60
61
62
63
64
65

761 TALE: transcription-activator-like effectors
762 qPCR: Quantitative PCR

1
2
3
4
5
6
7
8
9
10
11
12
13
14
15
16
17
18
19
20
21
22
23
24
25
26
27
28
29
30
31
32
33
34
35
36
37
38
39
40
41
42
43
44
45
46
47
48
49
50
51
52
53
54
55
56
57
58
59
60
61
62
63
64
65

763 **Reference:**

764 1. Jinek M, Chylinski K, Fonfara I, Hauer M, Doudna JA, Charpentier E: **A**
765 **programmable dual-RNA-guided DNA endonuclease in adaptive**
766 **bacterial immunity.** *Science* 2012, **337**:816-821.

767 2. Mali P, Yang L, Esvelt KM, Aach J, Guell M, Dicarlo JE, Norville JE, Church GM:
768 **RNA-Guided Human Genome Engineering via Cas9.** *Science* 2013.

769 3. Jinek M, East A, Cheng A, Lin S, Ma E, Doudna J: **RNA-programmed genome**
770 **editing in human cells.** *elife* 2013, **2**:e00471.

771 4. Cong L, Ran FA, Cox D, Lin S, Barretto R, Habib N, Hsu PD, Wu X, Jiang W,
772 Marraffini LA, Zhang F: **Multiplex genome engineering using CRISPR/Cas**
773 **systems.** *Science* 2013, **339**:819-823.

774 5. Johan Vad-Nielsen LL, Lars Bolund, Anders Lade Nielsen, Yonglun Luo
775 **Golden-Gate assembly of CRISPR gRNA Expression Array for**
776 **Simultaneously Targeting Multiple Genes.** *Cell Mol Life Sci* 2016.

777 6. Qi LS, Larson MH, Gilbert LA, Doudna JA, Weissman JS, Arkin AP, Lim WA:
778 **Repurposing CRISPR as an RNA-Guided Platform for Sequence-Specific**
779 **Control of Gene Expression.** *Cell* 2013, **152**:1173-1183.

780 7. Cheng AW, Wang H, Yang H, Shi L, Katz Y, Theunissen TW, Rangarajan S,
781 Shivalila CS, Dadon DB, Jaenisch R: **Multiplexed activation of endogenous**
782 **genes by CRISPR-on, an RNA-guided transcriptional activator system.**
783 *Cell Res* 2013, **23**:1163-1171.

784 8. Gilbert LA, Larson MH, Morsut L, Liu Z, Brar GA, Torres SE, Stern-Ginossar N,
785 Brandman O, Whitehead EH, Doudna JA, et al: **CRISPR-mediated modular**
786 **RNA-guided regulation of transcription in eukaryotes.** *Cell* 2013,
787 **154**:442-451.

788 9. Fujita T, Fujii H: **Efficient isolation of specific genomic regions and**
789 **identification of associated proteins by engineered DNA-binding**
790 **molecule-mediated chromatin immunoprecipitation (enChIP) using**
791 **CRISPR.** *Biochem Biophys Res Commun* 2013, **439**:132-136.

792 10. Chen B, Gilbert LA, Cimini BA, Schnitzbauer J, Zhang W, Li GW, Park J,
793 Blackburn EH, Weissman JS, Qi LS, Huang B: **Dynamic imaging of genomic**
794 **loci in living human cells by an optimized CRISPR/Cas system.** *Cell* 2013,
795 **155**:1479-1491.

796 11. Kearns NA, Pham H, Tabak B, Genga RM, Silverstein NJ, Garber M, Maehr R:
797 **Functional annotation of native enhancers with a Cas9-histone**
798 **demethylase fusion.** *Nat Methods* 2015, **12**:401-403.

799 12. Hilton IB, D'Ippolito AM, Vockley CM, Thakore PI, Crawford GE, Reddy TE,
800 Gersbach CA: **Epigenome editing by a CRISPR-Cas9-based**
801 **acetyltransferase activates genes from promoters and enhancers.** *Nat*
802 *Biotechnol* 2015, **33**:510-517.

803 13. Jones PA, Baylin SB: **The fundamental role of epigenetic events in cancer.**
804 *Nat Rev Genet* 2002, **3**:415-428.

805 14. Brena RM, Costello JF: **Genome-epigenome interactions in cancer.** *Hum*
806 *Mol Genet* 2007, **16 Spec No 1**:R96-105.

1
2
3
4
5
6
7
8
9
10
11
12
13
14
15
16
17
18
19
20
21
22
23
24
25
26
27
28
29
30
31
32
33
34
35
36
37
38
39
40
41
42
43
44
45
46
47
48
49
50
51
52
53
54
55
56
57
58
59
60
61
62
63
64
65

807 15. Vojta A, Dobrinic P, Tadic V, Bockor L, Korac P, Julg B, Klasic M, Zoldos V:
808 **Repurposing the CRISPR-Cas9 system for targeted DNA methylation.**
809 *Nucleic Acids Res* 2016.

810 16. McDonald JI, Celik H, Rois LE, Fishberger G, Fowler T, Rees R, Kramer A,
811 Martens A, Edwards JR, Challen GA: **Reprogrammable CRISPR/Cas9-based**
812 **system for inducing site-specific DNA methylation.** *Biol Open* 2016, **5**:866-
813 874.

814 17. Livak KJ, Schmittgen TD: **Analysis of relative gene expression data using**
815 **real-time quantitative PCR and the 2(-Delta Delta C(T)) Method.** *Methods*
816 2001, **25**:402-408.

817 18. Rohde C, Zhang Y, Reinhardt R, Jeltsch A: **BISMA--fast and accurate**
818 **bisulfite sequencing data analysis of individual clones from unique and**
819 **repetitive sequences.** *BMC Bioinformatics* 2010, **11**:230.

820 19. Wagner GP, Kin K, Lynch VJ: **Measurement of mRNA abundance using**
821 **RNA-seq data: RPKM measure is inconsistent among samples.** *Theory*
822 *Biosci* 2012, **131**:281-285.

823 20. Xi Y, Li W: **BSMAP: whole genome bisulfite sequence MAPping program.**
824 *BMC Bioinformatics* 2009, **10**:232.

825 21. Law JA, Jacobsen SE: **Establishing, maintaining and modifying DNA**
826 **methylation patterns in plants and animals.** *Nat Rev Genet* 2010, **11**:204-
827 220.

828 22. Pakneshan P, Szyf M, Farias-Eisner R, Rabbani SA: **Reversal of the**
829 **hypomethylation status of urokinase (uPA) promoter blocks breast**
830 **cancer growth and metastasis.** *J Biol Chem* 2004, **279**:31735-31744.

831 23. Gowher H, Jeltsch A: **Molecular enzymology of the catalytic domains of**
832 **the Dnmt3a and Dnmt3b DNA methyltransferases.** *J Biol Chem* 2002,
833 **277**:20409-20414.

834 24. Margot JB, Aguirre-Arteta AM, Di Giacco BV, Pradhan S, Roberts RJ, Cardoso
835 MC, Leonhardt H: **Structure and function of the mouse DNA**
836 **methyltransferase gene: Dnmt1 shows a tripartite structure.** *J Mol Biol*
837 2000, **297**:293-300.

838 25. Fu Y, Foden JA, Khayter C, Maeder ML, Reyon D, Joung JK, Sander JD: **High-**
839 **frequency off-target mutagenesis induced by CRISPR-Cas nucleases in**
840 **human cells.** *Nat Biotechnol* 2013.

841 26. Rivenbark AG, Stolzenburg S, Beltran AS, Yuan X, Rots MG, Strahl BD,
842 Blancafort P: **Epigenetic reprogramming of cancer cells via targeted DNA**
843 **methylation.** *Epigenetics* 2012, **7**:350-360.

844 27. Yang AS, Estecio MR, Doshi K, Kondo Y, Tajara EH, Issa JP: **A simple method**
845 **for estimating global DNA methylation using bisulfite PCR of repetitive**
846 **DNA elements.** *Nucleic Acids Res* 2004, **32**:e38.

847 28. Landan G, Cohen NM, Mukamel Z, Bar A, Molchadsky A, Brosh R, Horn-Saban
848 S, Zalcenstein DA, Goldfinger N, Zundelovich A, et al: **Epigenetic**
849 **polymorphism and the stochastic formation of differentially methylated**
850 **regions in normal and cancerous tissues.** *Nat Genet* 2012, **44**:1207-1214.

1
2
3
4
5
6
7
8
9
10
11
12
13
14
15
16
17
18
19
20
21
22
23
24
25
26
27
28
29
30
31
32
33
34
35
36
37
38
39
40
41
42
43
44
45
46
47
48
49
50
51
52
53
54
55
56
57
58
59
60
61
62
63
64
65

851 29. Wu H, Xu T, Feng H, Chen L, Li B, Yao B, Qin Z, Jin P, Conneely KN: **Detection**
852 **of differentially methylated regions from whole-genome bisulfite**
853 **sequencing data without replicates.** *Nucleic Acids Res* 2015, **43**:e141.

854 30. Kuscu C, Arslan S, Singh R, Thorpe J, Adli M: **Genome-wide analysis reveals**
855 **characteristics of off-target sites bound by the Cas9 endonuclease.** *Nat*
856 *Biotechnol* 2014, **32**:677-683.

857 31. Wu X, Scott DA, Kriz AJ, Chiu AC, Hsu PD, Dadon DB, Cheng AW, Trevino AE,
858 Konermann S, Chen S, et al: **Genome-wide binding of the CRISPR**
859 **endonuclease Cas9 in mammalian cells.** *Nat Biotechnol* 2014, **32**:670-676.

860 32. Jensen KT, Floe L, Petersen TS, Huang J, Xu F, Bolund L, Luo Y, Lin L:
861 **Chromatin accessibility and guide sequence secondary structure affect**
862 **CRISPR-Cas9 gene editing efficiency.** *FEBS Lett* 2017.

863 33. Bailey TL, Elkan C: **Fitting a mixture model by expectation maximization**
864 **to discover motifs in biopolymers.** *Proc Int Conf Intell Syst Mol Biol* 1994,
865 **2**:28-36.

866 34. Liu XS, Wu H, Ji X, Stelzer Y, Wu X, Czauderna S, Shu J, Dadon D, Young RA,
867 Jaenisch R: **Editing DNA Methylation in the Mammalian Genome.** *Cell*
868 2016, **167**:233-247 e217.

869 35. Bernstein DL, Le Lay JE, Ruano EG, Kaestner KH: **TALE-mediated epigenetic**
870 **suppression of CDKN2A increases replication in human fibroblasts.** *J*
871 *Clin Invest* 2015, **125**:1998-2006.

872 36. Meister GE, Chandrasegaran S, Ostermeier M: **Heterodimeric DNA**
873 **methyltransferases as a platform for creating designer zinc finger**
874 **methyltransferases for targeted DNA methylation in cells.** *Nucleic Acids*
875 *Res* 2010, **38**:1749-1759.

876 37. Stepper P, Kungulovski G, Jurkowska RZ, Chandra T, Krueger F, Reinhardt R,
877 Reik W, Jeltsch A, Jurkowski TP: **Efficient targeted DNA methylation with**
878 **chimeric dCas9-Dnmt3a-Dnmt3L methyltransferase.** *Nucleic Acids Res*
879 2016.

880 38. Suelves M, Carrio E, Nunez-Alvarez Y, Peinado MA: **DNA methylation**
881 **dynamics in cellular commitment and differentiation.** *Brief Funct*
882 *Genomics* 2016, **15**:443-453.

883 39. O'Geen H, Henry IM, Bhakta MS, Meckler JF, Segal DJ: **A genome-wide**
884 **analysis of Cas9 binding specificity using ChIP-seq and targeted**
885 **sequence capture.** *Nucleic Acids Res* 2015, **43**:3389-3404.

886 40. Zhang XH, Tee LY, Wang XG, Huang QS, Yang SH: **Off-target Effects in**
887 **CRISPR/Cas9-mediated Genome Engineering.** *Mol Ther Nucleic Acids*
888 2015, **4**:e264.

889 41. Duan J, Lu G, Xie Z, Lou M, Luo J, Guo L, Zhang Y: **Genome-wide**
890 **identification of CRISPR/Cas9 off-targets in human genome.** *Cell Res*
891 2014, **24**:1009-1012.

892 42. Kungulovski G, Nunna S, Thomas M, Zanger UM, Reinhardt R, Jeltsch A:
893 **Targeted epigenome editing of an endogenous locus with chromatin**
894 **modifiers is not stably maintained.** *Epigenetics Chromatin* 2015, **8**:12.

895
896

1
2
3
4
5
6
7
8
9
10
11
12
13
14
15
16
17
18
19
20
21
22
23
24
25
26
27
28
29
30
31
32
33
34
35
36
37
38
39
40
41
42
43
44
45
46
47
48
49
50
51
52
53
54
55
56
57
58
59
60
61
62
63
64
65

897

898 **Figure captions**

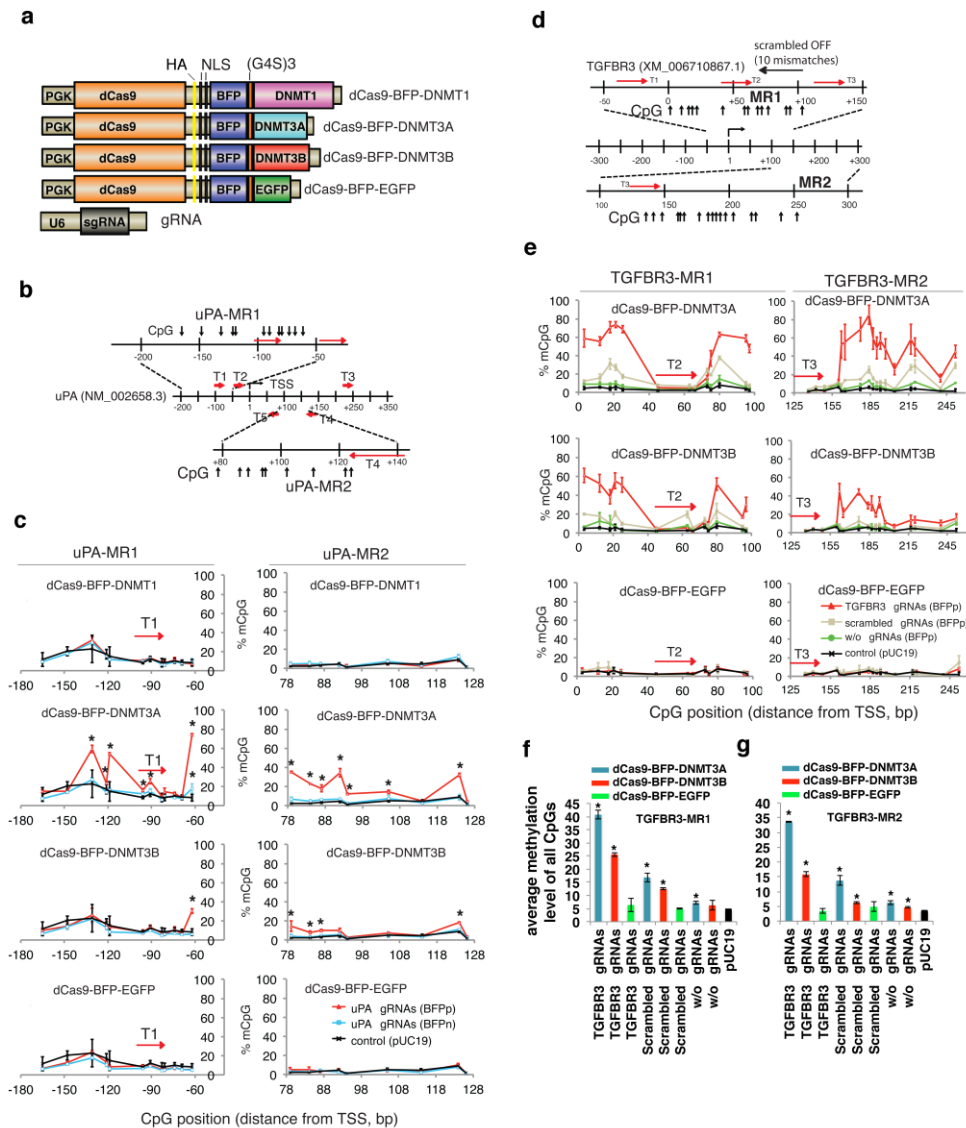


Fig. 1 De novo uPA and TGFBR3 methylation by RNA-guided dCas9 methyltransferases

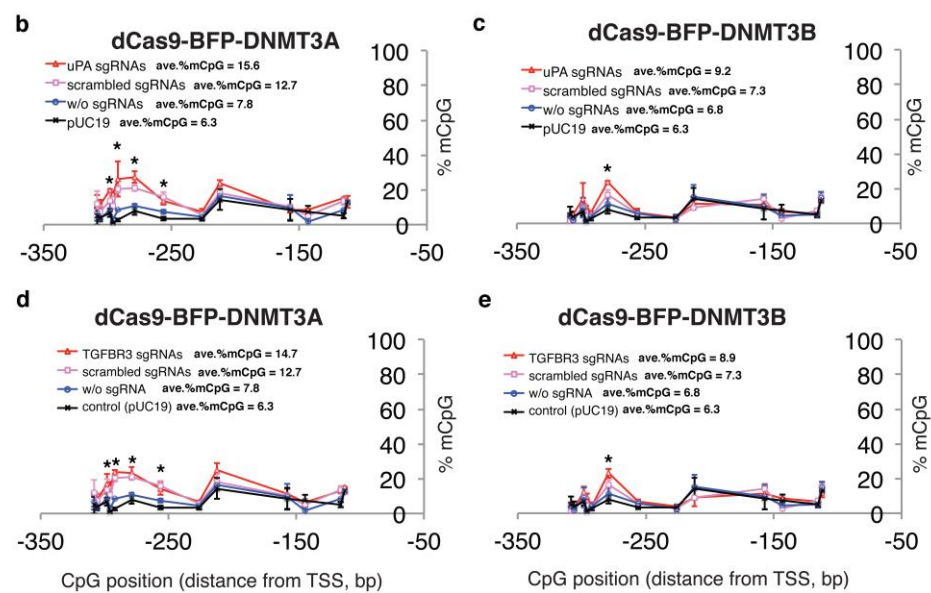
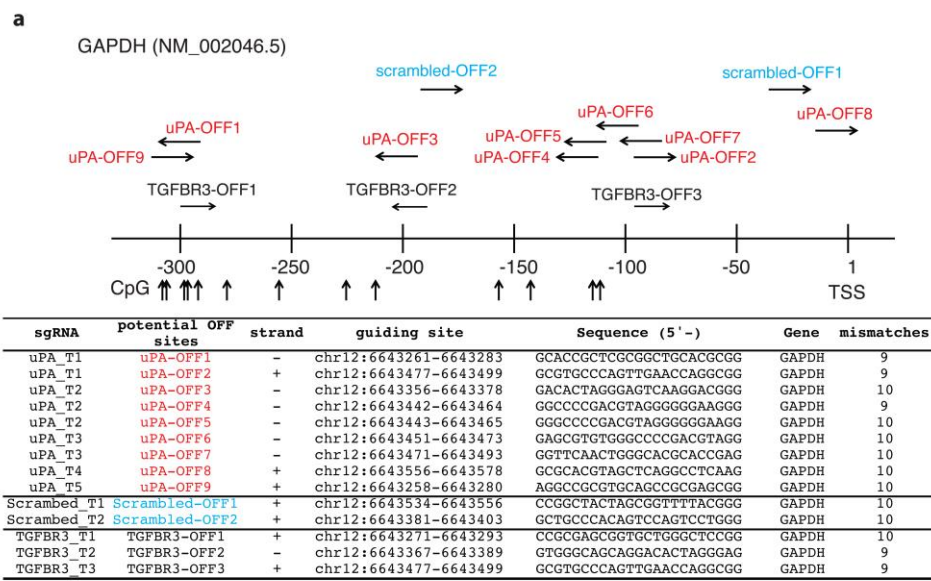
(a) Schematic illustration of the dCas9 methyltransferase expression vectors. PGK: phosphoglycerate kinase promoter; G4S: GGGGS linker; NLS: nuclear localization signal; U6: human U6 promoter.

(b) Schematic illustration of the uPA promoter and gRNA target sites (T1-T5), two uPA methylated regions (uPA-MR1, uPA-MR2) and CpGs analyzed by bisulfite pyrosequencing. TSS: Transcription start site. Numbers indicate distances in base pairs from TSS.

(c) Line plots of the percentage of methylated CpGs (mCpG). Red line: the BFP positive cells (BFPp). Light blue line: BFP negative cells (BFPn). Note that %mCpG in control cells transfected with pUC19 has been re-plotted as a reference (black line). BFPn cells include cells expressing

1
2
3
4
5
6
7
8
9
10
11
12
13
14
15
16
17
18
19
20
21
22
23
24
25
26
27
28
29
30
31
32
33
34
35
36
37
38
39
40
41
42
43
44
45
46
47
48
49
50
51
52
53
54
55
56
57
58
59
60
61
62
63
64
65

910 very low level of dCas9 methyltransferase. Each data point represents mean \pm SD (n = 2-4).
911 Asterisk (*) indicates statistical significance ($p < 0.05$) compared to the control after Bonferroni
912 correction.
913 **(d)** Schematic illustration of the human *TGFBR3* promoter locus, *TGFBR3* gRNA binding sites
914 (red arrows), potential off-target binding sites (black horizontal arrows) of the scrambled gRNA,
915 and CpG sites.
916 **(e)** Line plots of % mCpG at the *TGFBR3* promoter in cells expressing dCas9 methyltransferase
917 with (red line) or without (green line) *TGFBR3* gRNAs, or with the scrambled gRNAs (gray line).
918 Note that %mCpG in control cells transfected with pUC19 has been re-plotted as a reference
919 (black line). Each data point represents mean \pm SD (n = 2-5).
920 **(f-g)** Bar chart of average methylation levels for TGFBR3-MR1 **(f)** and TGFBR3-MR2 **(g)** CpG
921 sites. Values represent mean \pm SD (n = 3). Asterisk (*) represents P value < 0.05 compared to
922 pUC19 (ANOVA).
923
924



925
926

Fig. 2 Off-target methylation of GAPDH promoter by dCas9 methyltransferases and gRNAs

1
2
3
4
5
6
7
8
9
10
11
12
13
14
15
16
17
18
19
20
21
22
23
24
25
26
27
28
29
30
31
32
33
34
35
36
37
38
39
40
41
42
43
44
45
46
47
48
49
50
51
52
53
54
55
56
57
58
59
60
61
62
63
64
65

927 (a) Schematic illustration of the *GAPDH* promoter. Potential off target sites and CpGs analyzed
928 by bisulfite pyrosequencing are indicated. Sequences of potential off-target binding sites by *uPA*,
929 *TGFBR3* and scrambled gRNAs with maximum 10 mismatches are listed.

930 (b-d) Line plots of *GAPDH* promoter methylation in FACS-sorted HEK293T cells 48 hours after
931 transfection with dCas9 methyltransferases and gRNAs. The methylation profiles from the
932 pUC19-transfected samples were re-plotted as reference. Each data point in the graph
933 represents the mean \pm SD (n = 2 independent transfections). Average methylation levels for all
934 CpGs analyzed are presented next to line legends. Asterisks (*) represent P value < 0.05
935 compared to pUC19 (ANOVA).

936
937
938

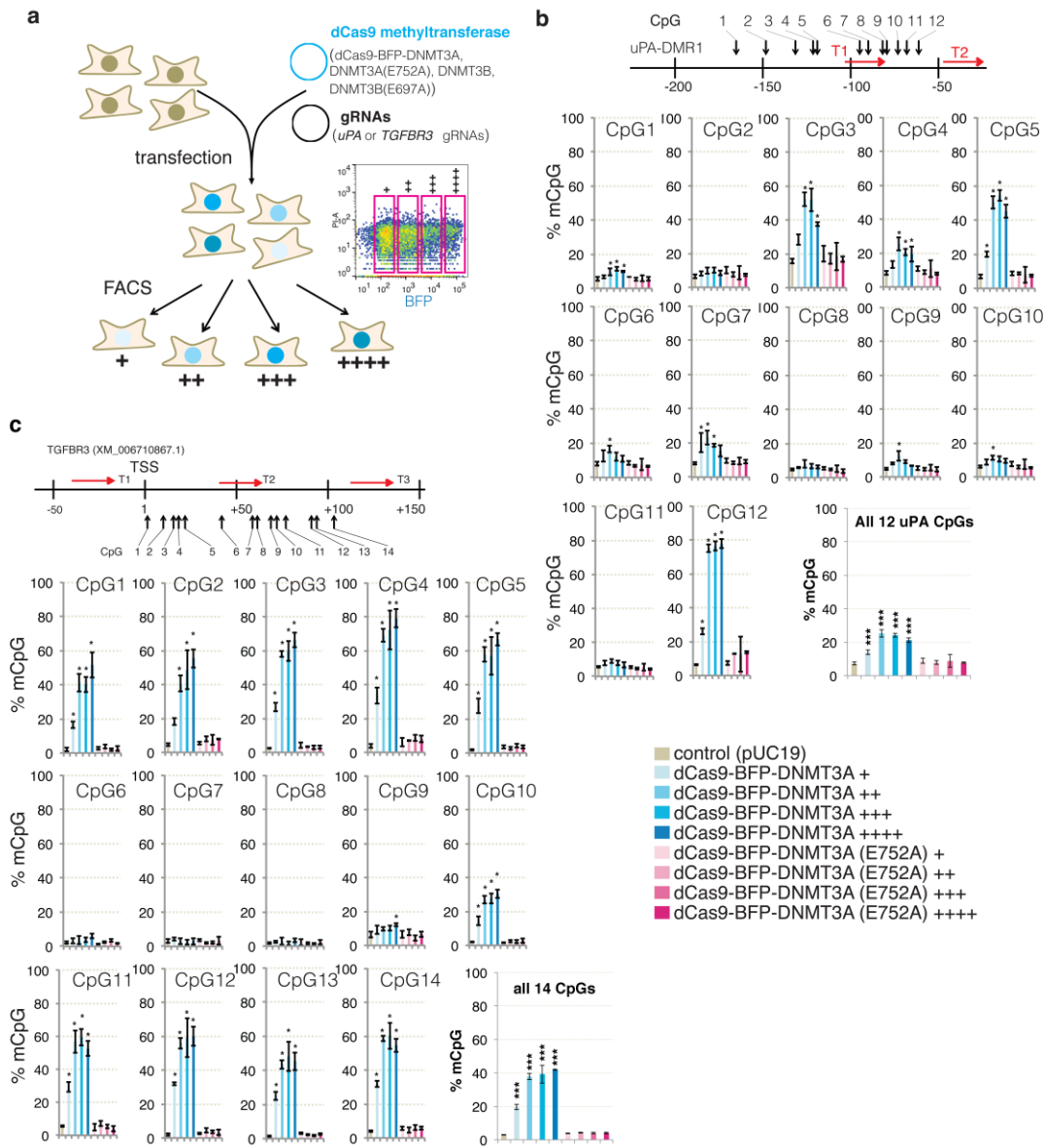


Fig. 3 On-target methylation by dCas9 methyltransferases

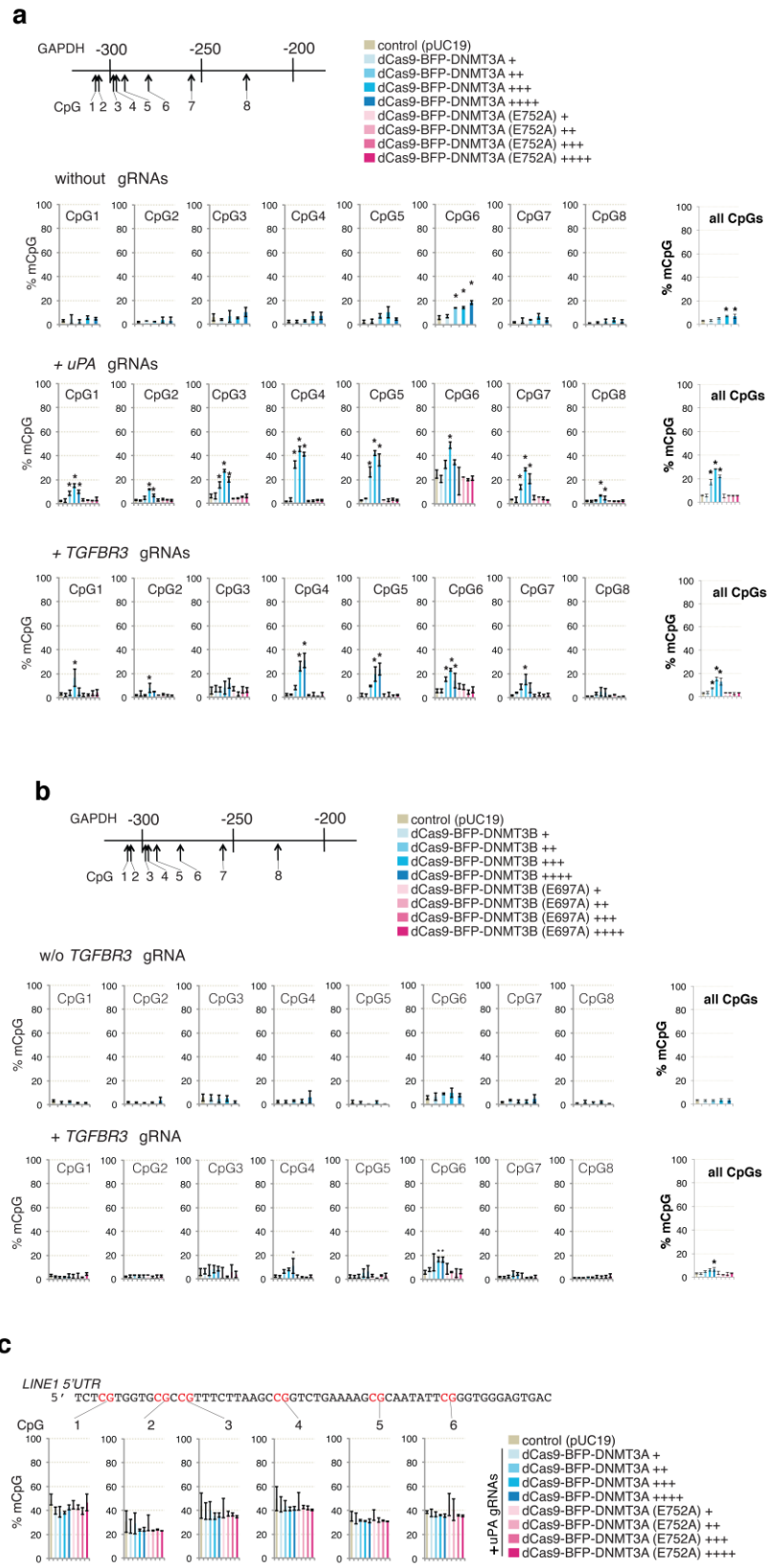
(a) Schematic illustration of the experiment. dCas9 methyltransferase-expressing cells were enriched by FACS 48 hours after transfection and sorted according to the BFP signal: +, ++, +++, +++++. Right: Representative FACS plot and gating.

(b-c) Bar charts indicating % mCpG for individual CpG and average values of all CpG sites in the uPA (b) and TGFBR3 (c) target regions. The schematic illustrations above the bar graphs show gRNA binding sites and CpG sites analyzed. Value represents mean \pm SD (n = 3). Asterisk (*) indicates statistical significance (p < 0.05, ANOVA) compared to the control after Bonferroni correction. Figure legend for bar graphs in (b) and (c) is presented at bottom-right.

1
2
3
4
5
6
7
8
9
10
11
12
13
14
15
16
17
18
19
20
21
22
23
24
25
26
27
28
29
30
31
32
33
34
35
36
37
38
39
40
41
42
43
44
45
46
47
48
49
50
51
52
53
54
55
56
57
58
59
60
61
62
63
64
65

950

1
2
3
4
5
6
7
8
9
10
11
12
13
14
15
16
17
18
19
20
21
22
23
24
25
26
27
28
29
30
31
32
33
34
35
36
37
38
39
40
41
42
43
44
45
46
47
48
49
50
51
52
53
54
55
56
57
58
59
60
61
62
63
64
65



1
2
3
4
5
6
7
8
9
10
11
12
13
14
15
16
17
18
19
20
21
22
23
24
25
26
27
28
29
30
31
32
33
34
35
36
37
38
39
40
41
42
43
44
45
46
47
48
49
50
51
52
53
54
55
56
57
58
59
60
61
62
63
64
65

952 **Fig. 4 Off-target methylation by dCas9 methyltransferases**

953 **(a)** Bar charts indicating % mCpG at individual CpGs and total % mCpG (8 CpG sites) for the
954 *GAPDH* promoter in cells expressing different levels (BFP signal: +, ++, +++, +++) of dCas9-
955 BFP-DNMT3A or dCas9-BFP-DNMT3A(E752A) alone or together with either *uPA* or *TGFBR3*
956 gRNAs.

957 **(b)** Bar charts indicating % mCpG in the *GAPDH* promote in cells expressing different levels (BFP
958 signal: +, ++, +++, +++) of dCas9-BFP-DNMT3B or dCas9-BFP-DNMT3B(E697A) alone or with
959 *TGFBR3* gRNAs.

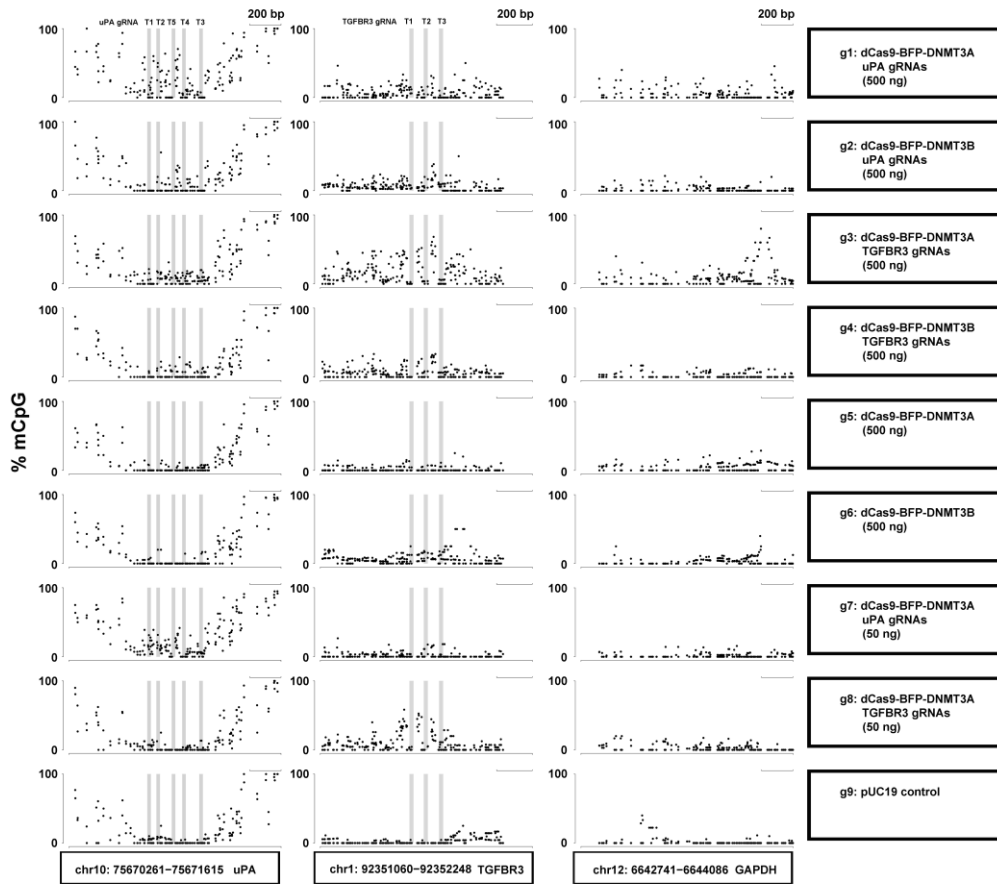
960 **(c)** *LINE1* 5'UTR methylation in cells expressing *uPA* gRNAs with different levels of either dCas9-
961 BFP-DNMT3A or dCas9-BFP-DNMT3A(E752A). Cells transfected with pUC19 were used as
962 controls. Values represent mean \pm SD (n = 3). Asterisks (*) represent P value < 0.05 (ANOVA)
963 compared to pUC19.

964

965

1
2
3
4
5
6
7
8
9
10
11
12
13
14
15
16
17
18
19
20
21
22
23
24
25
26
27
28
29
30
31
32
33
34
35
36
37
38
39
40
41
42
43
44
45
46
47
48
49
50
51
52
53
54
55
56
57
58
59
60
61
62
63
64
65

Fig. 5



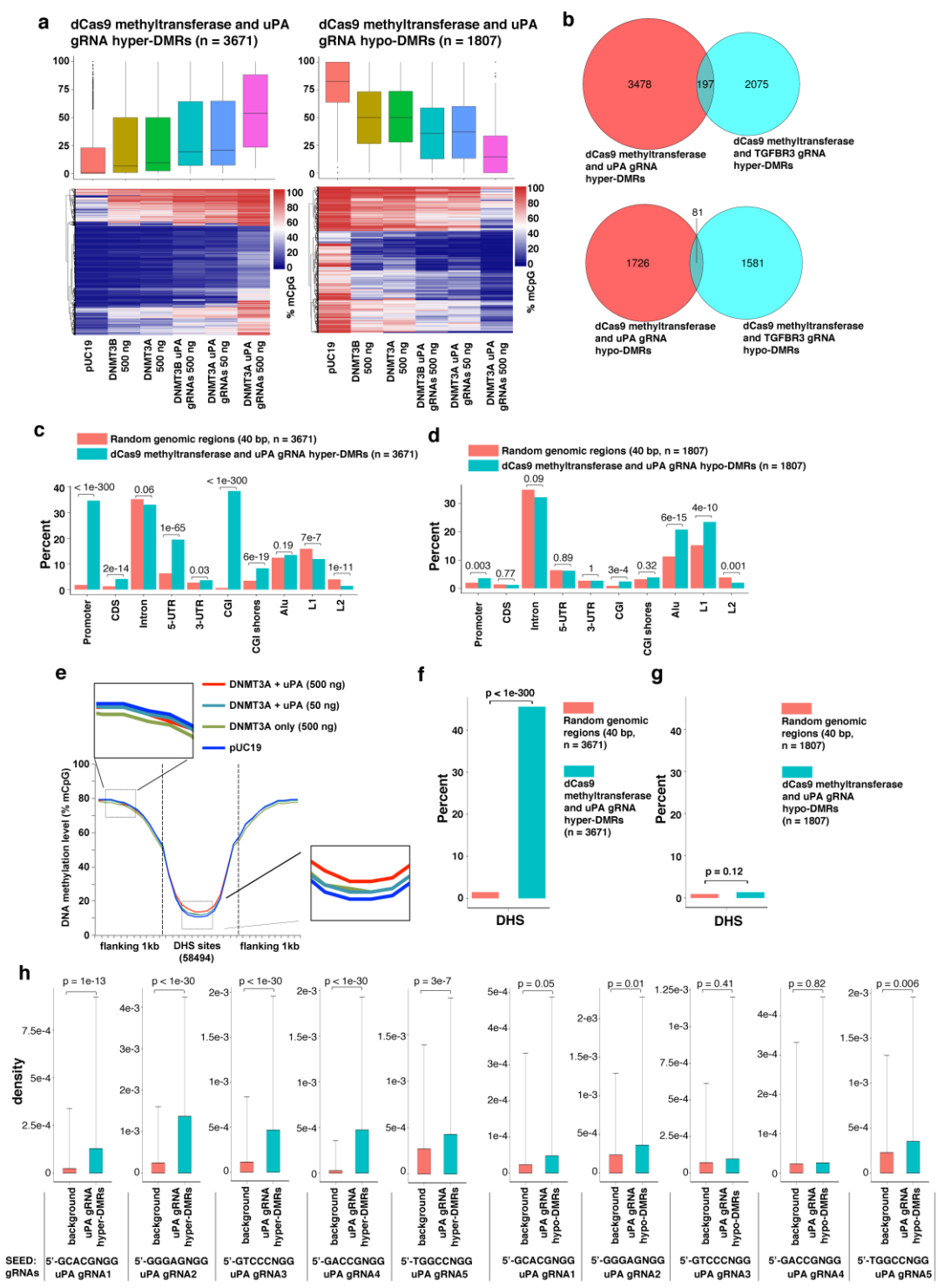
966
967
968

Fig. 5 De novo methylation of *uPA*, *TGFBR3* and *GAPDH* promoters by dCas9 methyltransferase measured with WGBS. Dot plots of % mCpG for individual CpG sites in the

1
2
3
4
5
6
7
8
9
10
11
12
13
14
15
16
17
18
19
20
21
22
23
24
25
26
27
28
29
30
31
32
33
34
35
36
37
38
39
40
41
42
43
44
45
46
47
48
49
50
51
52
53
54
55
56
57
58
59
60
61
62
63
64
65

969 *uPA*, *TGFBR3* and *GAPDH* promoter regions. Each dot represents one CpG site. Right panel
970 indicates the transfected plasmids. mCpG levels were quantified by WGBS. Scale bar, 200 bp.
971
972

1
2
3
4
5
6
7
8
9
10
11
12
13
14
15
16
17
18
19
20
21
22
23
24
25
26
27
28
29
30
31
32
33
34
35
36
37
38
39
40
41
42
43
44
45
46
47
48
49
50
51
52
53
54
55
56
57
58
59
60
61
62
63
64
65

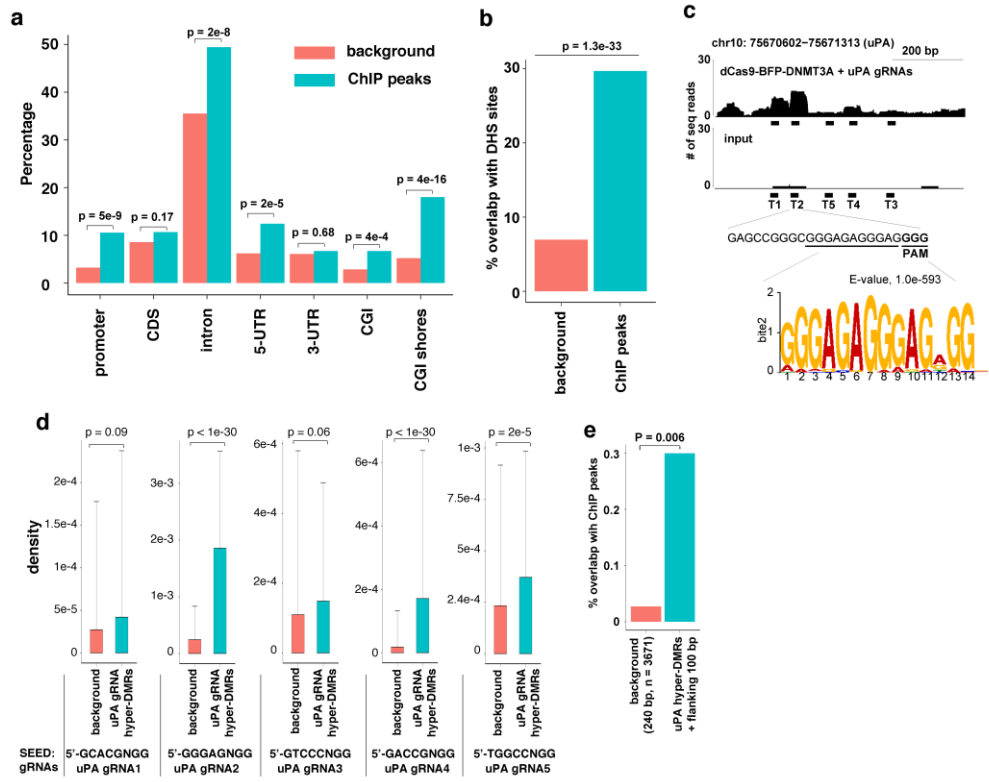


973
974 **Fig. 6 Genomic characteristics of off-target DMRs caused by dCas9 methyltransferases**
975 **and uPA gRNAs**

1
2
3
4
5
6
7
8
9
10
11
12
13
14
15
16
17
18
19
20
21
22
23
24
25
26
27
28
29
30
31
32
33
34
35
36
37
38
39
40
41
42
43
44
45
46
47
48
49
50
51
52
53
54
55
56
57
58
59
60
61
62
63
64
65

976 (a) Box plot (top) and heatmap clustering (bottom) of the hypermethylated (left) and
977 hypomethylated (right) DMRs resulting from dCas9 methyltransferases and *uPA* gRNAs.
978 (b) Venn diagram presentation of hypermethylated (top) or hypomethylated (bottom) DMRs
979 caused by dCas9 methyltransferases and *uPA* gRNAs compared to *TGFBR3* gRNAs.
980 (c-d) Bar chart illustrating the percentage of the identified uPA hypermethylated (c) or
981 hypomethylated (d) DMRs that fall into the different types of genomic regions indicated.
982 Background represents a random sample of the same number of similar sized genomic windows
983 that fall into the categories indicated. Values above bars are P values between background and
984 uPA-DMRs (Fisher's exact test).
985 (e) Metaplot of average CpG methylation levels in 58,494 DNase I hypersensitive sites (DHS) and
986 1 kb upstream and downstream flanking regions.
987 (f-g) Bar chart of % uPA hypermethylated (f) or hypomethylated (g) DMRs falling into DHS core
988 regions.
989 (h) Density of 5nt-SEED-NGG for uPA gRNAs (T1 to T5) in background genomic windows and
990 uPA DMRs + flanking 100 bp. Values represent median density with one standard deviation. P
991 values (t-test) are given above the bar charts.
992
993

1
2
3
4
5
6
7
8
9
10
11
12
13
14
15
16
17
18
19
20
21
22
23
24
25
26
27
28
29
30
31
32
33
34
35
36
37
38
39
40
41
42
43
44
45
46
47
48
49
50
51
52
53
54
55
56
57
58
59
60
61
62
63
64
65

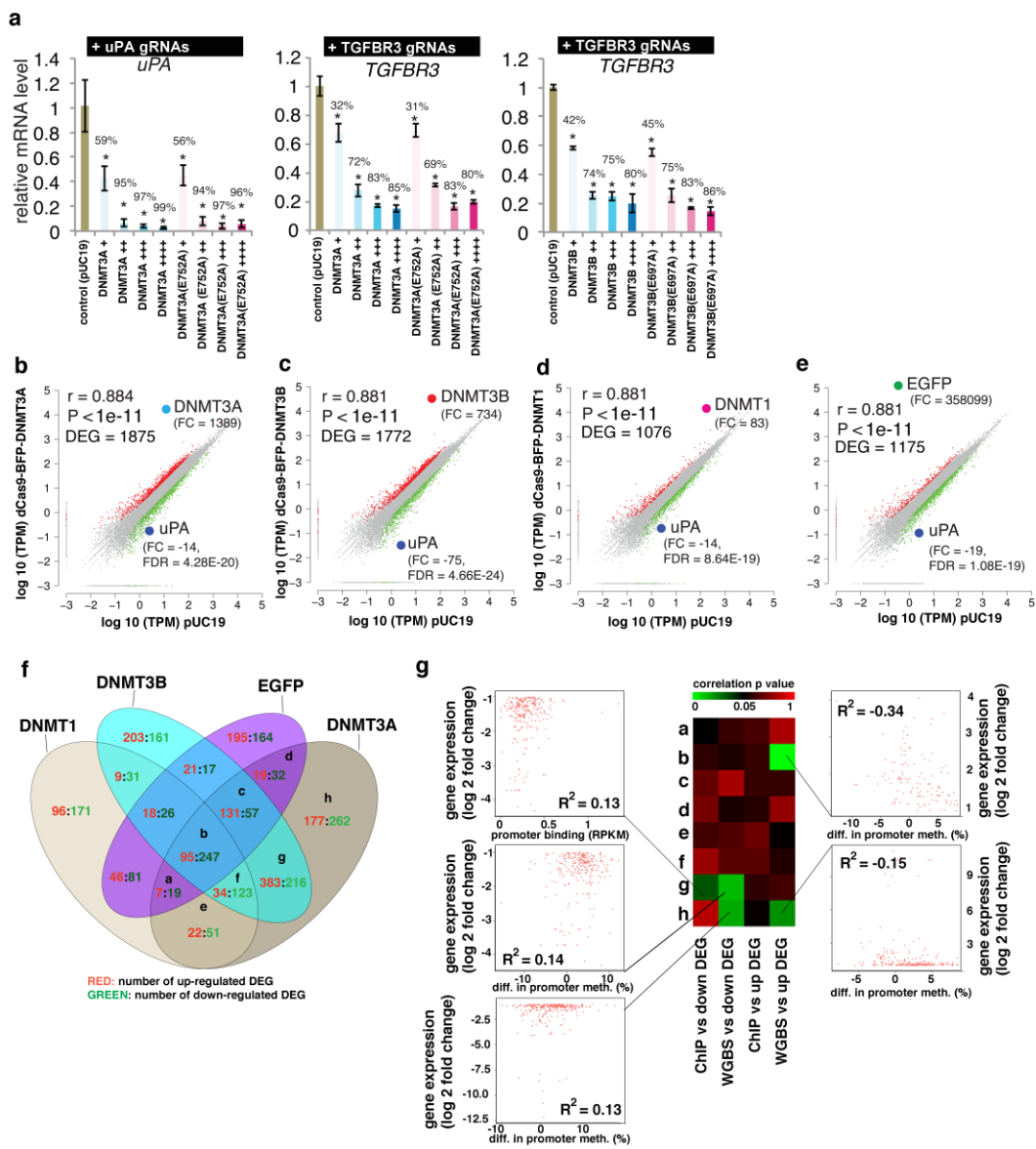


994
995 **Fig. 7 Correlation between dCas9-BFP-DNMT3A off-target binding and off-target**
996 **methylation**

1
2
3
4
5
6
7
8
9
10
11
12
13
14
15
16
17
18
19
20
21
22
23
24
25
26
27
28
29
30
31
32
33
34
35
36
37
38
39
40
41
42
43
44
45
46
47
48
49
50
51
52
53
54
55
56
57
58
59
60
61
62
63
64
65

- 997 (a) Bar chart illustrating the percentage of ChIP peaks from cells expressing dCas9-BFP-
- 998 DNMT3A and uPA gRNAs or background control regions (random sampling of the same number
- 999 of similar sized genomic windows as the ChIP peaks) falling into the different types of genomic
- 1000 regions indicated. P-values between background and ChIP peaks indicated above bars, Fisher's
- 1001 exact test.
- 1002 (b) Bar chart of % ChIP-peaks falling into DHS core regions.
- 1003 (c) Representative plot of ChIP-seq reads in the *uPA* promoter, uPA gRNA T2 sequences, and
- 1004 the top motif identified by MEME-ChIP.
- 1005 (d) Density of 5nt-SEED-NGG for uPA gRNAs (T1 to T5) ChIP peaks. Background is a random
- 1006 sample of the same number of similar sized genomic windows as ChIP peaks. Values represent
- 1007 median density with one standard deviation. P values are given for the indicated comparisons (t-
- 1008 test).
- 1009 (e) Bar plot of % ChIP peaks overlapping with hypermethylated DMRs caused by dCas9
- 1010 methyltransferase and *uPA* gRNAs. Background is a random sample of the same number of
- 1011 similar sized genomic windows as DMRs.
- 1012
- 1013

1
2
3
4
5
6
7
8
9
10
11
12
13
14
15
16
17
18
19
20
21
22
23
24
25
26
27
28
29
30
31
32
33
34
35
36
37
38
39
40
41
42
43
44
45
46
47
48
49
50
51
52
53
54
55
56
57
58
59
60
61
62
63
64
65



1014
1015

Fig. 8 Effect of dCas9 methyltransferases on gene expression

1
2
3
4
5
6
7
8
9
10
11
12
13
14
15
16
17
18
19
20
21
22
23
24
25
26
27
28
29
30
31
32
33
34
35
36
37
38
39
40
41
42
43
44
45
46
47
48
49
50
51
52
53
54
55
56
57
58
59
60
61
62
63
64
65

1016 **(a)** Relative gene expression levels of *uPA* and *TGFBR3* in cells expressing different levels of
1017 dCas9-BFP-DNMT3A, dCas9-BFP-DNMT3B, dCas9-BFP-DNMT3A(E752A), or dCas9-BFP-
1018 DNMT3B(E697A). mRNA expression was measured by qPCR and quantified as fold change
1019 compared to control cells transfected with pUC19. Bar charts depict mean change in mRNA level
1020 compared to pUC19 controls. Data represent mean \pm SD (n = 3 independent transfections). Mean
1021 percentage decrease in mRNA level compared to pUC19 is presented on top of bars. Asterisks
1022 (*) represent P value < 0.05 compared to pUC19.

1023 **(b-e)** Dot plots of log₁₀ (transcripts per million (TPM)) for all genes expressed in the BFP positive
1024 (BFPp) cells expressing *uPA* gRNAs (T1-T5) and dCas9-BFP-DNMT3A **(b)**, dCas9-BFP-
1025 DNMT3B **(c)**, dCas9-BFP-DNMT1 **(d)**, or dCas9-BFP-EGFP **(e)** plotted against log₁₀ (TPM) in a
1026 pUC19 control group. Differentially expressed genes (DEG) are marked in red (up-regulated) and
1027 green (down-regulated) (fold change \geq 2, FDR < 0.001). Fold changes compared to pUC19 and
1028 FDR p-values for DNMT1, *DNMT3A*, *DNMT3B*, *EGFP*, and *uPA* are shown.

1029 **(f)** Venn diagram representation of cross-comparison of DEGs.

1030 **(g)** Integrative analysis of gene expression change, promoter methylation and promoter binding
1031 caused by dCas9-BFP-DNMT3A and *uPA* gRNAs for the different clusters of DEGs. Heatmap
1032 represents linear regression p values. Dot plots were given for significant correlations (p < 0.05).

1033
1034
1035
1036
1037
1038

1
2
3
4
5
6
7
8
9
10
11
12
13
14
15
16
17
18
19
20
21
22
23
24
25
26
27
28
29
30
31
32
33
34
35
36
37
38
39
40
41
42
43
44
45
46
47
48
49
50
51
52
53
54
55
56
57
58
59
60
61
62
63
64
65

1039 **Supplementary Figure Legends**

1040

1041 **Supplementary Fig. S1 Validation of dCas9 methyltransferase expression and *uPA***
1042 **promoter methylation**

1043 (a) Schematic overview of the human DNA methyltransferases (DNMT1, DNMT3A and DNMT3B)
1044 with the N-terminal regulatory region, a C-terminal catalytic domain (CD), and the cytosine C5-
1045 DNA methyltransferase motifs highlighted. The first amino acid (a.a) residue of the C-terminal
1046 catalytic domain, which was fused to the dCas9, is indicated by an arrow.

1047 (b) Representative FACS sorting and Re-analysis of HEK293T cells 48 hours after transfection.
1048 Gating for BFP positive (BFPp) and negative (BFPn) cells are indicated.

1049 (c) Laser scanning microscopy of **dCas9 methyltransferase** expression in HEK293T cells, 48
1050 hours after transfection. The BFP signal from the dCas9-BFP-DNMT1 transfected cells was
1051 enhanced since the BFP signal from the dCas9-BFP-DNMT1 fusion was initially weaker
1052 compared to that from the other three fusion proteins. Scale bar: 20 μ m.

1053 (d) Validation of RNA-guided *uPA* methylation (*uPA*-MR1) by dCas9-BFP-DNMT3A using bisulfite
1054 Sanger sequencing.

1055

1056 **Supplementary Fig. S2 Validation of dCas9 methyltransferase-mediated *TGFBR3***
1057 **methylation in HEK293T cells by bisulfite Sanger sequencing**

1058 *TGFBR3* methylation by dCas9 methyltransferase and gRNAs was validated by bisulfite Sanger
1059 sequencing. CpG methylation status is indicated according to the absolute nucleotide position
1060 and color-coded as red, methylated; blue, unmethylated; or white, unknown methylation state
1061 based on the sequencing signal.

1062

1063 **Supplementary Fig. S3 Validation of *de novo* methylation of *uPA* by dCas9**
1064 **methyltransferase and *uPA* gRNAs**

1065 Line plots of *uPA*-MR2 methylation in cells transfected with pUC19 (control), dCas9-BFP-
1066 DNMT3A or dCas9-BFP-DNMT3B only, and dCas9-BFP-DNMT3A or dCas9-BFP-DNMT3B
1067 together with either *uPA* gRNAs or scrambled gRNAs.

1068

1069 **Supplementary Fig. S4 Effect of dCas9 methyltransferases on two potential off-target sites**
1070 **(*SH2D3C* and *FAM221A*).**

1071 (a-b) Schematic illustration of the *SH2D3C* (b) and *FAM221A* (c) off-target loci, with off-target
1072 sites indicated by red arrows. Sequences of *uPA* gRNA (T2), *SH2D3C*, and *FAM221A* off-target
1073 sites are given above, with the PAM (red letters) and mismatches (green letters) indicated. CpGs
1074 analyzed are indicated by black arrows; numbers indicate distances (in bp) from the transcription
1075 start site (TSS) of the gene (*SH2D3C*, NM_001252334.1) or (*FAM221A*, XM_011515369.1). Y-

1
2
3
4 1076 axis represents % mCpG level for each CpG site and X-axis represents distance (in bp) from
5 1077 TSS. The CpG methylation level from the control samples (pUC19 transfection) was re-plotted as
6 1078 a reference. Each data point in the graph represents the mean percentage of CpGs methylated \pm
7 1079 SD (n = 2, independent transfections).
8
9 1080
10 1081
11
12 1082 **Supplementary Fig. S5 Effects of DNMT3B catalytic activity and expression level on *de***
13 1083 ***novo* TGFBR3 methylation**
14
15 1084 Bar charts of % mCpG level for individual CpG sites of the *TGFBR3* targeted regions in dCas9
16 1085 methyltransferase-expressing cells. Cells were enriched by FACS 48 hours after transfection and
17 1086 sorted according to the BPF signal: +, ++, +++, +++++. The schematic illustrations above the bar
18 1087 charts show gRNA binding sites and CpG sites analyzed. Asterisk (*) indicates statistical
19 1088 significance (p < 0.05, ANOVA) compared to the pUC19 control group after Bonferroni correction.
20 1089 Percentage values represent % decrease of *TGFBR3* expression compared to pUC19.
21 1090
22 1091 **Supplementary Fig. S6 WGBS analysis of cells expressing dCas9 methyltransferase and**
23 1092 **gRNAs**
24
25 1093 (a) Summary of WGBS including clean data, clean reads, clean rate, mapped reads, uniquely
26 1094 mapped reads and rate, and bisulfite conversion rate, for each experimental group and control
27 1095 (pUC19).
28 1096 (b) Average percentage of methylated cytosine (% mC) for whole-genome CpG sites, CHG sites,
29 1097 and CHH sites. "H" represents A, C, and T.
30 1098 (c-d) Average mCpG level (percentage) stratified according to individual chromosome or whole
31 1099 genome for all samples measured by WGBS.
32 1100
33 1101 **Supplementary Fig. S7 Differentially methylated regions (DMRs) identified by DSS-single**
34 1102 **method.** DMRs were categorized as hypermethylated or hypomethylated compared to control
35 1103 sample (pUC19 transfection).
36 1104
37 1105 **Supplementary Fig. S8 Histogram charts of the distribution of DMR length (bp), and**
38 1106 **number of CpGs per DMR.** DMRs included in this figure are those remaining after the stringent
39 1107 filtering step (see methods). Mean DMRs length (in bp) and mean number of CpG per DMR were
40 1108 given for each chart.
41 1109
42 1110 **Supplementary Fig. S9 Genomic characteristics of off-target DMRs caused by dCas9**
43 1111 **methyltransferases and *TGFBR3* gRNAs**

1
2
3
4 1112 (a) Box plot (top) and heatmap clustering (bottom) of the hypermethylated (left) and
5 1113 hypomethylated (right) DMRs caused by dCas9 methyltransferases and *TGFBR3* gRNAs.
6
7 1114 (b-c) Bar chart illustrating the percentage of the identified *TGFBR3* hypermethylated (c) or
8 1115 hypomethylated (d) DMRs that fall into the different types of genomic regions indicated.
9
10 1116 Background represents of a random sample of the same number of similar sized genomic
11 1117 windows that fall into the categories indicated. Values above bars are P values between
12 1118 background and *TGFBR3* DMRs, Fisher's exact test.
13
14 1119 (d) Metaplot of average CpG methylation levels in 58,494 DNase I hypersensitive sites (DHS)
15 1120 and 1 kb upstream and downstream flanking regions.
16
17 1121 (e-f) Bar chart of % *TGFBR3* hypermethylated (f) or hypomethylated (g) DMRs falling into DHS
18 1122 core regions.
19
20 1123 (h) Density of 5nt-SEED-NGG for *TGFBR3* gRNAs (T1 to T3) in background genomic windows
21 1124 and *TGFBR3* DMRs + flanking 100 bp. Values represent median density with one standard
22 1125 deviation. P values (t-test) are given above the bar charts.
23
24 1126
25
26
27 1127 **Supplementary Fig. S10 Average methylation levels of seven genomic regions in all**
28 1128 **annotated genes (hg19).** (a-d) Each line indicates the genome-wide average methylation levels
29 1129 across seven genomic regions: upstream 2kb of the transcription start site, first exon, first intron,
30 1130 internal exons, internal introns, last exon, and downstream 2kb of the last exon.
31
32 1131
33
34 1132
35
36 1133 **Supplementary Fig. S11 The average methylation level in ChIP-peaks and flanking regions.**
37 1134 Bar chat presents the average methylation level of all dCas9-BFP-DNMT3A and uPA gRNA off-
38 1135 target binding sites (n = 7754) found by ChIPseq, as well as the 2kb upstream and downstream
39 1136 region.
40
41 1137 **Supplementary Fig. S12 Effect of dCas9 methyltransferases and uPA gRNAs on cell**
42 1138 **growth.** Cell growth was determined by counting the number of cell clones derived from 1,000
43 1139 BFP positive cells after transfection. Values represent mean and one standard deviation from 6
44 1140 experimental repeats. Asterisks represent a p value < 0.05 (ANOVA) compared to pUC19
45 1141 transfection control.
46
47 1142
48 1143
49
50 1144 **Supplementary Fig. S13 Effects of dCas9 methyltransferases on mCherry expression in**
51 1145 **fluorescence reporter cell lines**
52
53 1146 (a) Schematic illustration of the mCherry fluorescence transgene expression cassette. The target
54 1147 sites of the gRNAs within the CMV promoter are indicated by red arrows (5'-3', targeting sense or
55 1148 antisense strands).

1
2
3
4
5
6
7
8
9
10
11
12
13
14
15
16
17
18
19
20
21
22
23
24
25
26
27
28
29
30
31
32
33
34
35
36
37
38
39
40
41
42
43
44
45
46
47
48
49
50
51
52
53
54
55
56
57
58
59
60
61
62
63
64
65

1149 (b) Southern blot analysis of five cell clones with the transgene cassette randomly and stably
1150 integrated into the genome.

1151 (c) Flow cytometry-based analysis of the percentage of BFP positive cells in the fluorescence
1152 reporter cells at 2, 5, 8 and 14 days after transient transfection with CMV gRNAs (T1-T3) and
1153 dCas9-BFP-DNMT1, dCas9-BFP-DNMT3A, dCas9-BFP-DNMT3B, or dCas9-BFP-EGFP.

1154 (d-h) % mCherry fluorescence median intensity in these five clones at day 2, 5, 8, and 14 days
1155 following transient transfection with CMV gRNAs (T1-T3) and dCas9-BFP-DNMT1, dCas9-BFP-
1156 DNMT3A, dCas9-BFP-DNMT3B, or dCas9-BFP-EGFP. Control cells were transfected with
1157 pUC19. Percent inhibition of mCherry expression was calculated by normalizing the median
1158 mCherry fluorescence intensity to that from the pUC19 transfected cells at each time point.
1159 Figures are plotted using the mean % mCherry median \pm SD (n = 3, independent transfections).
1160 ANOVA with Bonferroni comparison was performed for cell clone 2. "a", "b", "c", and "d," indicates
1161 a p-value < 0.05 compared to the pUC19 control for the corresponding transfection group.

1162
1163 **Supplementary Fig. S14 Validation of hypermethylated DMRs and DHS methylation caused**
1164 **by dCas9-BFP-DNMT3A and uPA gRNAs by WGBS**

1165 (a) Box plot of % methylation level of hypermethylated DMRs dCas9 found in previous WGBS
1166 experiment. The WGBS in the repeat experiment was conducted as described in the methods
1167 sections, but cells were not FACS enriched and sequenced in lower depth than previous
1168 experiment.

1169 (b) Metaplot of average CpG methylation levels in 58,494 DNase I hypersensitive sites (DHS)
1170 and 1 kb upstream and downstream flanking regions. P value represents Wilcoxon matched pairs
1171 signed rank test between treated and control groups.

1172
1173 **Supplementary Table S1** List of plasmids deposited to Addgene, qPCR primers, gRNA
1174 sequences, bisulfite PCR primers, bisulfite pyrosequencing primers, and DNA regions analyzed
1175 for methylation.

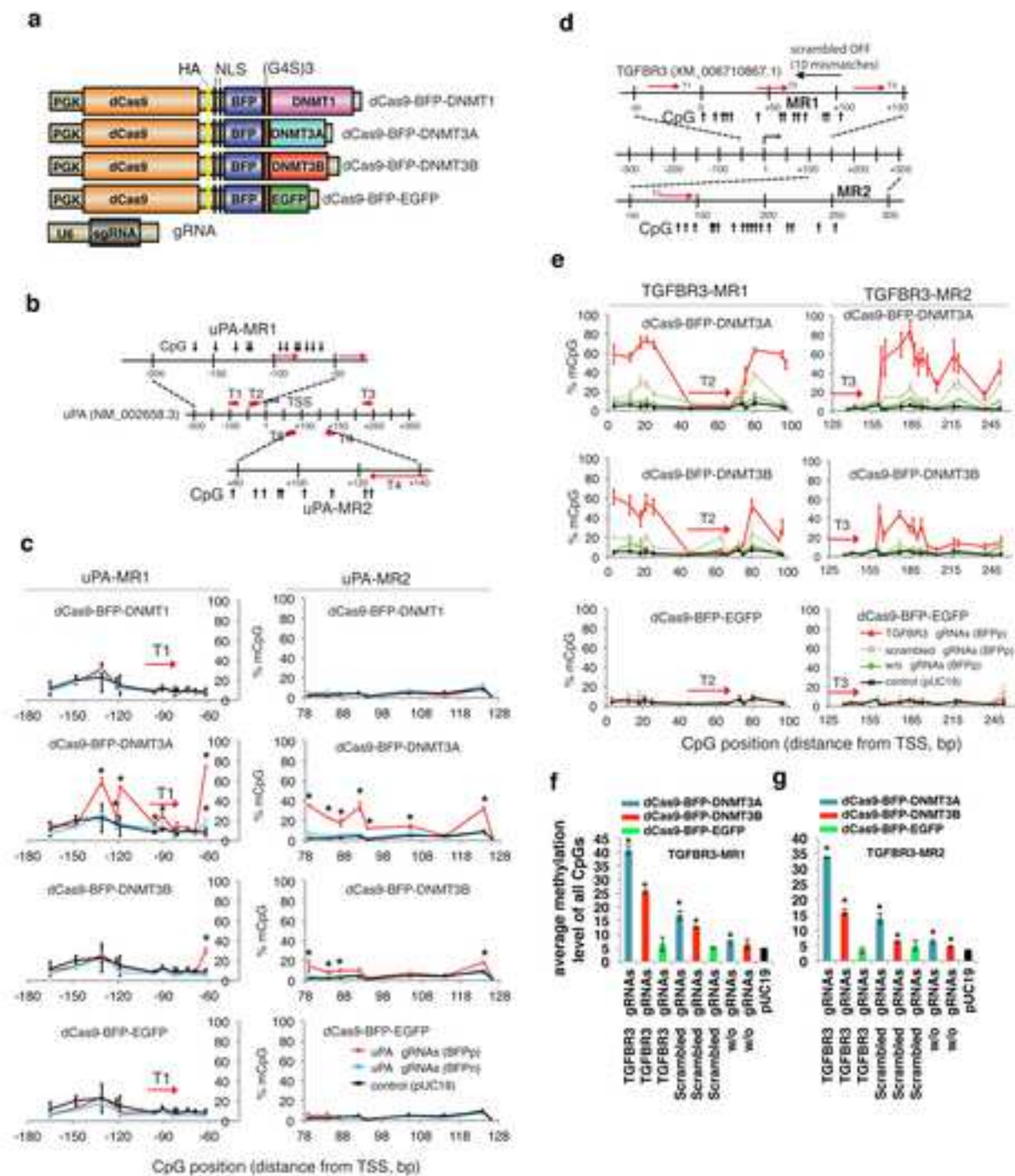
1176 **Supplementary Table S2** List of hypermethylated DMRs caused by dCas9 methyltransferases
1177 and uPA gRNAs

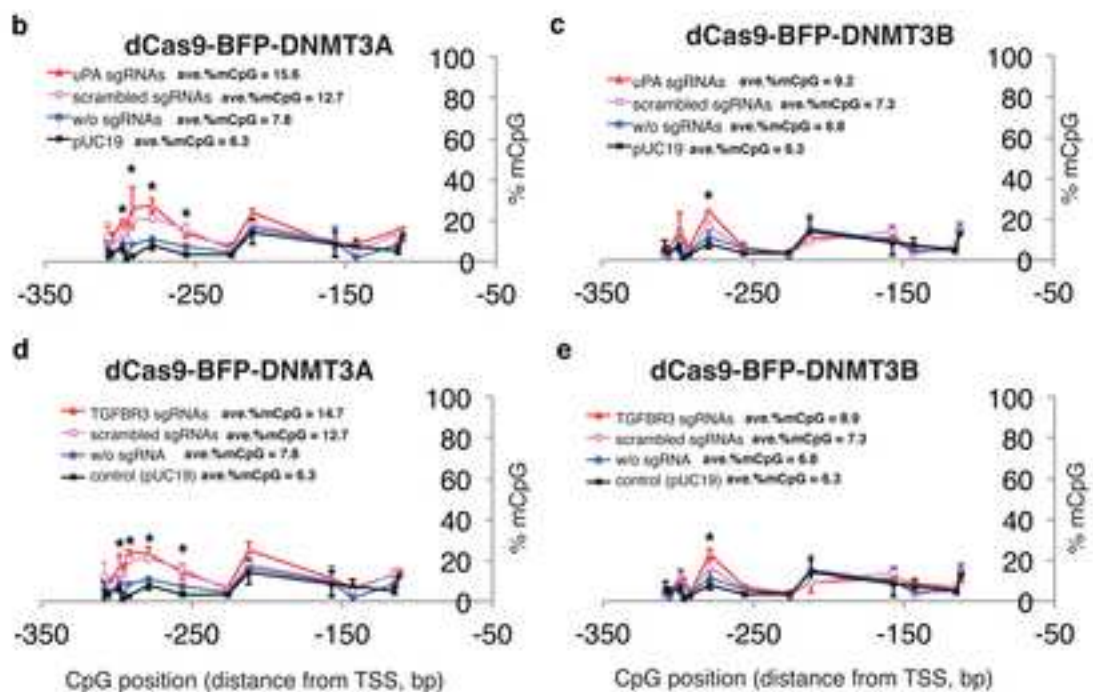
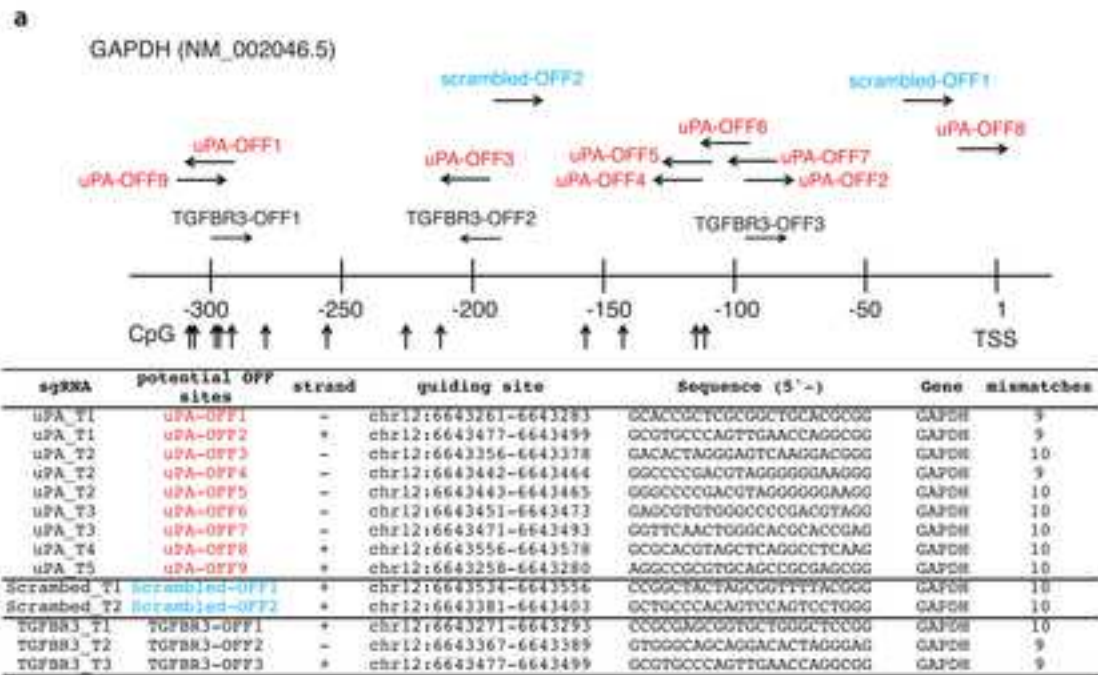
1178 **Supplementary Table S3** List of hypomethylated DMRs caused by dCas9 methyltransferases
1179 and uPA gRNAs

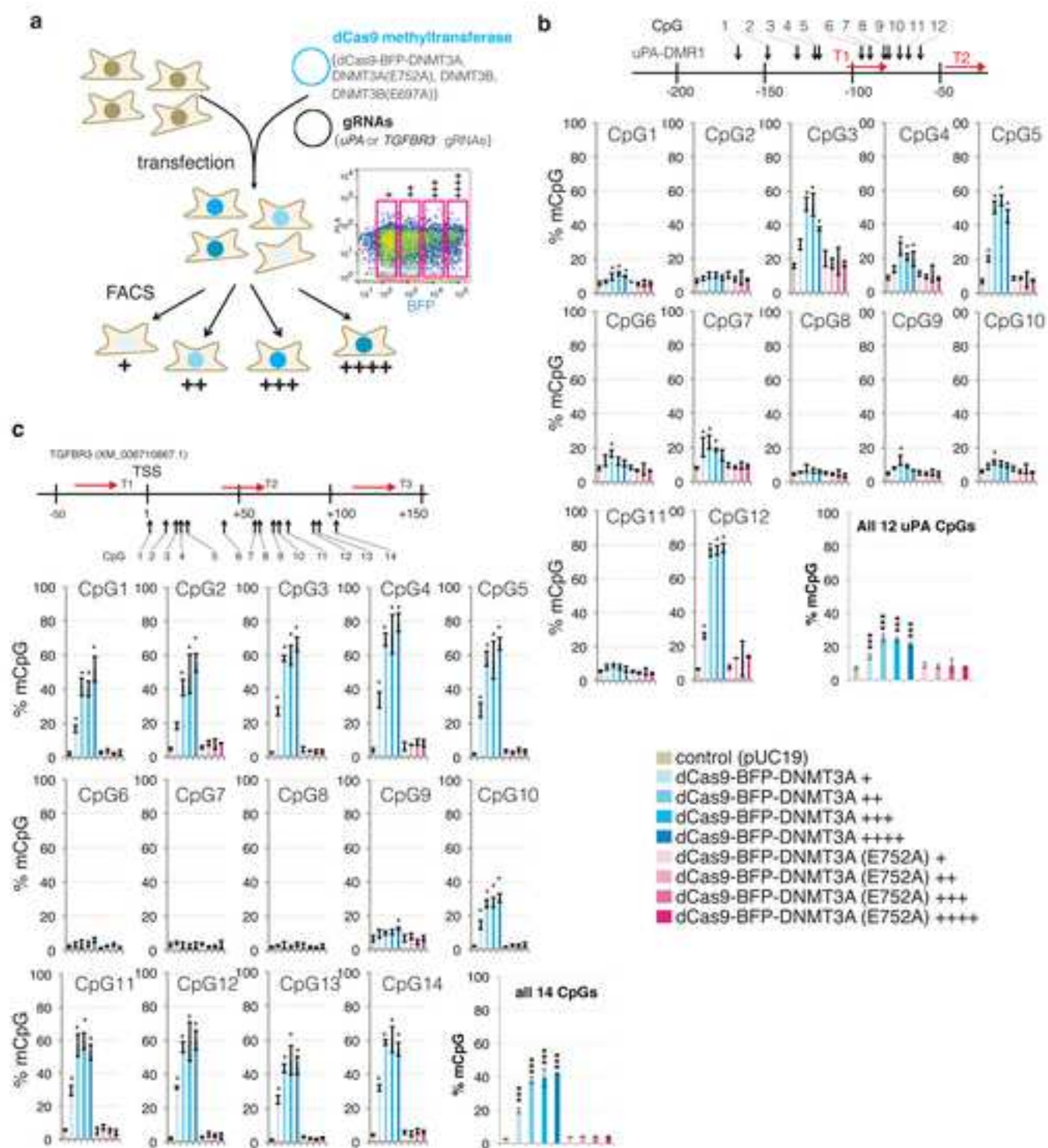
1180
1181 **Supplementary Table S4** List of hypermethylated DMRs caused by dCas9 methyltransferases
1182 and TGFBR3 gRNAs

1183
1184 **Supplementary Table S5** List of hypomethylated DMRs caused by dCas9 methyltransferases
1185 and TGFBR3 gRNAs

1	
2	
3	
4	1186
5	
6	1187 Supplementary Table S6 List of binding peaks caused by dCAs9-BFP-DNMT3A and uPA
7	1188 gRNAs
8	
9	1189
10	1190 Supplementary File 1 Extended discussion and results
11	
12	1191
13	
14	
15	
16	
17	
18	
19	
20	
21	
22	
23	
24	
25	
26	
27	
28	
29	
30	
31	
32	
33	
34	
35	
36	
37	
38	
39	
40	
41	
42	
43	
44	
45	
46	
47	
48	
49	
50	
51	
52	
53	
54	
55	
56	
57	
58	
59	
60	
61	
62	
63	
64	
65	







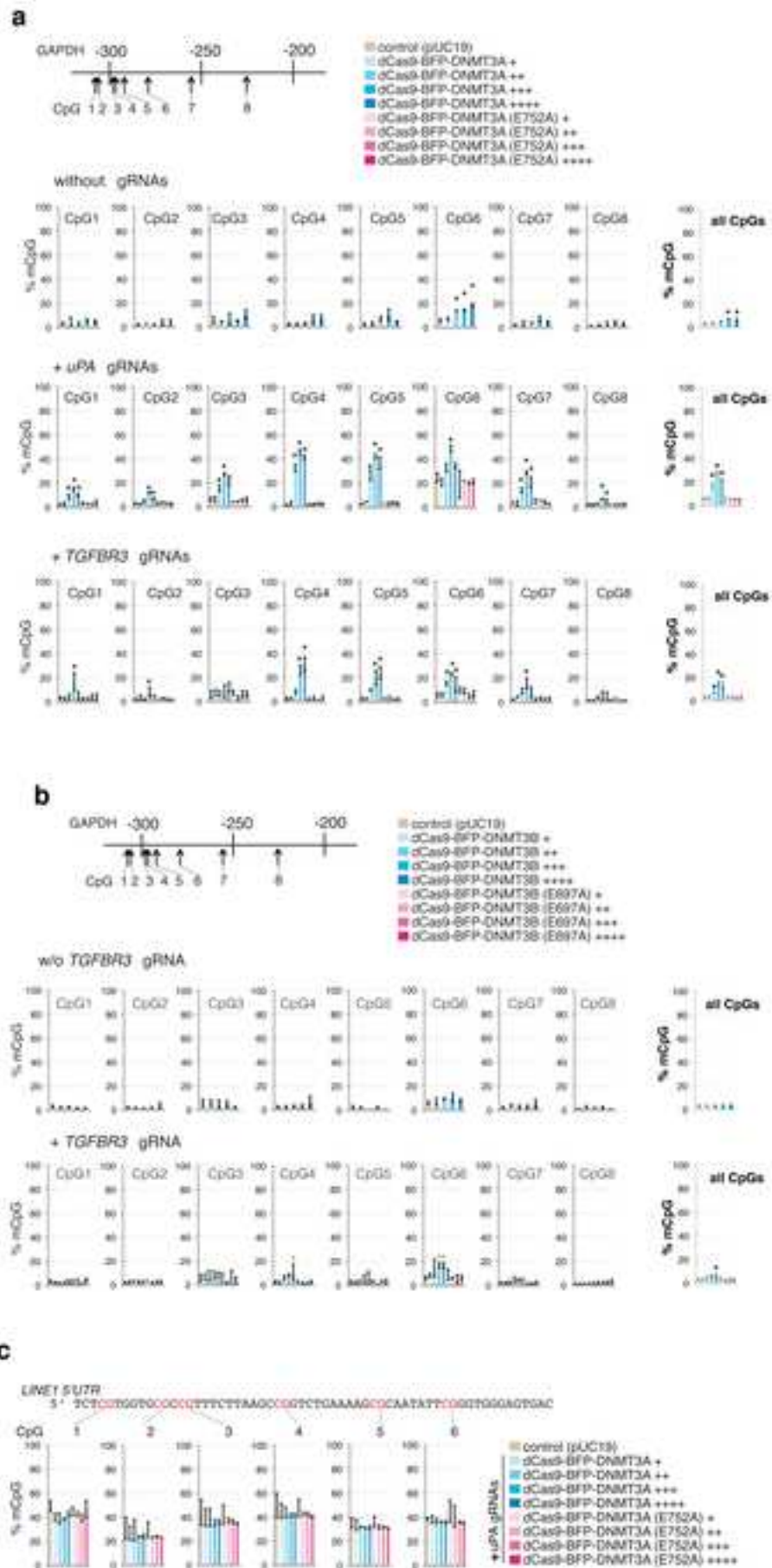
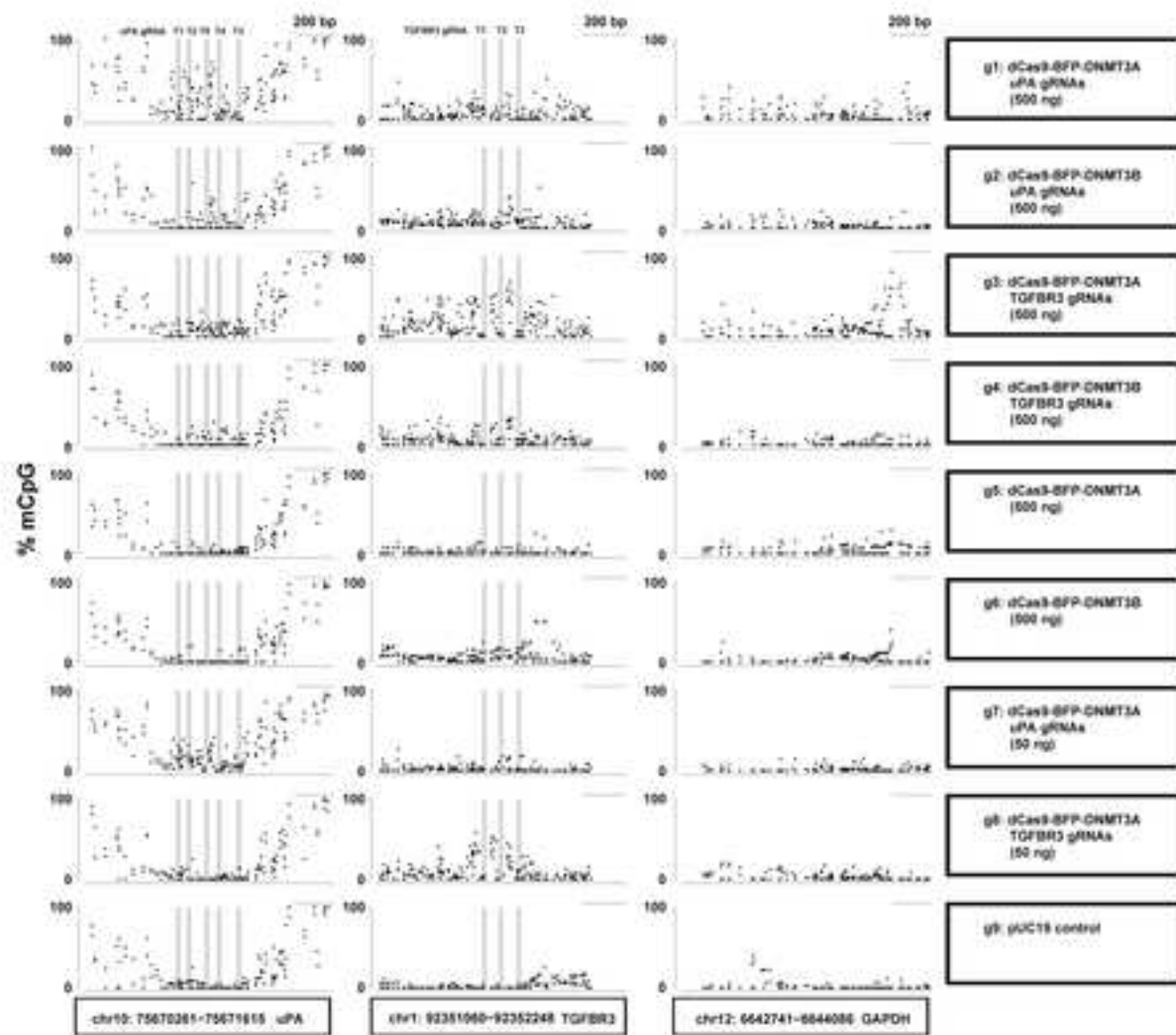
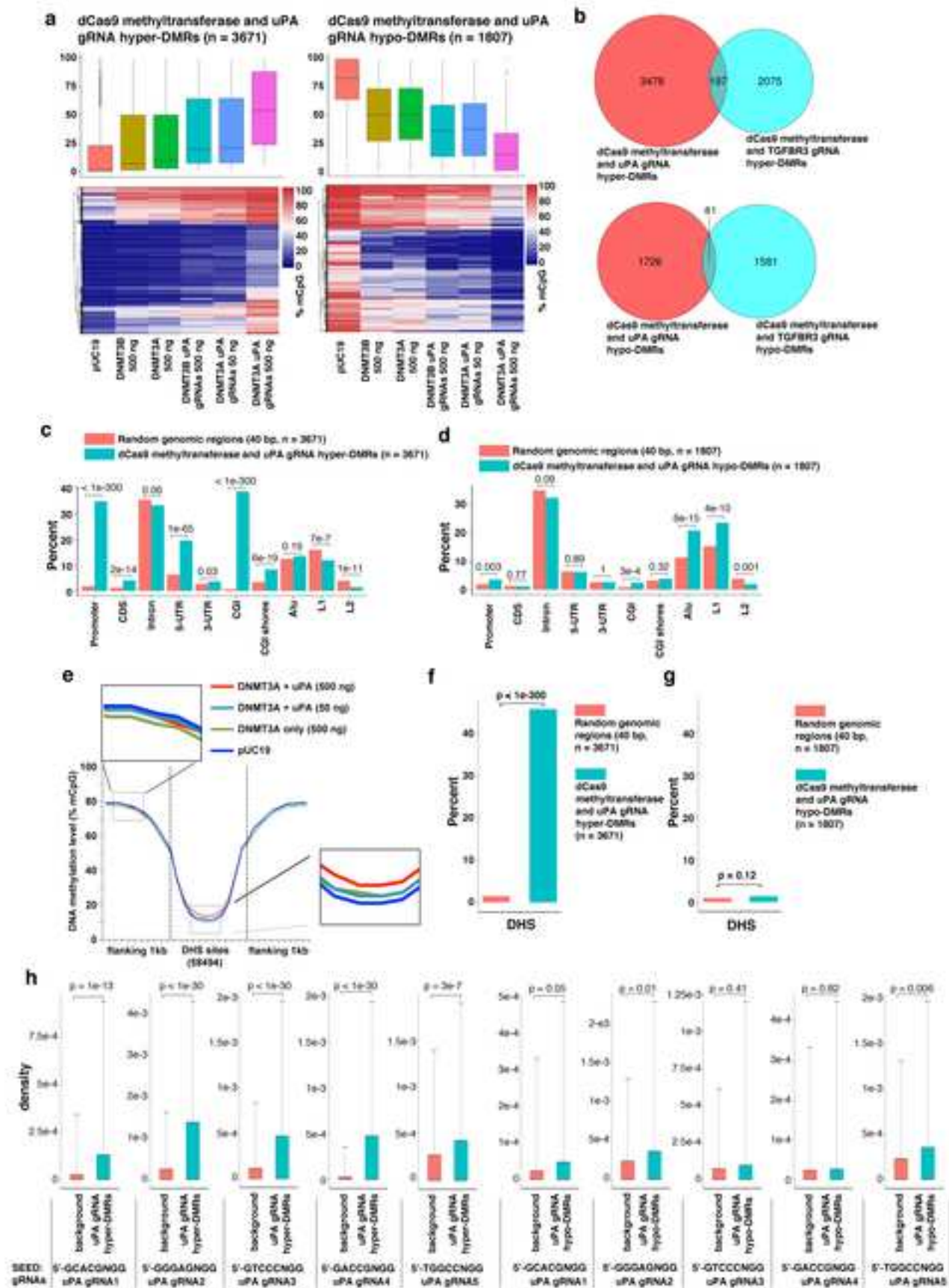
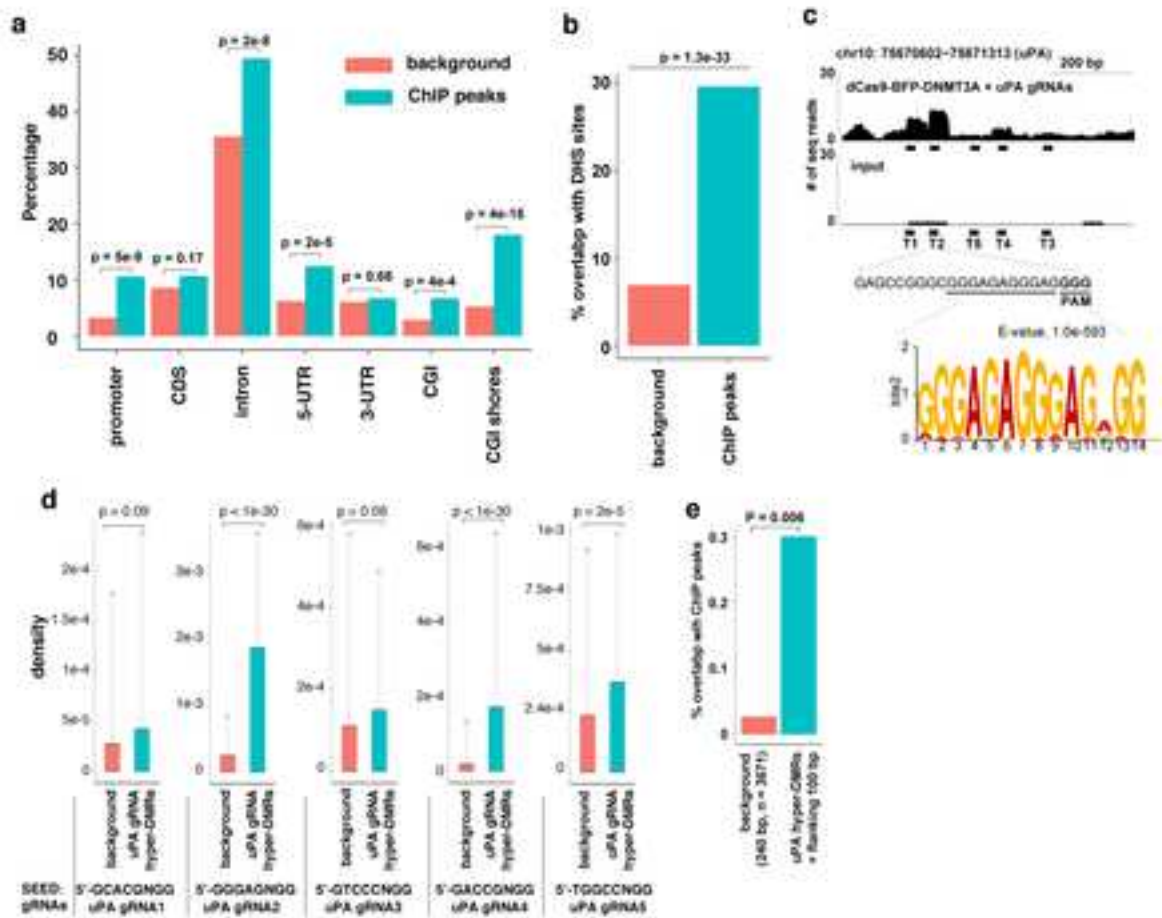
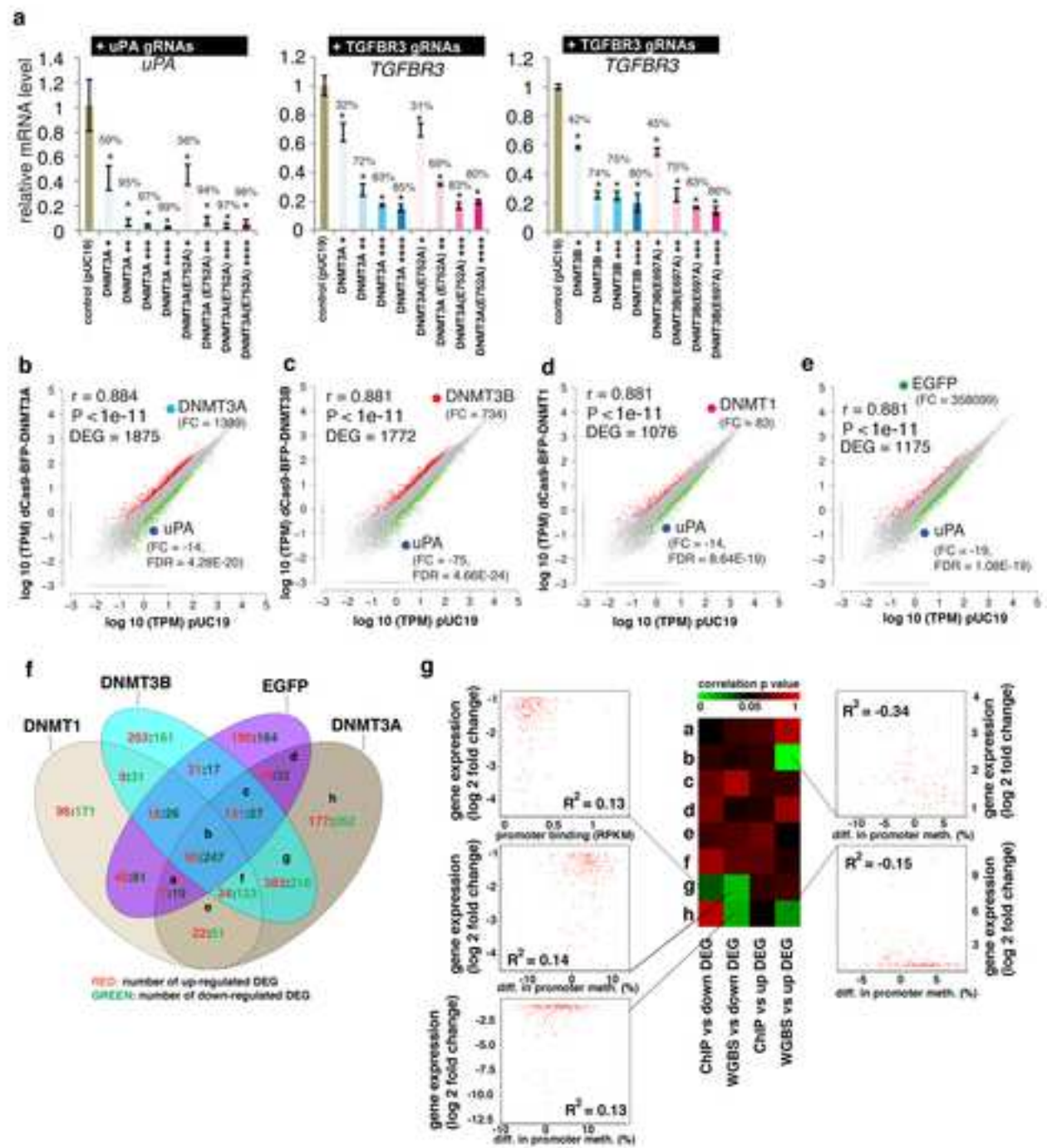


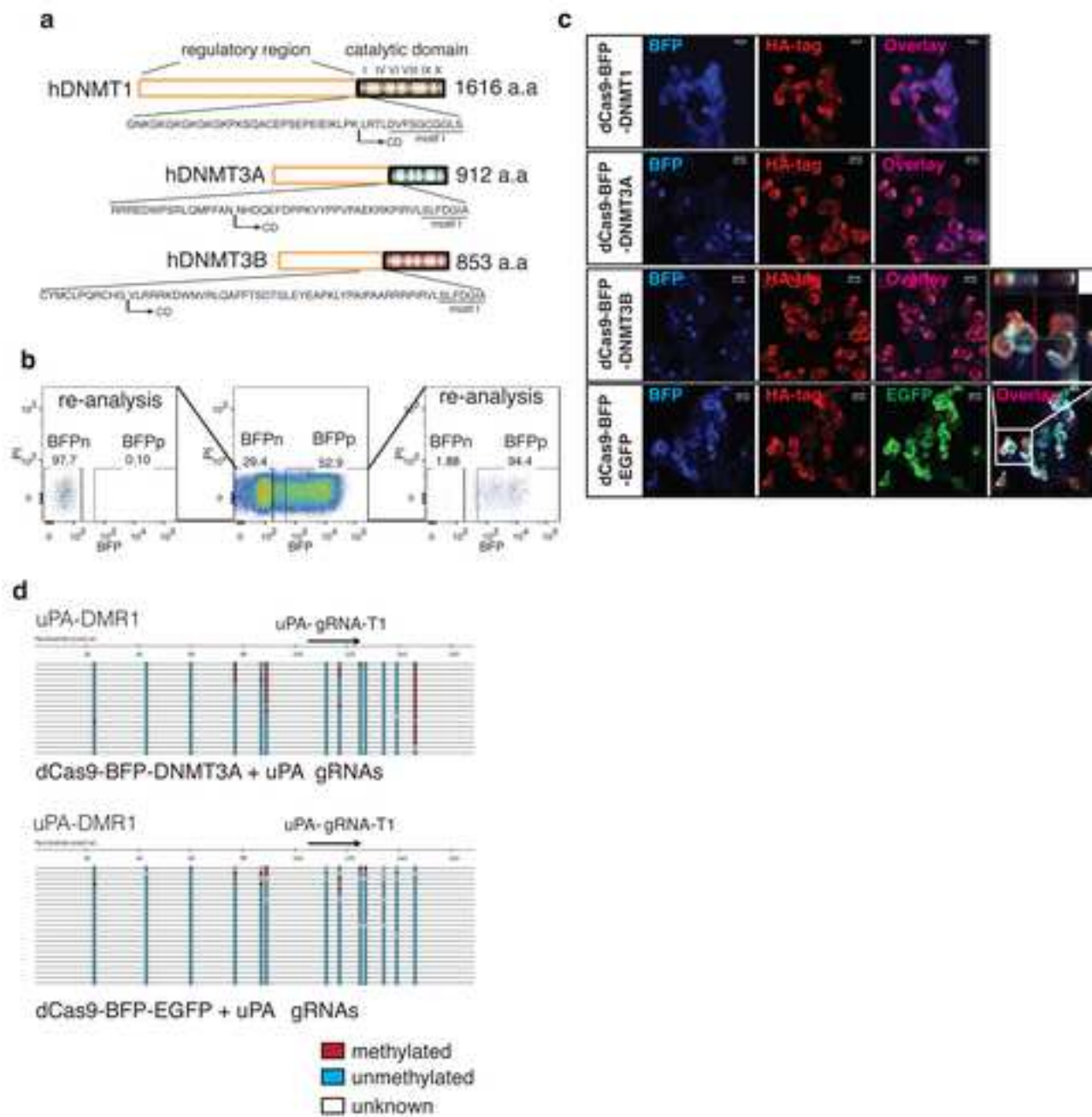
Fig. 5

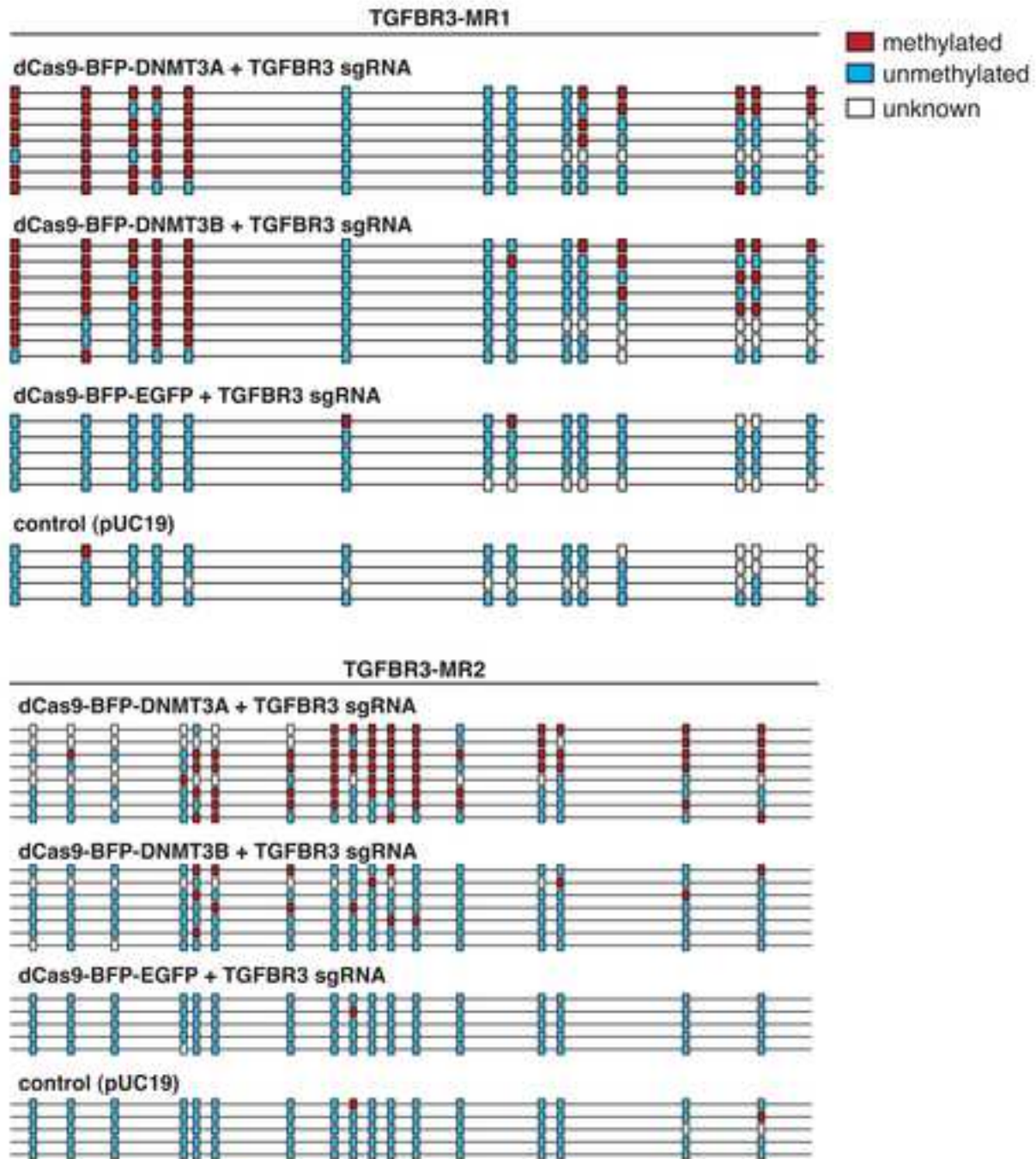


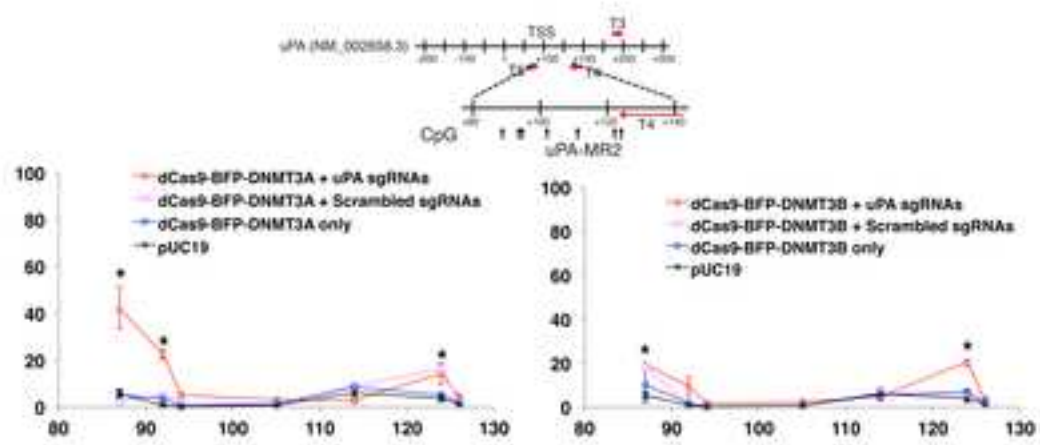


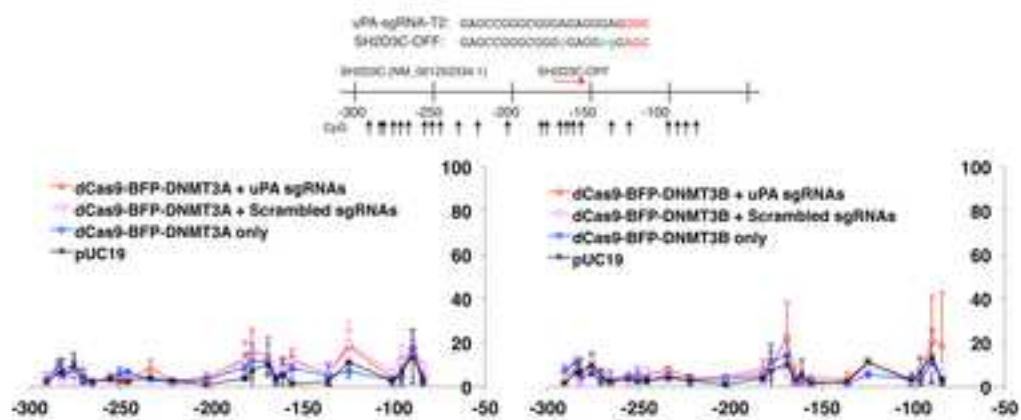
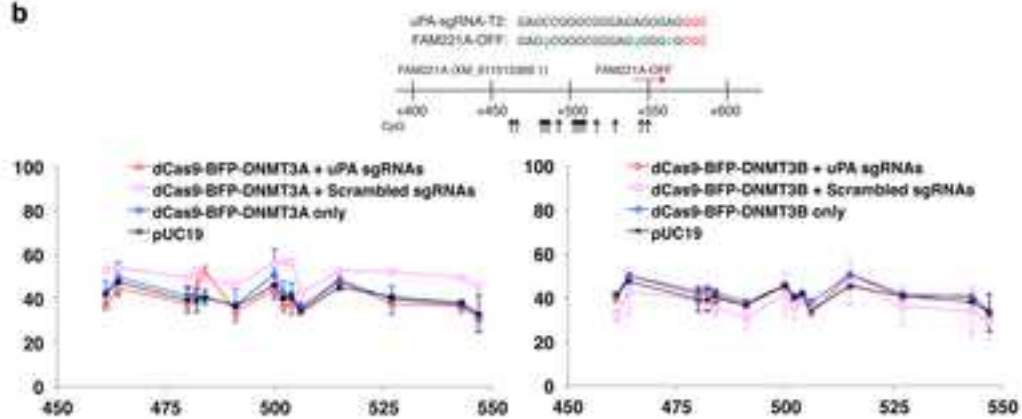


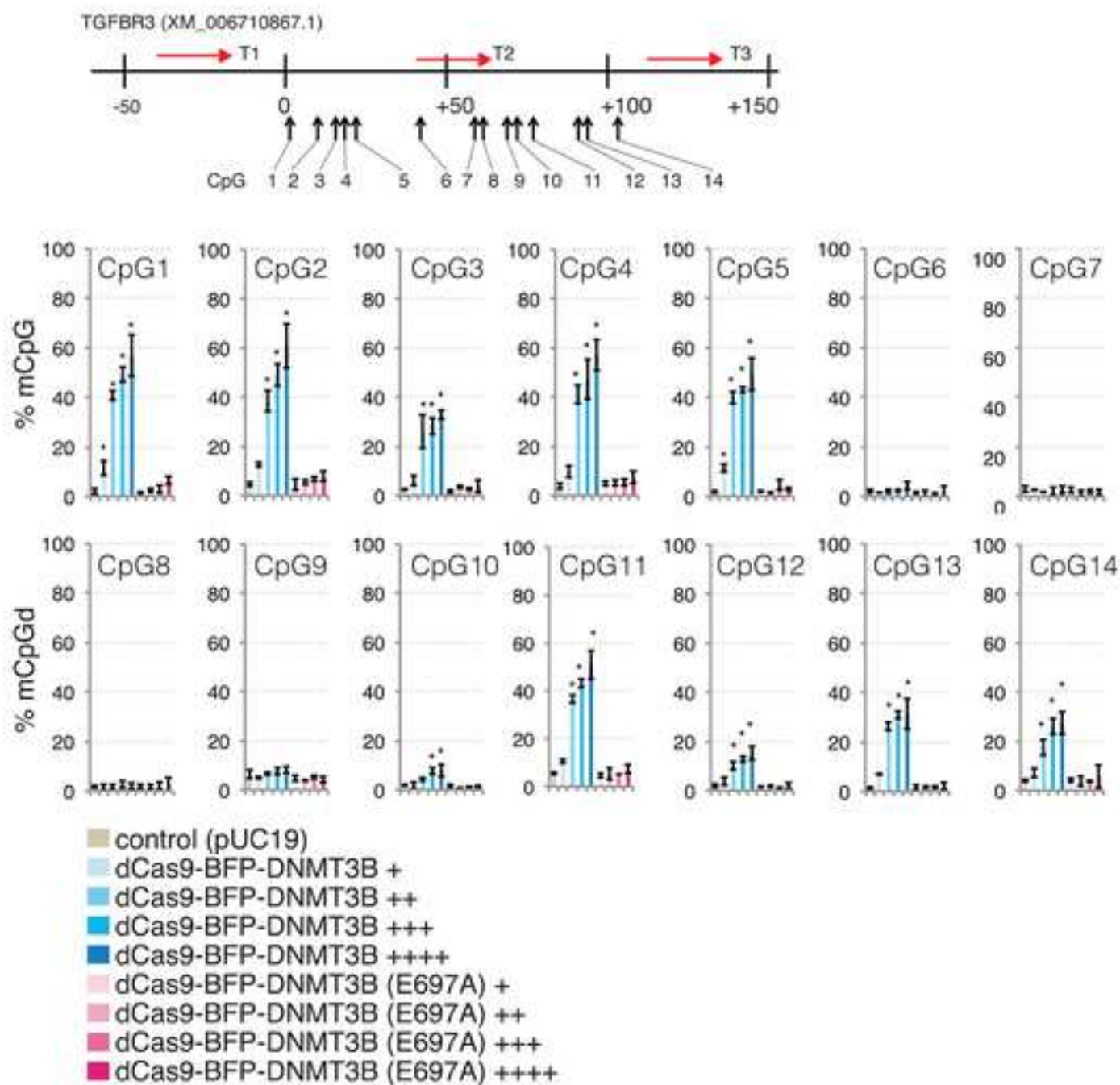








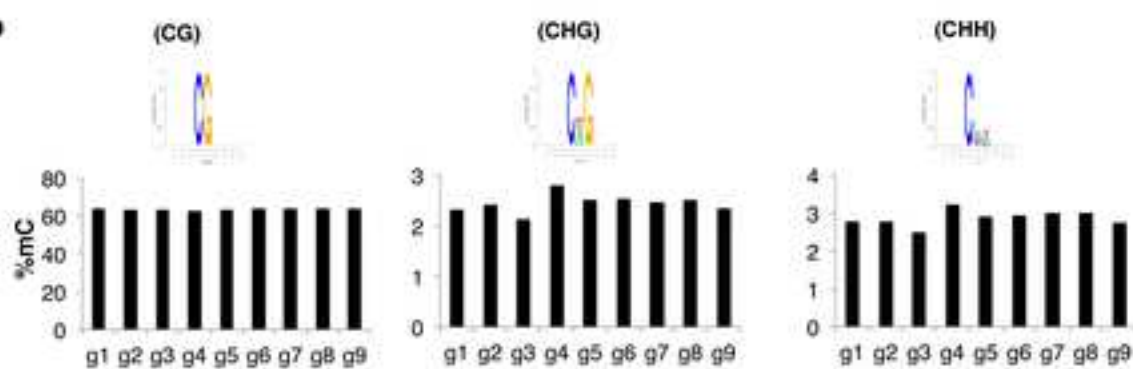
a**b**



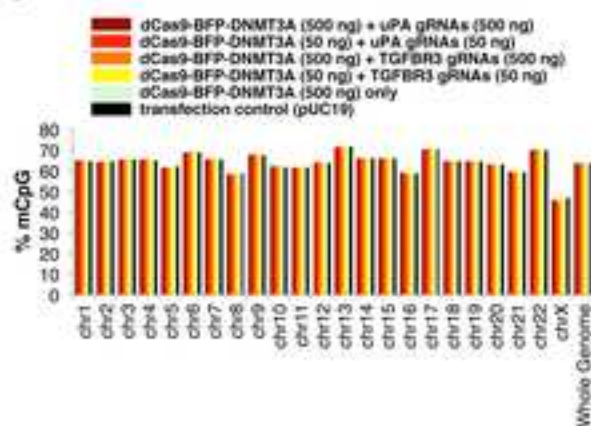
a

Sample ID	Description	Clean Data Size(bp)	Clean Reads Number	Clean Rate(%)	Mapped Reads	Mapping Rate (%)	Uniquely Mapped Reads	Uniquely Mapping Rate (%)	Bisulfite Conversion Rate (%)
g1	dCas9-BFP-DNMT3A (500 ng) + uPA gRNAs (500 ng)	100,601,409,600	670,676,064	95.06	558316453	83.25	558316453	83.25	99.63
g2	dCas9-BFP-DNMT3B (500 ng) + uPA gRNAs (500 ng)	103,778,694,600	691,857,964	95.64	575422550	83.17	575422550	83.17	99.52
g3	dCas9-BFP-DNMT3A (500 ng) + TGFBR3 gRNAs (500 ng)	117,505,796,100	783,371,974	94.06	651431832	83.16	651431832	83.16	99.65
g4	dCas9-BFP-DNMT3B (500 ng) + TGFBR3 gRNAs (500 ng)	109,001,895,600	726,679,304	90.85	604104613	83.13	604104613	83.13	99.63
g5	dCas9-BFP-DNMT3A (500 ng) only	105,265,839,000	701,772,260	90.36	562464794	83	562464794	83	99.62
g6	dCas9-BFP-DNMT3B (500 ng) only	118,394,522,400	789,296,816	95.6	660303371	83.66	660303371	83.66	99.6
g7	dCas9-BFP-DNMT3A (50 ng) + uPA gRNAs (50 ng)	117,366,362,100	762,442,414	67.18	645181340	82.46	645181340	82.46	99.6
g8	dCas9-BFP-DNMT3A (50 ng) + TGFBR3 gRNAs (50 ng)	101,372,416,500	675,616,110	65.25	561172295	83.04	561172295	83.04	99.49
g9	pUC19 control	80,429,413,600	536,196,092	90.08	444407297	82.88	444407297	82.88	99.46

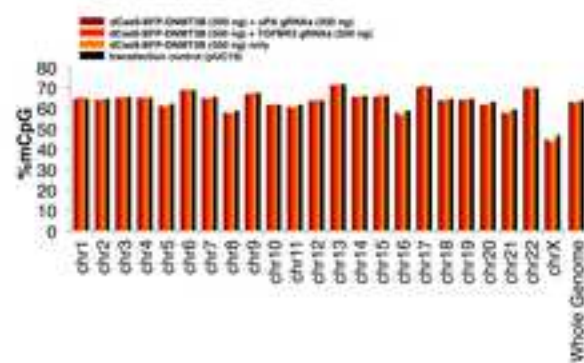
b

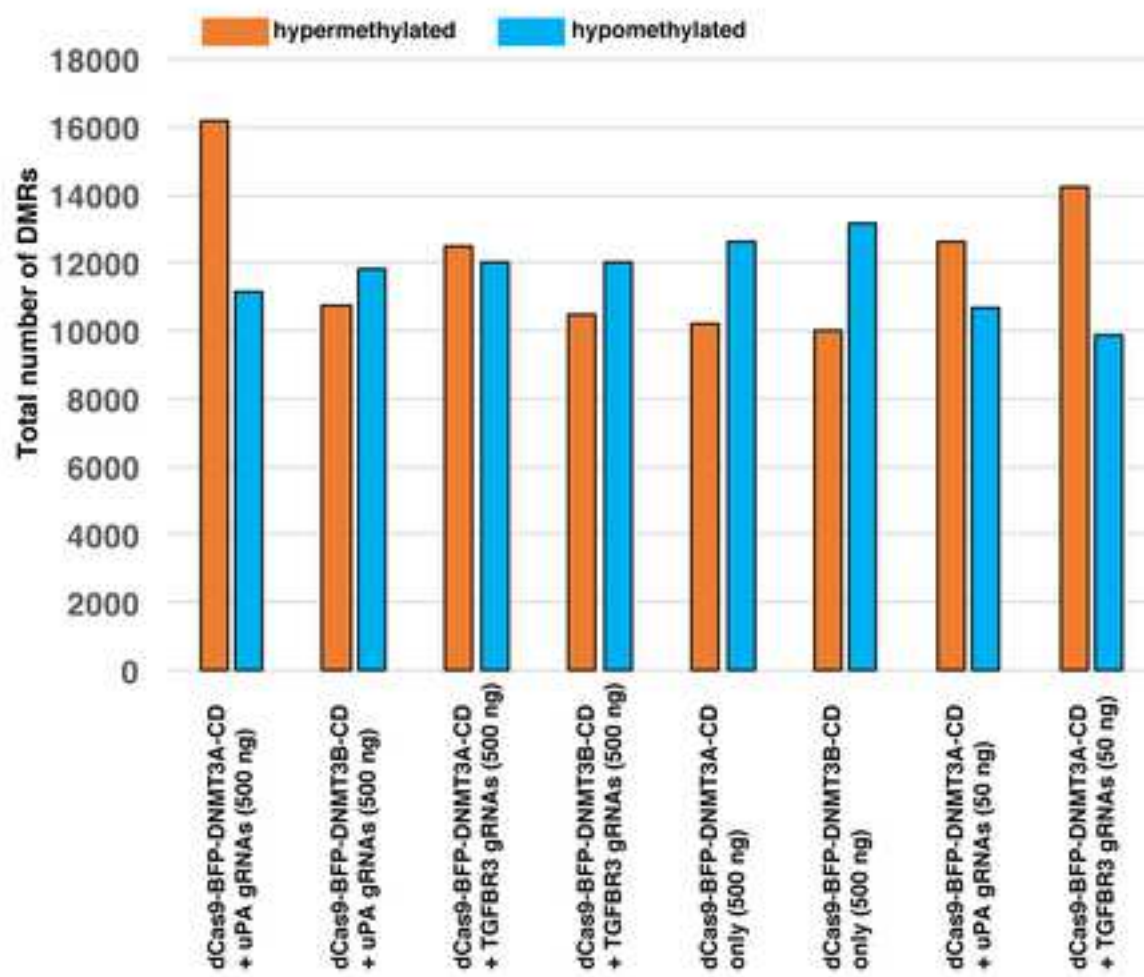


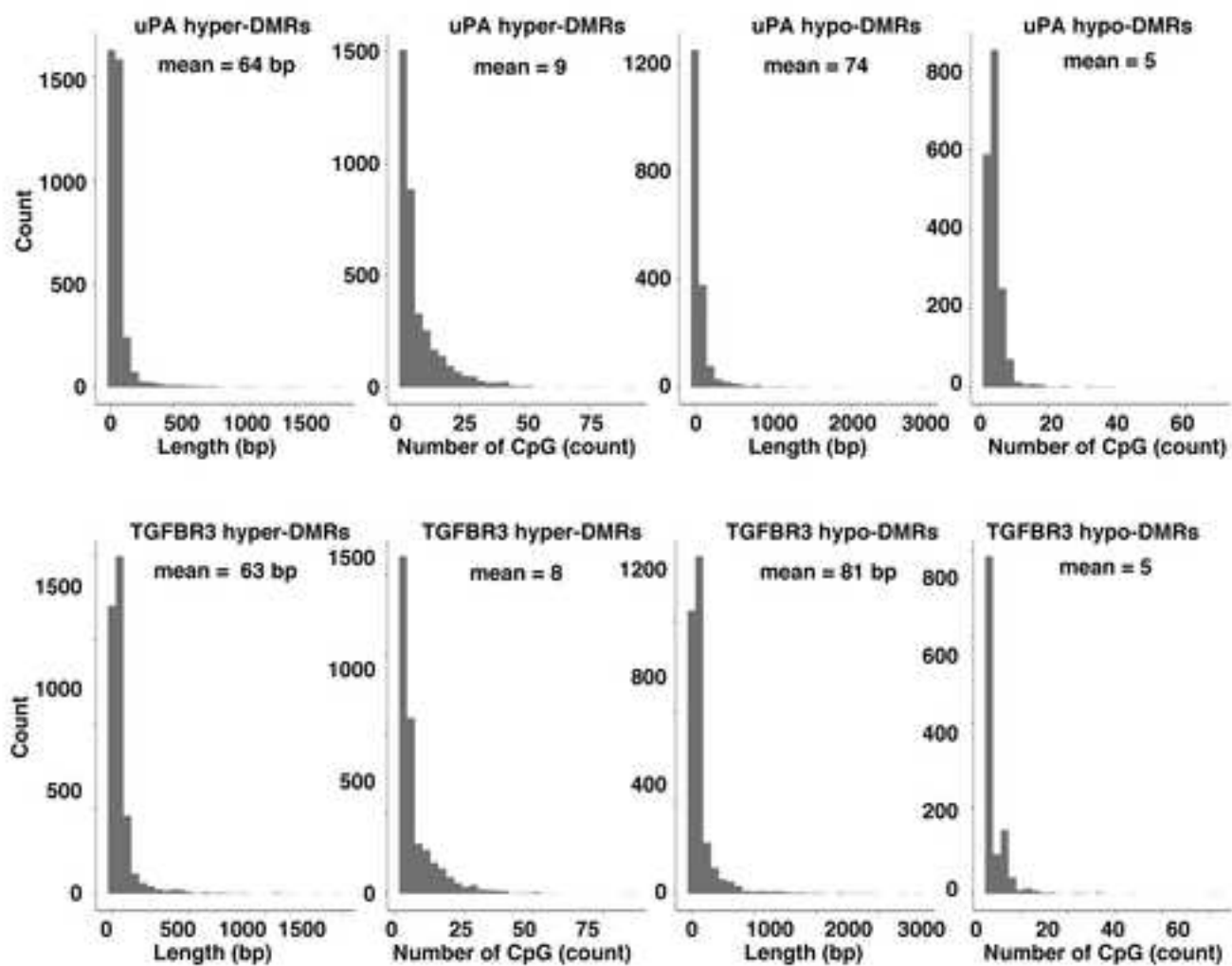
c

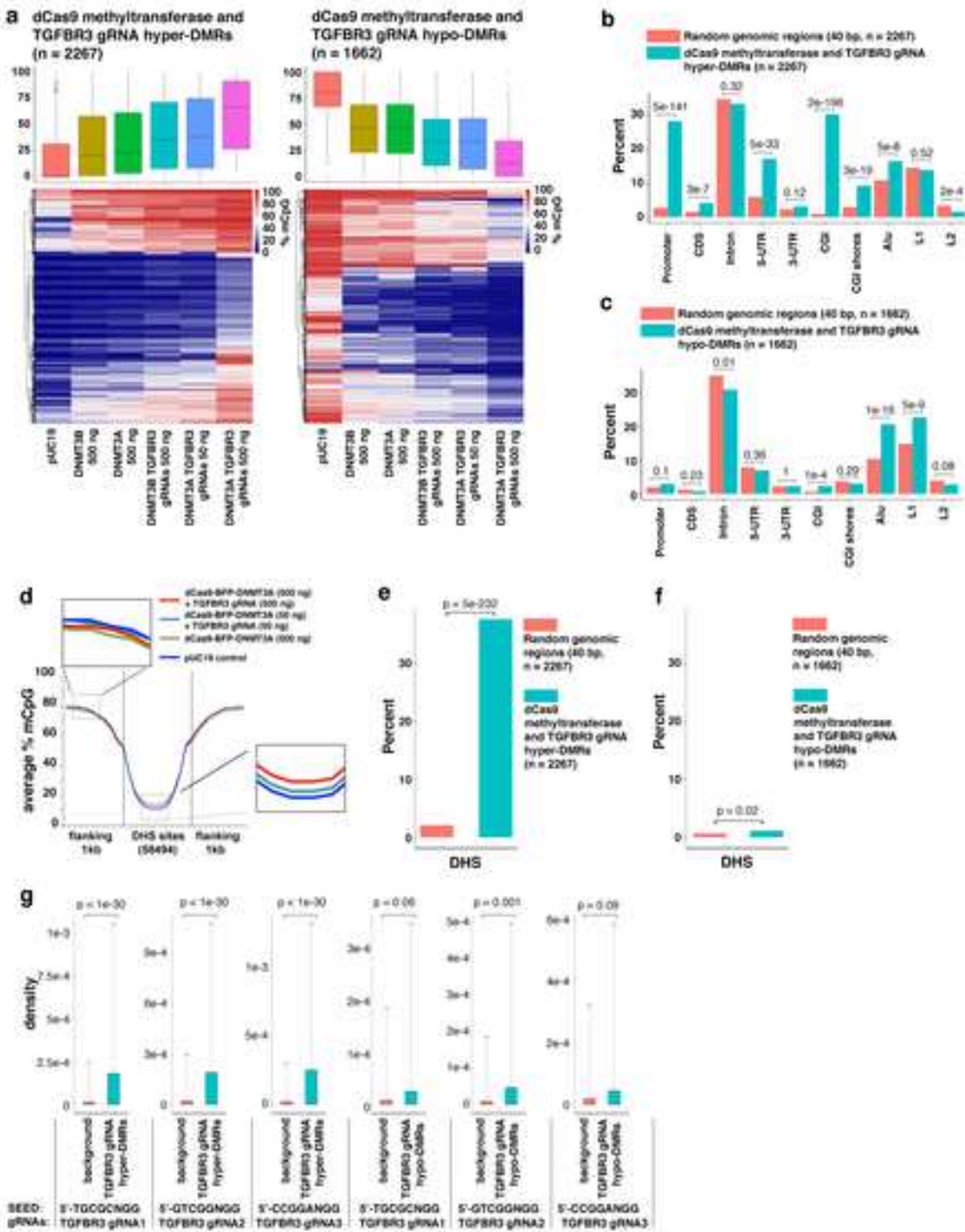


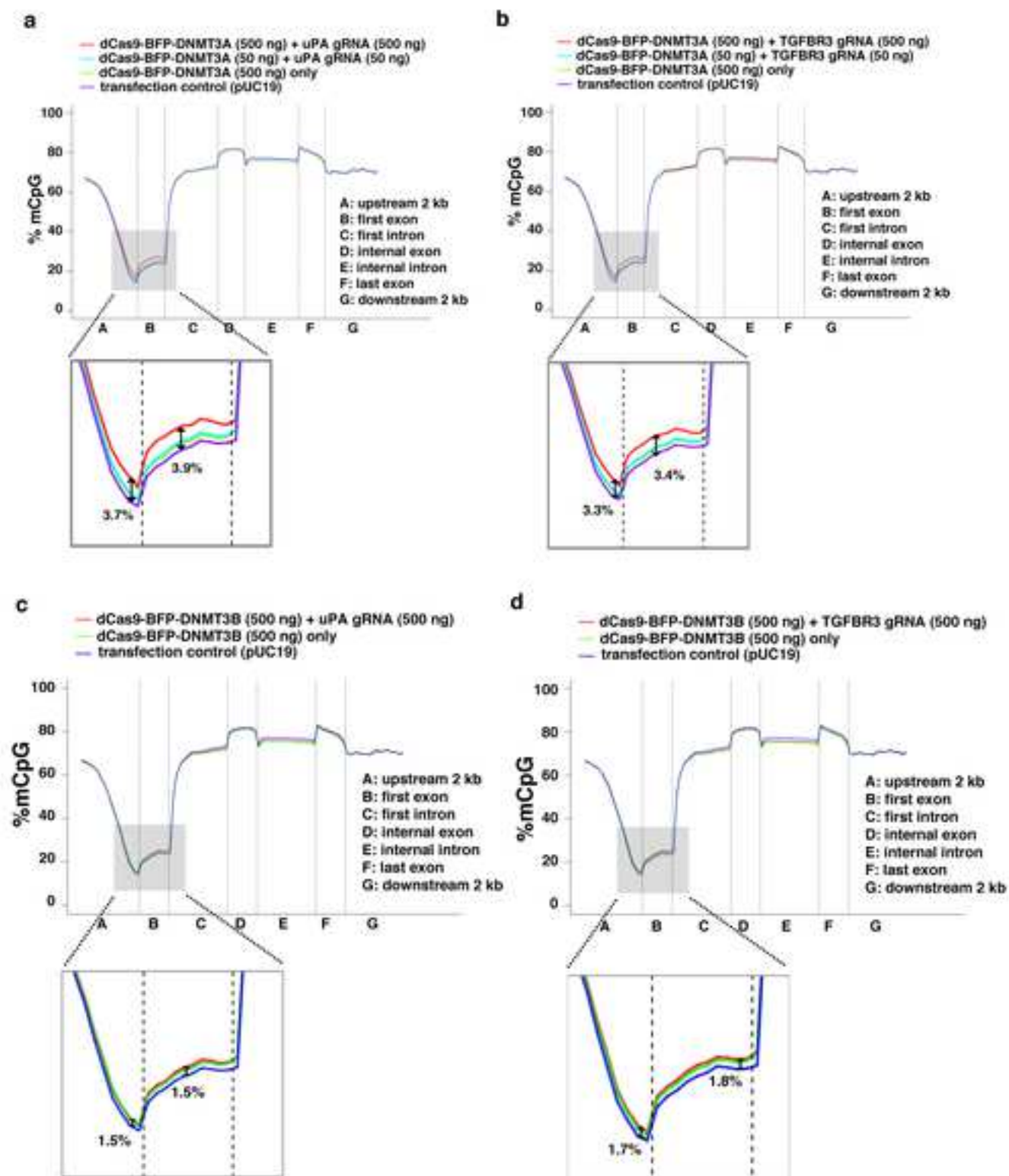
d

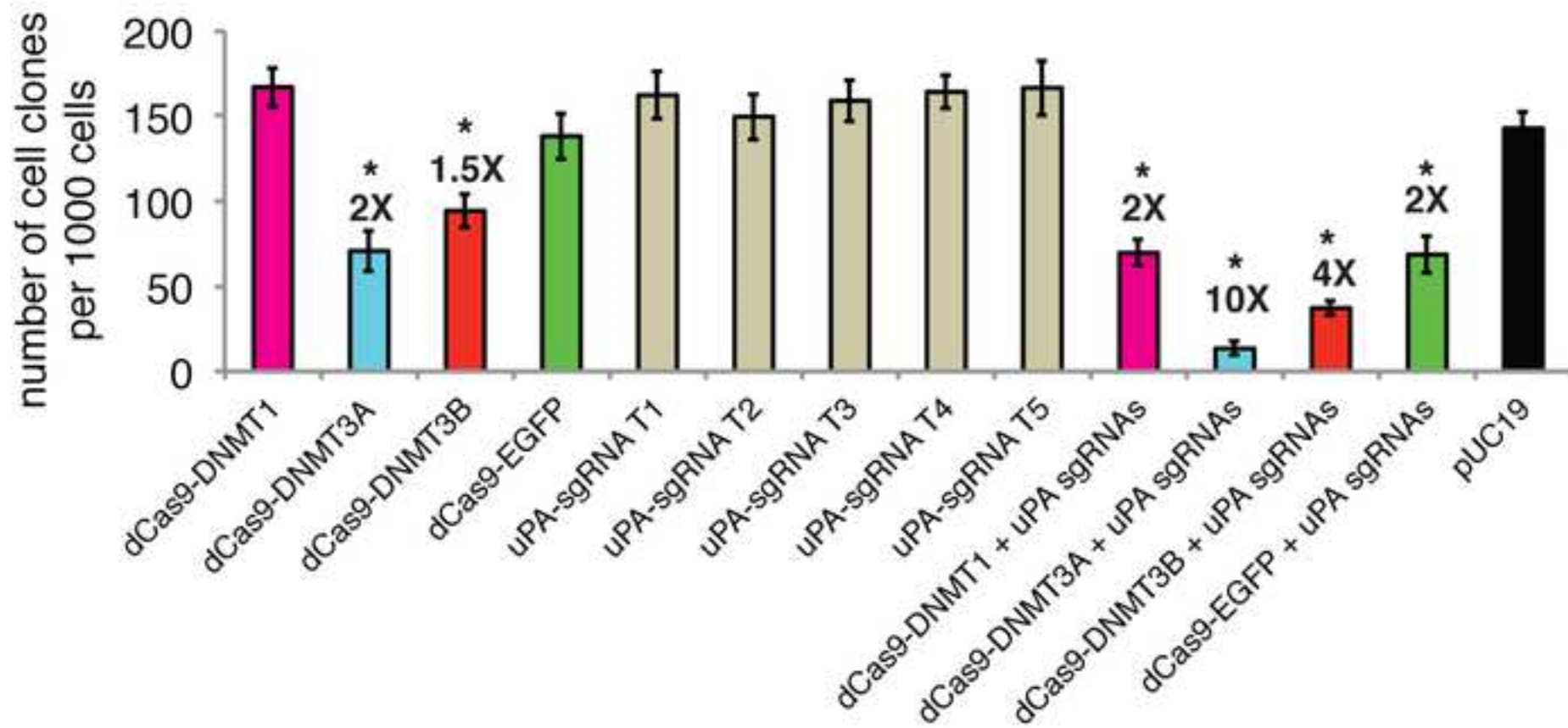


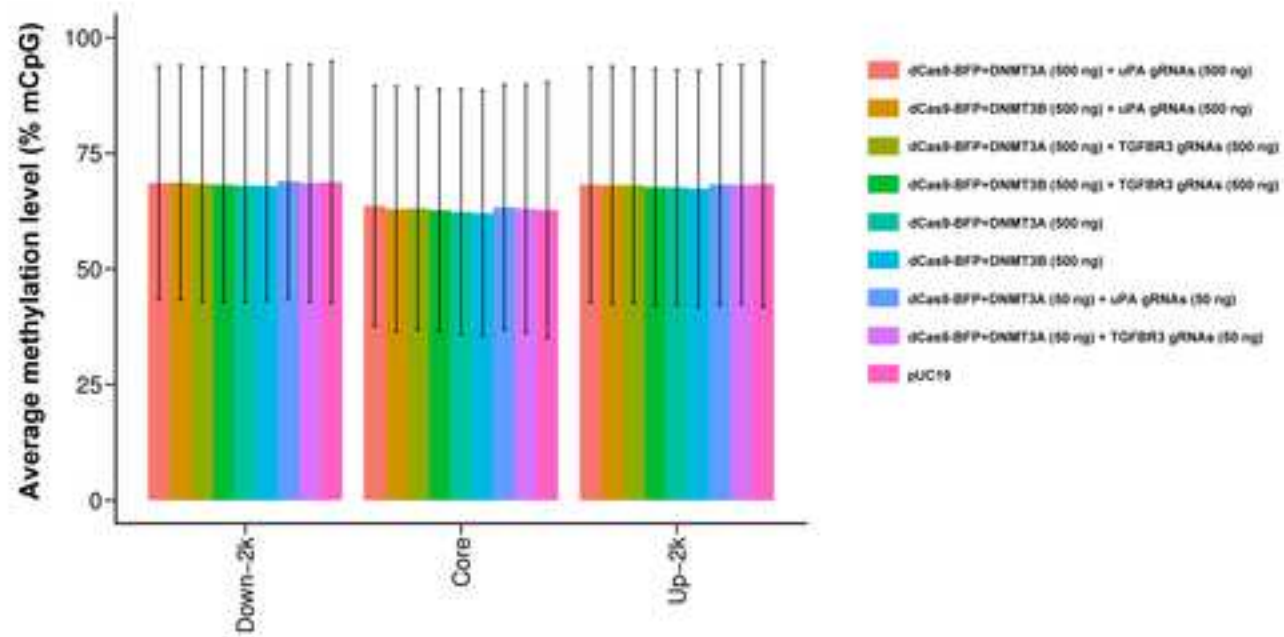


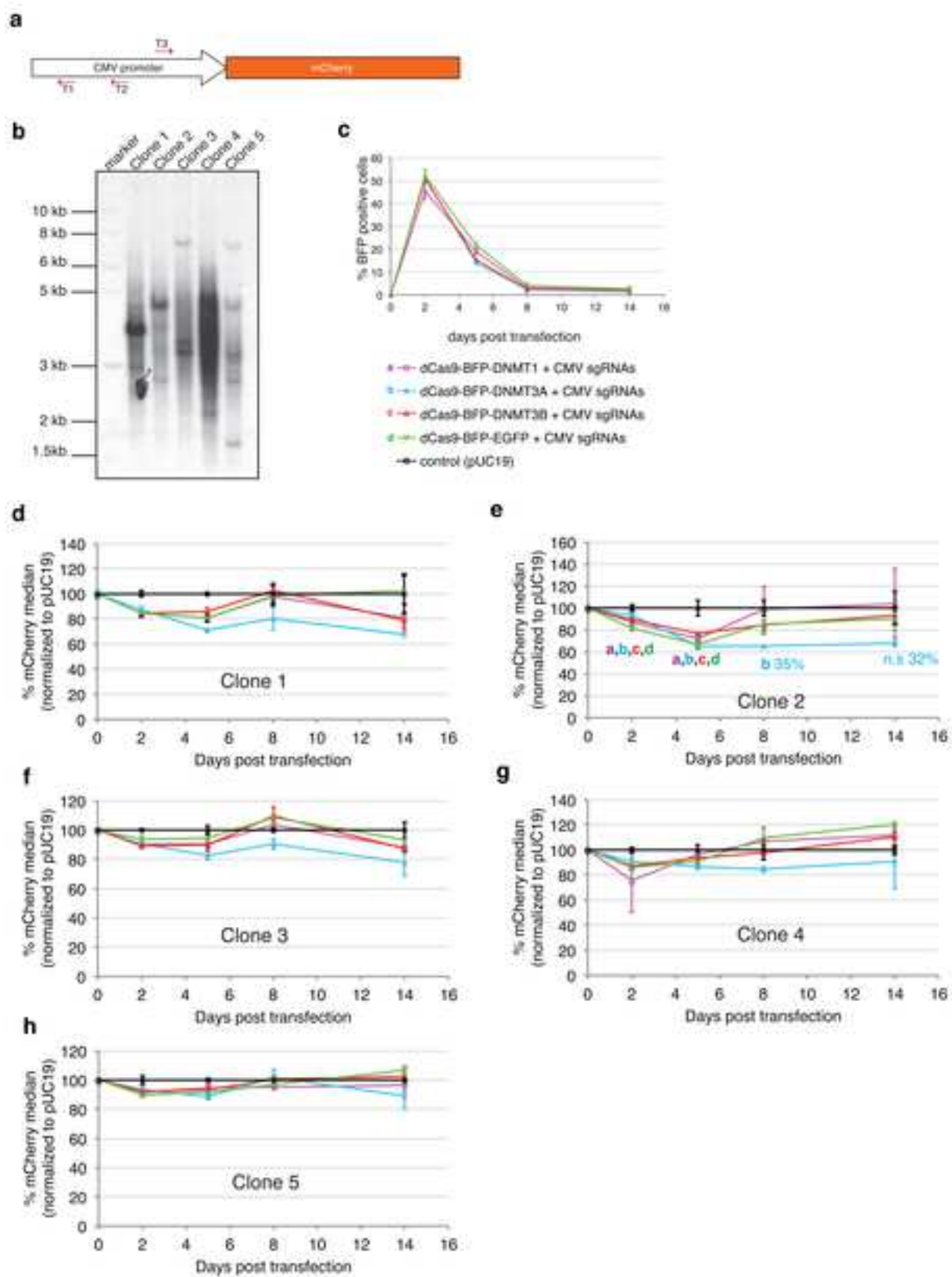






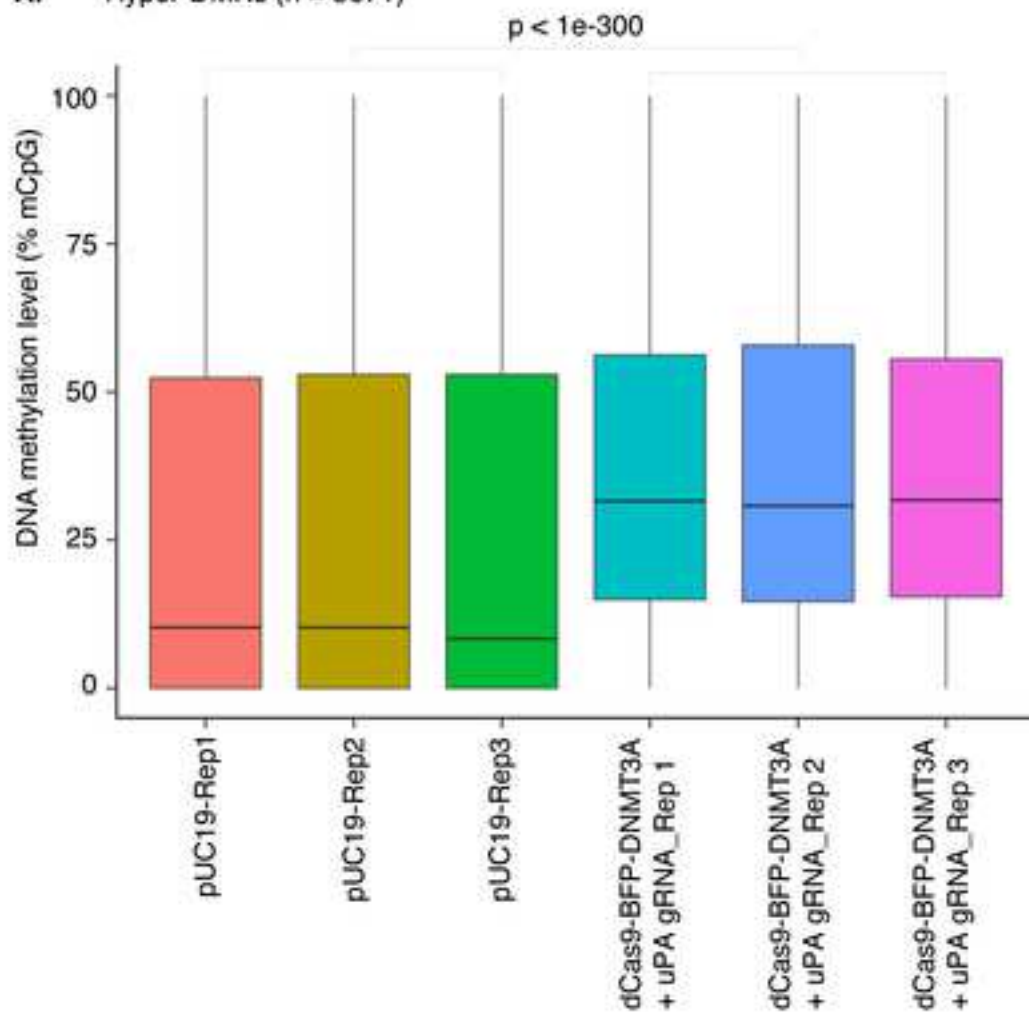




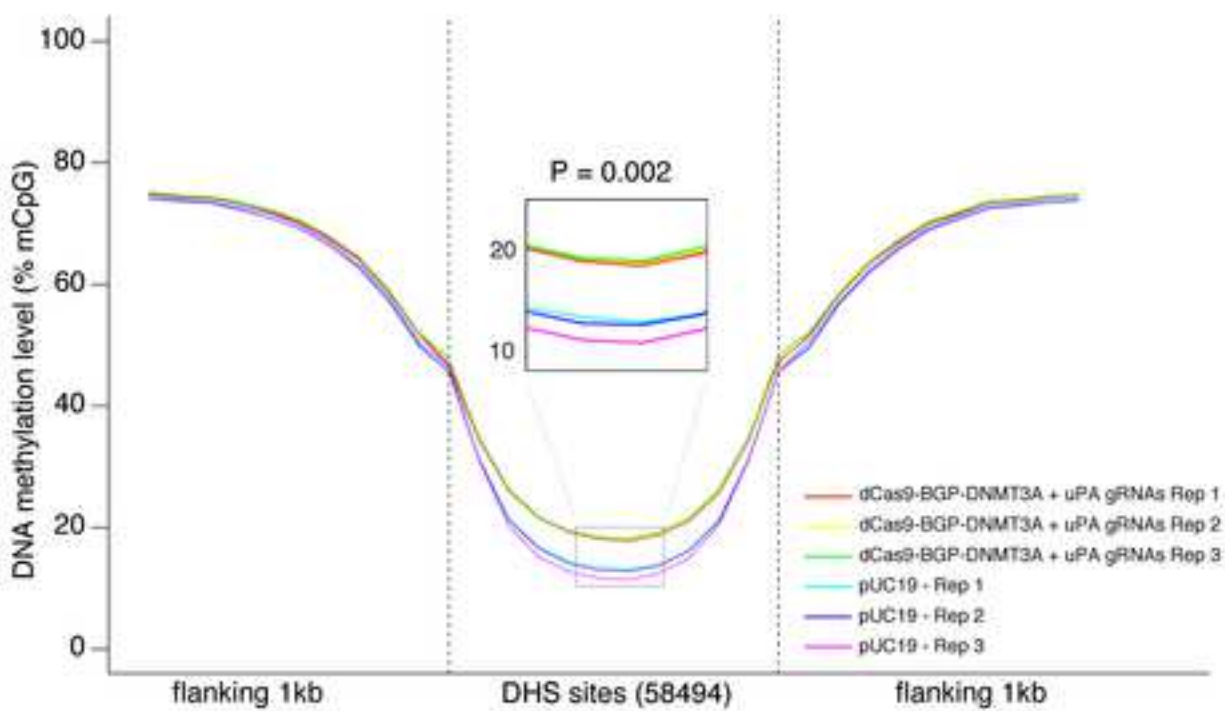


Supplementary Figure 14

A. Hyper-DMRs (n = 3671)



B.



Supplementary File 1: extended text and discussion

DNMT3A and DNMT3B catalytic domain causes gRNA-independent off-target methylation

Lin Lin^{1,7,§}, Yong Liu^{1,§}, Jinrong Huang^{2,3,§}, Fengping Xu^{2,3,4,§}, Tina Fuglsang Daugaard¹, Trine Skov Petersen¹, Bettina Hansen¹, Lingfei Ye², Qing Zhou^{2,3}, Fang Fang^{2,3}, Shengting Li^{1,2}, Lasse Fløe¹, Kristopher Torp Jensen¹, Ellen Shrock⁶, Huanming Yang^{2,4}, Jian Wang^{2,4}, Xun Xu^{2,3,*}, Lars Bolund^{1,2,7}, Anders Lade Nielsen¹, Yonglun Luo^{1,2,7,8*}

Affiliations for authors:

1. Department of Biomedicine, Aarhus University, Aarhus, Denmark
 2. BGI-Shenzhen, Shenzhen 518083, China
 3. China National GeneBank-Shenzhen, BGI-Shenzhen, Shenzhen 518083, China
 4. Department of Biology, University of Copenhagen, Copenhagen, Denmark
 5. James D. Watson Institute of Genome Sciences, Hangzhou 310058, China
 6. Department of Genetics, Harvard Medical School, Boston, MA, USA.
 7. Danish Regenerative Engineering Alliance for Medicine (DREAM), Department of Biomedicine, Aarhus University, Aarhus, Denmark
 8. BrainStem - Stem Cell Center of Excellence in Neurology, Copenhagen, Denmark
- §. These authors contributed equally to the study
- *. All correspondence should be addressed to Xun Xu (XUXUN@GENOMICS.CN) and Yonglun Luo (ALUN@BIOMED.AU.DK)

Main text:

Upon staining of the dCas9-BFP-DNMT3A and dCas9-BFP-DNMT3B fusion proteins in HEK293T cells, it is evident that most fusion protein is located in the cytoplasm rather than in the nucleus. This is probably due to the large size of the fusion proteins hindering efficient nuclear entry. We therefore reduced the size of the fusion proteins by removing the BFP domain in order to increase the nuclear entry efficiency of dCas9 methyltransferase. Furthermore, to enable enrichment of transfected cells, we introduce a blasticidin expression cassette.

Five expression vectors were constructed encoding the human-codon-optimized dCas9 protein flanked by two copies of an NLS and conjugated to the DNMT3A or DNMT3B catalytic domains, or DNMT3A (E752A), DNMT3B (E697A) or GFP, as well as a blasticidin resistance domain (**Fig. SF1a**). In the system utilized for the experiment, the blasticidin domain is cleaved from the fusion protein upon translation via the self-cleaving 2A peptide.

We first evaluated the *de novo* DNA methylation efficiency of dCas9-DNMT3A and dCas9-DNMT3B (**Fig. SF1b-c**). 10-fold and 3-fold increases of *de novo* methylation of the *TGFBR3* promoter were achieved in cells expressing *TGFBR3* gRNAs with dCas9-DNMT3A or dCas9-DNMT3B, respectively, compared to pUC19 or dCas9-EGFP controls (*P* value < 0.001, ANOVA). As expected, dCas9-DNMT3A(E752A) or dCas9-DNMT3B(E697A) lacked *de novo* methylation capacity. However, compared to the dCas9-BFP-DNMT3A and dCas9-BFP-DNMT3B fusions, the dCas9-DNMT3A and dCas9-DNMT3B fusions have higher gRNA-independent unspecific methylation (**Fig. SF1d**).

We speculated that the increased unspecific methylation by dCas9-DNMT3A and dCas9-DNMT3B was related to increased gene expression and/or nuclear localization efficiency. Thus, we used fluorescence

imaging to quantify the expression level and nuclear localization of the three EGFP control plasmids: dCas9-BFP-EGFP, dCas9-EGFP, and EF1a-EGFP, our results showed that both expression and nuclear entry levels of dCas9-EGFP is significantly higher (P value < 0.05 , ANOVA) than dCas9-BFP-EGFP (**Fig. SF2a**). Furthermore, we analyzed *GAPDH* promoter methylation in cells expressing dCas9-BFP-DNMT3A, dCas9-DNMT3A, or EF1a-DNMT3A (a control plasmid expressing the DNMT3A catalytic domain under transcriptional control of the EF1a promoter). Our results showed that cells expressing dCas9-DNMT3A and EF1a-DNMT3A showed notably higher mCpG levels than cells transfected with pUC19 (mean diff. mCpG level = 11.7% and 38.5%, P value = 0.012, Wilcoxon matched-pairs signed-rank test), while the difference between cells expressing dCas9-BFP-DNMT3A (CRISPRme1.0) and pUC19 was much smaller (mean diff. mCpG level = 2.3%, P value = 0.012, Wilcoxon matched-pairs signed-rank test) (**Fig. SF2b**).

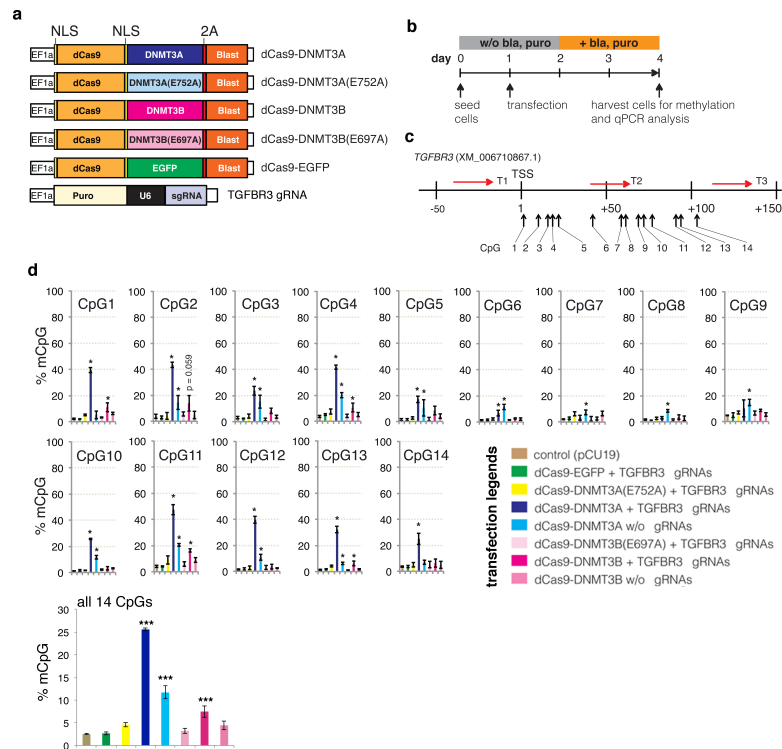
We next measured *LINE1* 5'UTR methylation. There was no significant difference in *LINE1* 5'UTR DNA methylation between cells expressing dCas9-BFP-DNMT3A and dCas9-DNMT3A (**Fig. SF2c**). However, cells transfected with the expression vector EF1a-DNMT3A had significantly higher *LINE1* methylation levels compared to pUC19 control cells (mean diff. % mCpG = 3.1, P value = 0.028, Wilcoxon matched-pairs signed-rank test) (**Fig. SF2c**), suggesting that increased CRISPRme expression and nuclear entry is accompanied by increased gRNA-independent off-target methylation of DNMT3A and DNMT3B fusion proteins.

We also investigated whether titration of the dCas9-DNMT3A and dCas9-DNMT3B plasmids used for transfection could reduce gRNA-independent off-target methylation. To test this, we transfected HEK293T cells with a varying amount of dCas9-DNMT3A plasmid (5, 25, 50, 100, 250, and 500 ng) alone or together with *TGFBR3* gRNAs. Titration of dCas9-DNMT3A caused a concordant decrease in both *TGFBR3* and *GAPDH* methylation (**Fig. SF3a-d**). Next, we tested whether decreasing the gRNA expression level could minimize gRNA-dependent off-target effects. We transfected HEK293T cells with various combinations of the amounts of dCas9-DNMT3A plasmid (5, 25, and 50 ng) and *TGFBR3* gRNAs (5, 25, 50, and 500 ng). Bisulfite pyrosequencing results showed that titration of gRNA transfection quantities decreased both on-target (*TGFBR3*) and off-target (*GAPDH*) methylation concordantly (**Fig. SF3e-h**). Collectively, our results suggest that increasing the expression of dCas9-DNMT3A and gRNAs results in enhancement of both on-target and off-target DNA methylation.

In conclusion, we have shown that fusion of dCas9 to catalytic domains of DNA methyltransferases can achieve RNA-guided methylation of targeted genomic regions. However, since these catalytic domains are active per se, cautions should be taken when delivering high amount of the fusion proteins/plasmids into cells, as these could cause unspecific methylation of genomic regions. Although GWBS was not conducted for the dCas9-DNMT3A and dCas9-DNMT3B fusions, the genomic regions prone to gRNA-independent methylation are most likely those located in open chromatin regions and CpG islands.

Figures and Figure Captions

Fig. SF1. Generation and validation of dCas9-DNMT3A and dCas9-DNMT3B methyltransferases



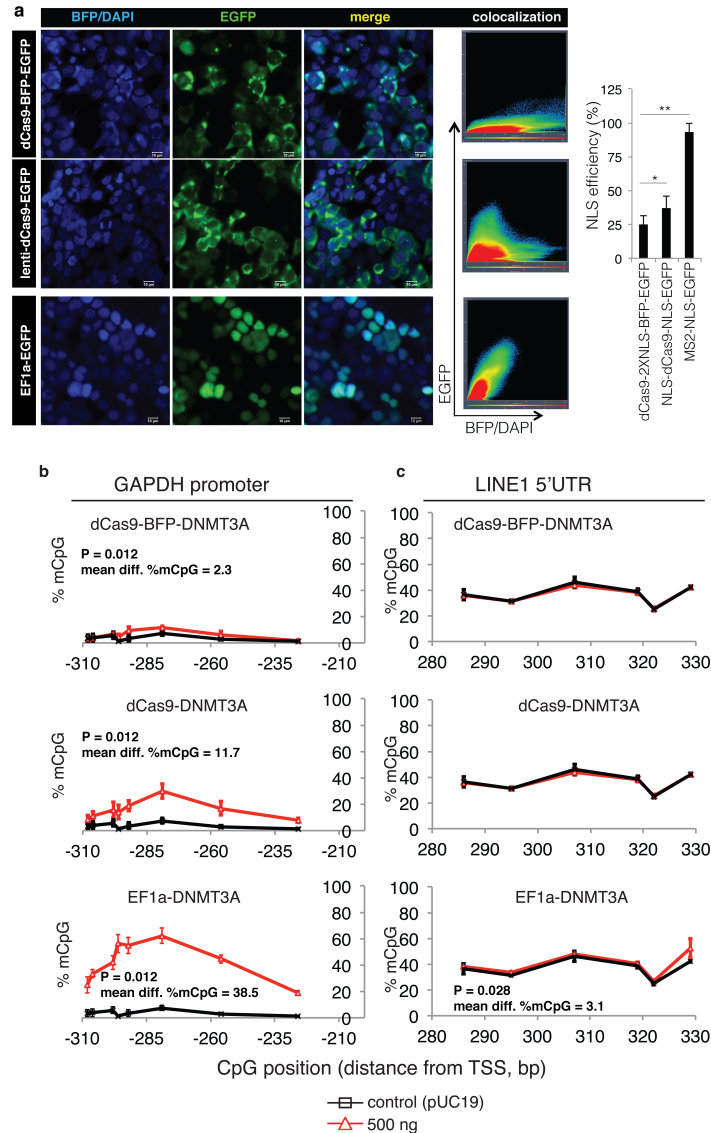
(a) Schematic illustration of CRISPRme 2.0 expression vectors encoding dCas9 flanked by nuclear localization signals (NLS) and fused to (i) a DNMT3A or DNMT3B catalytic domain, (ii) a DNMT3A (E752A) or DNMT3B (E697A) catalytically inactivated domain, or (iii) EGFP, and a blasticidin resistance gene. Expression of the fusion proteins was constitutively driven by the elongation factor-1 alpha (EF1a) promoter.

(b) Schematic illustration of the experiment. Transfected cells were enriched by blasticidin (10 ug/mL) and puromycin (10 ug/mL) antibiotic selection.

(c) *TGFBFR3* promoter with gRNA target sites and CpGs used for subsequent analysis by pyrosequencing.

(d) Bar charts depicting % mCpG for individual and all *TGFBFR3* CpG sites in cells expressing dCas9-DNMT3A, dCas9-DNMT3B, dCas9-DNMT3A(E752A), or dCas9-DNMT3B(E697A) with or without *TGFBFR3* gRNAs. Cells transfected with pUC19 or a dCas9-EGFP fusion were used as negative controls. % mCpG and relative gene expression values are presented as mean \pm SD (n = 3 independent transfections). Asterisks represent P value < 0.05 (*) and < 0.001 (***) (ANOVA). Percentage decrease in gene expression levels compared to pUC19 are presented on top of bars in (d).

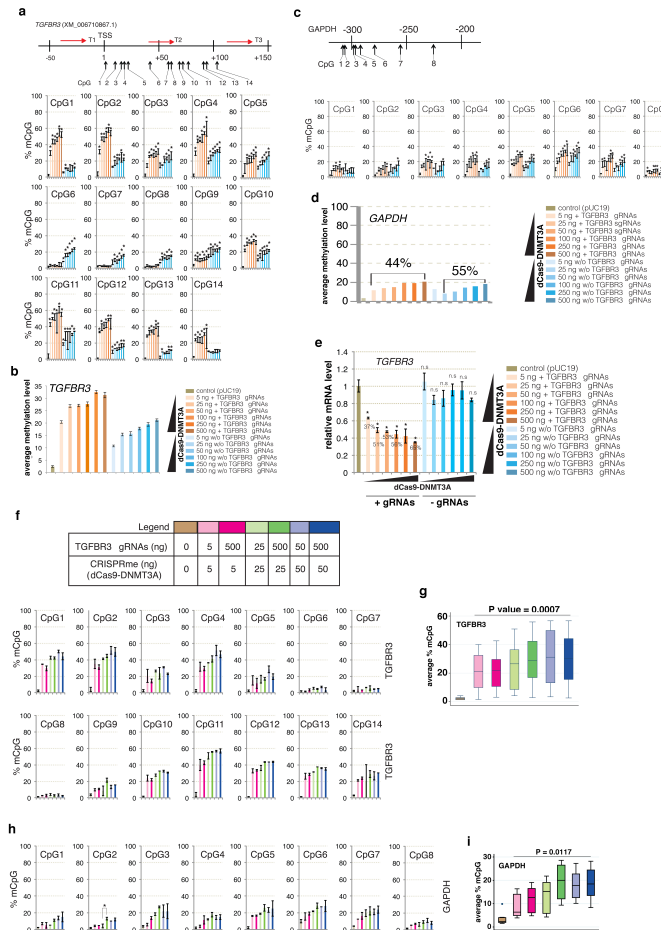
Fig. SF2 Comparison of dCas9 methyltransferase expression, nuclear entry efficiency, and the effects on specificity



(a) Laser scanning fluorescent microscopy of HEK293T cells expressing three EGFP fusion proteins. NLS, nuclear localization signal; BFP, blue fluorescent protein; MS2, the MS2 bacteriophage coat protein. Co-localization of EGFP and BFP/DAPI is observed. Nuclear localization was estimated using Image J. *, p-value < 0.05; **, p-value < 0.01 by ANOVA.

(b-c) Percentage methylation of *GAPDH* (b) and *LINE1* 5'UTR (c). Each data point is presented as mean \pm SD (n = 3, independent transfections). % mCpG levels were analyzed in cells 48 hours after transfection with dCas9-BFP-DNMT3A, lenti-dCas9-DNMT3A, or EF1a-DNMT3A plasmids (500 ng). Cells transfected with an identical amount of the pUC19 plasmid were used as control and re-plotted for the different treatments as reference. Average difference in % mCpG levels between experimental groups and controls are shown together with Wilcoxon matched-pairs signed-rank test P values.

Fig. SF3. Effects of titrating dCas9-DNMT3A, dCas9-DNMT3B and gRNA plasmids on on-target and off-target methylation



(a-b) Bar charts illustrating % mCpG levels for the 14 individual *TGFBR3* CpG sites (a) and the average methylation level for all 14 CpG sites. (b) in HEK293T cells expressing various amounts (5, 25, 50, 100, 250, and 500 ng) of the dCas9-DNMT3A plasmid with or without (w/o) *TGFBR3* gRNAs (500 ng).

(c-d) Bar charts illustrating % mCpG levels for individual CpG sites (c) or average methylation levels (d) in the *GAPDH* promoter in cells expressing different levels (5, 25, 50, 100, 250, and 500 ng) of dCas9-DNMT3A with or without *TGFBR3* gRNAs (500 ng). Cells transfected with pUC19 were used as controls. Asterisk (*) indicates statistical significance ($p < 0.05$, ANOVA) after Bonferroni correction.

(e) Bar charts of relative *TGFBR3* mRNA levels compared to control cells transfected with pUC19. Both CpG methylation and gene expression data represent mean \pm SD ($n = 3$ independent transfections). Asterisk (*) indicates statistical significance (P value < 0.05 , ANOVA) after Bonferroni correction.

(f) (top) Transfection legend. HEK293T cells were co-transfected with various amounts of dCas9-DNMT3A (5, 25, and 50 ng) and the *TGFBR3* gRNAs (5, 25, 50, and 500 ng). (bottom), bar charts of % mCpG for individual CpG sites in the *TGFBR3* promoter (TGFBR3-DMR1).

(g) Box plot of the average of % mCpG for all 14 CpG sites in the *TGFBR3* promoter for each experimental group.

(h) Bar charts illustrating % mCpG for individual CpG sites in the *GAPDH* promoter.

(i) Box plot of the average % mCpG for all 8 CpG sites in the *GAPDH* promoter for each experimental group.

Figures (f, h) are plotted as mean \pm SD ($n = 2$, independent transfections). (g, i) P values are from Wilcoxon matched-pairs signed-rank tests between the 5 ng and 500 ng experimental groups.



Click here to access/download
Supplementary Material
Supplementary Table S1.docx





Click here to access/download
Supplementary Material
Supplementary Table S2.xls



Click here to access/download
Supplementary Material
Supplementary Table S3.xls



Click here to access/download
Supplementary Material
Supplementary Table S4.xls





Click here to access/download
Supplementary Material
Supplementary Table S6.xls

